Dipl.-Ing. Dr.techn. Andreas Hackl, BSc

# Experimental Validation of an Electric Circuit based Battery Cell Model Approach for Automotive Applications

Master's Thesis

to achieve the university degree of

Diplom-Ingenieur

Master's degree programme: Electrical Engineering

submitted to

Graz University of Technology

Supervisors:

Dipl.-Ing. Dr.techn. Bernhard Schweighofer

Assoc.Prof. Dipl.-Ing. Dr.techn. Hannes Wegleiter

Institute of Electrical Measurement and Measurement Signal Processing

Graz, December 2019

# Acknowledgement

*Andreas Hackl*
*Graz, December 2019*

# Affidavit

I declare that I have authored this thesis independently, that I have not used other than the declared sources/resources, and that I have explicitly indicated all material which has been quoted either literally or by content from the sources used. The text document uploaded to TUGRAZonline is identical to the present doctoral thesis.

_____          _____
         Date                               Signature

# Abstract

To meet the growing demand of increasing comfort, reduced greenhouse gases and the usage of renewable energy in the daily live, are clearly visible nowadays. Due to the increasing number of hybrid and electrified vehicles, these changes are also given within the automotive industry. Nevertheless, the bottlenecks for a faster growth are currently two main facts, price and range. While price is constantly decreasing during the last years, managing the energy available from the battery system is defined as main challenge. To handle this problem in addition to reduce development time and save costs, modelling and simulation have become a state-of-the-art tool during the last years. Therefore, this thesis deals with the modelling, simulation and validation of the main part, needed in each battery pack system, namely the battery cell itself.

The first part of the thesis starts with the requirements and functionalities of battery cells, as fundamental knowledge for the modelling process. In detail, different chemical cell compositions are evaluated and advantages and disadvantages discussed. Finally, it will be shown that lithium-ion technologies are a good choice, based on the requirements nowadays, in automotive applications. Hence, functionalities of lithium-ion cells and fundamental chemical effects are presented as introduction to the modelling process. Following, three common model applications, namely electro chemical models, neuronal networks and models based on equivalent electric circuits are evaluated and validated based on a literature study. Thus, focus is held on accuracy, parameterability and calculation time. Finally, it will be presented that modelling a battery cell based on an equivalent electric circuit proves to be a satisfactory opportunity.

The second part of this thesis deals with the battery cell modelling process itself. Based on fundamental cell behaviour, a strategy is defined to separate the process into a steady-stated part, implemented as open circuit voltage versus state of charge characteristic, and a transient part, based on electric elements. Thereto, well known methods to generate the steady-state behaviour are presented, evaluated and discussed based on measurement data. Special focus is given within the accuracy versus measurement time as well as the hysteresis effect during charging and discharging. Following, an equivalent electric circuit is elaborated as second step. Thus, a method called electrical impedance spectroscopy is presented where cell behaviour is transformed into the frequency domain. Within this method a modelling from the engineering point of view can be realised.

After modelling the steady-state and transient part separately, both types of models are combined and evaluated based on measurement data. Thus, this will be done by validating different external influences, like SOC level, ambient temperature and load currents, respectively c-rate. In detail, it will be shown that the parameters are dependent on these effects, but the model approach is able to handle all influences quite satisfactorily. For the purpose of completeness, parameterisation results within time and frequency domain will be compared and evaluated. In summary, an equivalent electric circuit model approach will be presented which is able to handle various external influences as well as different parameterisation methods.

# Kurzfassung

Der wachsenden Bedarf an höheren Komfort, Reduzierung der Treibhausgase sowie der Nutzung von erneuerbaren Energien führt auch zu erhöhten Anforderung in der Technik. In der Automobilindustrie sind diese Trends durch den stetigen Zuwachs von hybrid- und elektrifizierten Fahrzeugen auch schon deutlich ersichtlich. Nichtsdestotrotz, bildet der hohe Preis als auch die geringe Reichweite oft noch den Flaschenhals für stärkeres Wachstum. Während die Preise in den letzten Jahren schon deutlich gesunken sind, stellt das perfekte managen jener Energie welche in den Batterien gespeicherten sind, eine große Herausforderung dar. Um dieses Problem bestmöglich zu managen hat sich die Modellbildung und Simulation zu einem wichtigen Werkzeug entwickelt. Somit beschäftig sich diese Arbeit mit der Modellbildung und Simulation von jener Komponente, welche für ein Batteriesystem unumgänglich ist, nämlich der Batteriezelle.

Als Grundlage für den Modellierungsprozess, beginnt der erste Teil der Arbeit mit den Anforderungen und Funktionalitäten von Batteriezellen. Dabei werden verschiedene chemische Zellzusammensetzungen bewertet, sowie deren Vor- und Nachteile diskutiert. Resultierend daraus, kann gezeigt werden, dass Lithium-Ion Technologien die heutigen Anforderungen bestmöglich erfüllen. Basierend auf einer Literaturrecherche werden im Anschluss daran drei gängige Modellansätze, elektrochemische Modelle, neuronale Netze und Modelle aufbauend auf äquivalente elektrische Schaltungen, vorgestellt. Fokus wird dabei auf Modellgenauigkeit, Parametrierbarkeit und Rechenzeit gelegt. Abschließend kann gezeigt werden, dass eine Modellierung mittels äquivalenter elektrischer Schaltungen die meisten Vorteile mit sich bringt.

Der zweite Teil der Arbeit beschäftigt sich mit der Modellbildung der Batteriezelle selbst. Basierend auf dem grundlegenden Zellverhalten wird eine Strategie definiert welche die Modellierung in einen stationären Part, beschrieben mittels Spannung versus Ladezustandscharakteristik, sowie einen transienten Part, aufbauend auf ein elektrisches Ersatzschaltbild, unterteilt. Des Weiteren werden bekannte Methoden zur Generierung dieses stationären Verhaltens vorgestellt, diskutiert und auf Basis von Messdaten bewertet. Besonderes Augenmerk wird auf die Modellgenauigkeit, Messzeit sowie den entstehenden Hysterese Effekt beim Laden und Entladen gelegt. Im Folgenden wird das elektrische Ersatzschaltbild ausgearbeitet. Dabei wird eine Methode vorgestellt, welche das Zellverhalten in den Frequenzbereich transformiert um eine einfache technische Modellierung durchzuführen.

Nach der getrennten Modellbildung der stationären sowie transienten Charakteristik, werden beide Modellteile kombiniert und anhand von Messdaten evaluiert. Besonderes Augenmerk wird dabei auf die unterschiedlichen Ladezustände, Umgebungstemperaturen und Ladeströme gelegt. Im Detail kann gezeigt werden, dass die Modellparameter von diesen Einflüssen abhängen, jedoch das Modell im Stande ist alle Einflüsse ausreichend genau zu modellieren. Abschließend werden noch die Ergebnisse aus der Parametrierung aus dem Zeit- und Frequenzbereich verglichen und evaluiert. Zusammenfassend kann gezeigt werden, dass der ausgearbeitete Modellansatz in der Lage ist verschiedene Einflüsse gut nachzubilden als auch mit unterschiedlichen Methoden parametriert werden kann.

# Contents

# Abbreviations

**AC** Alternating current

**ADC** Analog to digital converter

**BMS** Battery management system

**BV** Buttler Volmer

**CFD** Compuational Fluid Dynamics

**CPE** Constant phase element

**DOD** Depth of discharge

**EC** Equivalent electric circuit

**ECH** Electrochemical

**EIS** Electrical impedance spectroscopy

**EV** Electric vehicle

**HEV** Hybrid electric vehicle

**LCO** Lithium-cobalt-oxide

**LFP** Lithium-iron-phosphate

**LMO** Lithium-manganese-oxide

**LTI system** Linear time invariant system

**LTO** Lithium-titanate

**NCA** Lithium-nickel-cobalt-aluminum-oxide

**NMC** Lithium-nickel-manganese-cobalt-oxide

**NN** Neuronal network

**OCV** Open circuit voltage

**PDE** Partial differential equation

**SEI** Solid electrolyte interphase

**SOC** State of charge

**SOH** State of health

# Symbols

## Parameters and scalar variables

| | |
|---|---|
| $c_s$ | Conservation of lithium |
| $f$ | Frequency |
| $j$ | Reaction current |
| $l$ | Diffusion length |
| $o$ | Output |
| $r$ | Radius |
| $t$ | Time |
| $w$ | Weighting factor |
| $x$ | Input variable |
| | |
| $C$ | Capacity |
| $D$ | Diffusion coefficient |
| $D_e$ | Electrolyte phase $Li^+$ diffusion coefficient |
| $D_s$ | Solid phase Li diffusion coefficient |
| $F$ | Faraday constant |
| $I$ | Current |
| $I_a$ | Battery cell current |
| $L$ | Length |
| $Q$ | Electric charge |
| $R$ | Resistance |
| $R_s$ | Particle radius |
| $T$ | Temperature |
| $U$ | Voltage |
| $U_a$ | Battery cell voltage |
| $Z$ | Impedance |
| | |
| $\omega$ | Rotational speed |
| $\varphi$ | Phase delay |
| $\psi$ | Depression factor |
| | |
| $\Phi$ | Electric potential |
| $\Theta$ | Generalised capacity |

# Indices

| | |
|---|---|
| 0 | Initial condition |
| $\infty$ | Infinity |
| | |
| a | Ambient, anode |
| appr | Approximation |
| avg | Average |
| c | Cathode |
| ct | Charge transfer |
| diff | Diffusion |
| dl | Double layer |
| kp | Key points |
| meas | Measured |
| max | Maximum |
| min | Minimum |
| opt | Optimised |
| r | Relaxation time |
| s | Sample |
| | |
| N | Nominal |
| S | Steady-state |
| W | Warburg |
| | |
| $i$ | Index variable |

# 1

# Introduction

Nowadays, the customer-based technology is undergoing constant evolution. Expressions like *digitalisation*, *decentralised automation* or *electrification* are just a few examples which become key notes of today's everyday life. Where higher comfort and more prosperity for the population are named as main goal of this trend. Nevertheless, this change not only brings advantages, but also new challenges for sustainability and environmental compatibility. In addition to the functionality and recyclability of all these new products, the energy issue is probably one of the biggest challenges in near future. As a result, an efficient development procedure and the usage of renewable energy are becoming more and more important during this days.

Fortunately, not only private people recognised the energy saving principles but also politics tend to go in this direction. In November 2018, the political commission of the European Union called for a climate neutral Europe by the year 2050. Furthermore, the published key document with the title *A Clean Planet for all - a European strategic long-term vision for a prosperous, modern, competitive and climate neutral economy* includes, inter alia, the specification of reducing greenhouse gases and using renewable energy sources, [European Commission, 2018a] & [European Commission, 2018b]. As detailed example, the share of renewable energy should be increased from 17% in 2017 up to 32% in 2030, [European Commission, 2018c].

But this trend is not only visible in political broadcasts, also industries like the automotive engineering are undergoing constant evolution and following this trend. Key notes, like *digitalisation*, *electro mobility* and *autonomous driving*, are still in progress. Increasing comfort for final consumers on the one hand but also reduce green house gases and using renewable energy on the other hand is the aim of this branch as well. Not only statements from Volkswagen at the International Motor Show in Frankfurt, Germany 2017, that they will bring 80 new electrified vehicles to the market by 2025 or Daimler that they will invest 10 billion Euro in the expansion in the field of electric vehicles within the next few years, confirm this trend, [Müller-Wondorf, 2017]. Even a simple look around while driving is enough to recognise the increase in hybrid and fully electric vehicles as well as vehicles with a high degree of driver assistance systems. Taking all of this one step further, pioneers in the automotive industry are already talking about electric driven autonomous vehicles in the near future.

Although, the percentage of electric and hybrid vehicles is still rather low, but studies have shown that customer acceptance of electro mobility has increased significantly during the recent years. As an example, a study from [Statista GmbH, 2019a] shows the record number of new registrations of about 36000 electric vehicles just in Germany by the year 2018. That means almost a tripling since year 2015, see Figure 1.1 above. In addition, the constant growth of new registrations leads to an exponential number of overall *electric vehicle*s (EVs) for the next years, see Figure 1.1 below, [Statista GmbH, 2019b].

However, in order to achieve the desired goal of minimising emission greenhouse gases, requirements to continue these trends are different for final customers, business and research. While for consumers properties like comfort, vehicle consumptions, driving range or furthermore just the price are hard facts for a purchasing decisions, for business and research such trends usually bring very different questions and requirements. In summary, the bottleneck for a faster growth of the EVs and *hybrid electric vehicle*s (HEVs) are currently two main points, price and short range.
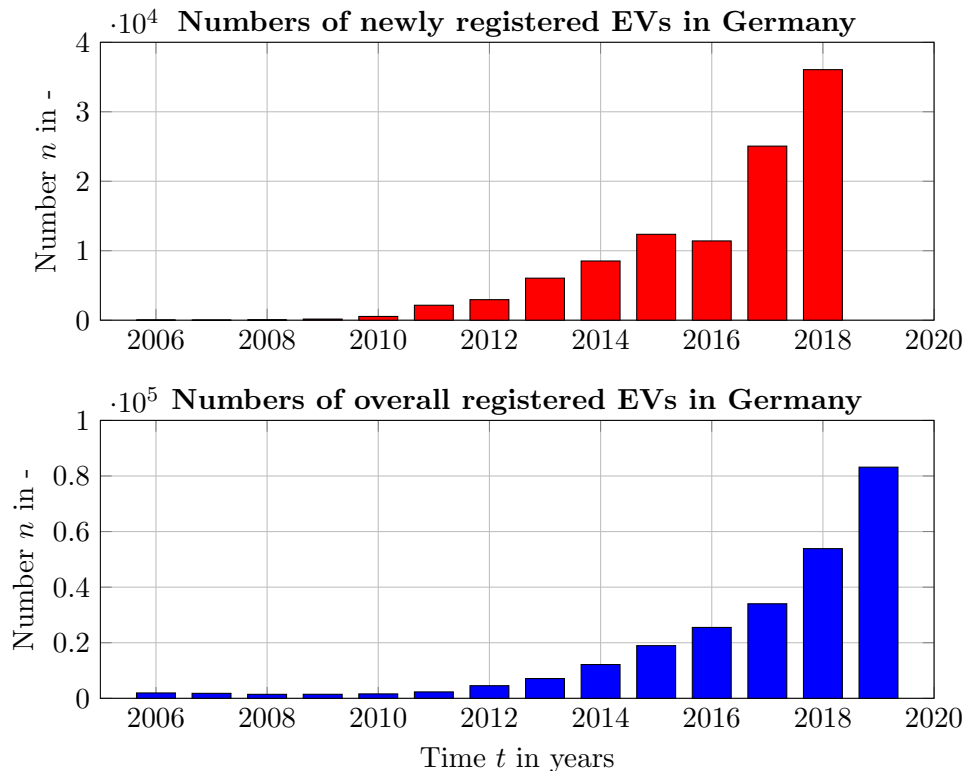


Figure 1.1.: Numbers of newly- and overall registered *electric vehicles* (EVs) in Germany from 2006 to 2019, Source: [Statista GmbH, 2019a] and [Statista GmbH, 2019b]

Where the price are mainly reflected in the cost of the battery pack respectively the cells, this tendencies are going in the right direction. Thus, the price of lithium-ion batteries, which are currently widely used in the automotive industry, has been roughly quartered in the last seven years, see Figure 1.2 adapted from [Statista GmbH, 2019c], and will definitely decrease with increasing number of EVs and HEVs.

Anyhow, to increase range by using a battery pack with more cells does not always fit due to the installation space and is also not very efficient because of the increasing vehicle mass. Therefore, using the available energy density in a most sufficient way leads to be a quite more economical and technical solution. In summary, beside efficient hardware components, a satisfactory energy management strategy is needed for maximising the range by a sufficient use of the energy storage system.

But how can just strategies be designed and evaluated in most efficient way and furthermore within even shorter development time? The answer of this question leads us to the virtual product development. The goal of this trend is to bring a larger part of the development process into the virtual world of modelling, simulation and testing. Starting with the problem description, continuing with the controller design and followed by testing, validation and tuning of overall energy management strategies should be done virtual, see e.g. [Kraus, 2016]. This brings the advantage that physical testing can be done in shorter time and under different surroundings. Especially validation and testing within vehicle and component limits as well as under extreme conditions can be done without any safety risks and be repeated all the time. Furthermore, all possible traffic and environment scenarios can be generated to evaluate the programmed algorithms under each feasible condition.

Nonetheless, practicality and applicability of these simulations are reflected on model accuracy or rather how good such models represent the real world behaviour. Therefore, an increase in virtual world complexity which is synonymously to a more detailed modelling process concludes on these challenges. However, a more detailed modelling



Figure 1.2.: Worldwide price development for lithium-ion batteries from 2013 to 2020 in Euro/kWh, Source: [Statista GmbH, 2019c]

process does not increase the computation accuracy automatically. More often it only leads to a more complicated parametrisation process which brings high computational effort. Finally, a higher model accuracy only counts with accurate model parameters and more calculation power. To summarise, in most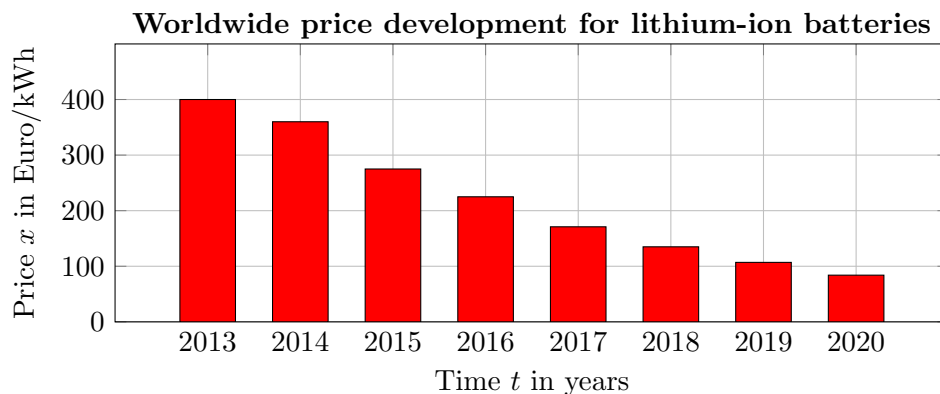 technical and economical cases a trade-off between model accuracy, parametrisability and computation time has to be solved.

## 1.1. Significance of battery cell modelling for energy management strategies of EVs and HEVs

Energy management systems are indispensable to increase the range of EVs and HEVs by using available energy in most sufficient way. To develop, evaluate and validate such strategies, modelling and simulation have become a major tool during the last years. But, a vehicle model itself is hardly capable to describe real world conditions by its own. In addition to a realistic vehicle model, an environment description, a driver- and furthermore a drivetrain model is needed to handle all interactions in a quite realistic way. This statement shows two main facts. First, high modelling effort is needed for a satisfactory overall simulation in general. Second, if only one part of the comprehensive model includes inaccuracies, it will effect the management system evaluation and validation process considerably. This leads to the point that within higher vehicle strategy requirements, increasing demands on modelling and simulation accuracies of each model part are given as well.

Nevertheless, one of the core components of an electric drivetrain is defined by the energy storage system, which is given by the battery pack in most applications. This leads to the fact that for simulation based evaluation and testing of energy management strategies the model accuracy of the battery pack is of great importance. But modelling a whole battery pack is a sophisticate problem to solve. Beside the interaction between electronic components like, *battery management system* (BMS), pre-/discharge board and the cells, see e.g. [Dubarry et al., 2019], also thermal behaviour and its impact on cell/pack characteristics is a big challenge to handle, see e.g. [Jeon & Baek, 2011], [Khan & Kaer, 2016].

However, before these interactions and thermal influences can be investigated, the battery cell as core component has to be modelled and understood first. Therefore, focus of this project is spent on battery cell modelling which can be seen as foundation for further fundamental investigations on battery storage systems. As an additional requirement, focus on computational effort has to be taken into account to use the battery model application for testing the energy management algorithm under realistic conditions. Furthermore, because parameterability interacts in most cases with measurement time, which equally means costs, a parameterisation process from the engineering point of view is preferred. In summary, a battery model within the trade-off accuracy, parameterability and computational effort is needed.

For that purpose, still a lot of research is ongoing on cell and battery modelling. Based on the literature, three main groups have emerged during the last years. The main group is application-based on equivalent electric circuit, followed from electro chemical models and neuronal networks as well as black box model approaches, see in detail Chapter 2. While neuronal networks bring good accuracy when a lot of measurement data are available for the generation and training process, electric circuit and electro chemical based models have advantages in terms of programming and handling. In this case, advantages and disadvantages have to be evaluated and the appropriate type of model which has to be used, depending on the application.

In summary, different types of model applications are already available for modelling a battery cell behaviour. Based on the application case and usage in automotive operations each type brings advantages and disadvantages in usability, accuracy and complexity. Nevertheless, requirements in the area of model accuracy within a wide range of *state of charge* (SOC), charge and discharge current rates as well as temperatures are given. In addition, low demands on measurement manoeuvre and parameterisation time save costs and bring a good benefit to effort ratio. Thus, a wide range of requirements is given for modelling and simulation of a battery cell.

## 1.2. Thesis contribution and outline

Modelling and simulation have become a state of the art tool in the field of automotive engineering to reduce development time and save costs. In order to meet the even growing demands on hybrid and vehicle strategies of EVs and HEVs, increasing demands on component modelling are given in addition. This means in detail, that shorter calculation time, higher accuracy and easier parameterability are main requirements. As core item of the electric drivetrain, model accuracy of the battery pack respectively the cell application plays an important role for the overall model approach. Nevertheless, a detailed modelling process does not increase model computation automatically. In most technical and economical cases a trade-off between model accuracy, parametrisability and computation time has to be solved.

Therefore, the goal of the present thesis is the experimental validation of various battery cell model approaches including their parameterisation processes. Special attention is paid on simple but effective model operation for automotive relevant applications with focus on model accuracy, parameterisation practicality and computation time, which equally means costs. To achieve this goal, a literature study is carried out on common and practicable types of battery cell models in the first part of the thesis.

This study provides an overview of the model availability on the market, but is also used to define a model structure for further detailed investigations. Based on the type of model application, the two well-known methods to generate the *open circuit voltage* (OCV) versus *state of charge* (SOC) characteristics (constant and puls charge/discharge current), are compared with special focus on the hysteresis effect and low SOC situations.

Following, different electric circuit based model approaches to describe the transient behaviour of the battery are presented and validated. For the parameterisation process of these models, *electrical impedance spectroscopy* (EIS) and pulse manoeuvres are used and the results compared. Furthermore, changes in environment temperatures and charge/discharge rates (short C-rate) are investigated in more detail. In addition, a semi-physical model approach is developed to describe the influences of the so called *Buttler Volmer* (BV) effect and its influence on cell behaviour.

Finally, a final model recommendation is presented which is able to handle different SOC, temperature and load spectrum situations. For all investigations a $LiNiCoAlO_2$ test cell with $3500\,mAh$ is used. Furthermore, all Matlab based model files are available and will be provided on request by contacting the author.

In order to achieve these goals, the presented thesis is structured as following:

**Chapter 1** provides an overview of the significance of modelling and simulation of battery cell modelling for EVs and HEVs strategies. Following, the relationship between energy management system and component accuracy is presented. Furthermore, focus is spent on battery cell modelling where a short overview of different types of models is given. Finally, an outlook on the thesis structure is presented.

**Chapter 2** begins with basic physical and chemical battery cell properties with focus on lithium-ion technologies. Following, a common literature based classification of different types of cell model approaches divided in three main groups (electrochemical models, equivalent electric circuit modelling and neuronal networks) is presented and evaluated based on automotive applications. Based on this literature study, one model approach is finally defined and used for detailed investigations in the next chapters.

**Chapter 3** starts with basic considerations on the voltage potential of a battery cell. Based on these fundamental investigations, the strategy to split the cell modelling into a steady-state and a transient part is confirmed. Afterwards, a short overview of the measurement equipment as well as the used test cell is given. The second part of this chapter focuses on the steady-state modelling part of a cell, which is implemented as the well-known open circuit voltage versus state of charge characteristics. Two literature based methods, to generate the behaviour, are investigated in detail and compared. Finally, the experimental generation forms the foundation of the transient model part, presented in the next chapter.

**Chapter 4** describes the modelling process of the transient battery cell behaviour. First, the state of the art method, called EIS, to investigate battery behaviour as well as parameterise cell models is presented. Following, an extended literature based model approach is given out of the EIS results. Next, this extended approach is revised, based on the thesis requirements and cell behaviour. Finally, a thesis model approach is elaborated, based on the *Monte-Carlo analysis* method. This approach, in combination with the OCV versus SOC characteristic, is used and validated in the next chapter.

**Chapter 5** presents the evaluation process of the elaborated electric circuit model based on external influences. Thus, changes in SOC, ambient temperature and load current, respectively C-rate are investigated and results compared with the model with focus on the parameter influences. Furthermore, a semi-physical model approach to handle the BV effect is presented and evaluated. Finally, parameterisation process within the time domain is compared with results generated out of the EIS measurements.

**Chapter 6** summarises the main findings of this thesis and provides a final statement. Finally, an outlook represents the next steps for further research projects.

# 2

# Modelling and simulation applications of battery cells

The first chapter concludes that a well structured and organised battery cell model forms the foundation for an accurate overall system simulation as well as for testing new control algorithms. Further, to guarantee a well defined model behaviour in case of accuracy, parameterability and computational effort, a balanced relationship between all model components of interest has to be given.

In order to be able to handle the modelling process of a battery pack, to simulate and validate the system behaviour as well as test new vehicle strategies. A well defined battery cell model forms the foundation therefore. Nevertheless, before focus on the modelling process is given in the next chapter, requirements and functionality of a battery cell should be investigated in more detail. Thus, the first part of this chapter starts with the requirements and properties of battery based energy storage systems. Different demands on high power as well as high energy cases are presented and discussed. Following, various chemically based state of the art types of cells, which fit requirements best today and maybe in future, are compared and evaluated.

Because the outcome of this comparison shows that lithium-ion technology chemistries fulfil requirements best and are widely used in the field of automotive engineering, this type is investigated in more detail. After presenting different chemical compositions, focus on the basic physical process during charging and discharging inside the battery is given. This fundamental understanding of the functionality serves as a basis for the subsequent model evaluation and the development process.

The second part of the chapter focuses on the comparison of different literature based types of model structures. Where the main groups are subdivided into electrochemical models, followed by equivalent electric circuits and neuronal networks, or also named black box model approaches. Focus of the evaluation process is held on parameterability, accuracy and computational effort based on automotive applications.

In addition, one type of model approach is selected and serves as foundation for further investigations in this project. Finally, this chapter ends with a conclusion and a transition to the next two chapters.

## 2.1. Requirements and functionality of battery cells

Before detailed investigations of different types of battery model applications are presented in the second part of this chapter, focus on requirements and functionality of battery cells is given in this section. Therefore, requirements for electrical energy storage systems, including a preferred energy to weight ratio, are discussed first. Following, different state of the art chemical based type of batteries are presented and evaluated. It is shown that lithium-ion technologies are currently a suitable solution for a battery based electrochemical storage systems. Afterwards, different types of lithium-ion technologies are presented and the fundamental functionality of lithium-ion battery cell types explained.

### 2.1.1. Battery requirements versus cell types

Like in most technical approaches, different requirements are necessary, depending on the needed applications. Because for automotive operations a rechargeable battery is the only option. So called secondary cell types are used in all cases. This means in detail, long live cycles and minimum ageing effects are major goals for a cell anyhow.

Nevertheless, different requirements require different solutions. Like in usual car concepts, classifying in high power and efficiency applications is quite common. This means, for quite efficient system demands, cells with high energy density are preferred, while for power applications, like in upper class cars, high power density cells are preferable. Based on the use case, cell types with different discharge or charge rate, energy to weight ratios and further properties are needed. A summary on requirements for both, energy and power based battery cells, is presented in Table 2.1.

Table 2.1.: Requirements on battery based energy storage systems, adapted from [Wegleiter & Schweighofer, 2017]

| **Energy based type $\mathrel{\widehat{=}}$ low charge/discharge rate** |
| --- |
| - High number of operating hours |
| - Energy management oriented |
| - High energy efficiency |
| - High energy harvesting |
| - Essential SOC determination |
| => **Approx. 250 Wh/kg preferred** |

| **Power based type $\mathrel{\widehat{=}}$ high charge/discharge rate** |
| --- |
| - Short term energy storage behaviour |
| - High energy buffering possibility |
| - High thermal capability |
| => **Approx. 120 Wh/kg preferred** |

Based on the partition from Table 2.1, it is feasible that the type used, depends on the field of application. Nevertheless, in most automotive operations, energy based cells are preferred because of their better energy to weight ratio. Anyhow, by comparing state of the art cell types like lead-acid, nickel-metal, natrium-nickelchlorid and lithium-ion based on energy and power density, is clearly visible why lithium-ion technology is widely used in the field of automotive engineering, see Figure 2.1 adapted from [Wegleiter & Schweighofer, 2017]. Within the different available internal chemical compositions of lithium-ion types, a larger energy density as well as a higher discharge and charge level is possible.

Anyhow, in order to promote the steady growth of electrified vehicles, research on new battery technologies is still ongoing. In Figure 2.1 on the right side, two promising chemical compositions for generation IV battery technologies are presented, see [Wegleiter & Schweighofer, 2017] and [Lösche-ter Horst, 2015] for more details. Both lithium based types promise an increase in energy as well as suitable power density. Especially with the lithium-air technology, more than a quadrupling in energy density could be possible. Nevertheless, until this technologies are ready to market, a few challenges need to be solved, e.g. high self-discharge behaviour of the lithium-sulphur or the instability of electrolytes at lithium-air technologies are just a few examples, [Lösche-ter Horst, 2015].

In summary, there are still a few challenges to master in order to close the energy density gap between electrified and conventional vehicles with combustion engines. But like the increasing number of newly registered electrified vehicles, research is still ongoing. These days, lithium-ion technologies meet the requirements best and have also the prerequisites to further increase their potential. Therefore, different chemical based compositions including advantages and disadvantages are presented in the next subsection.
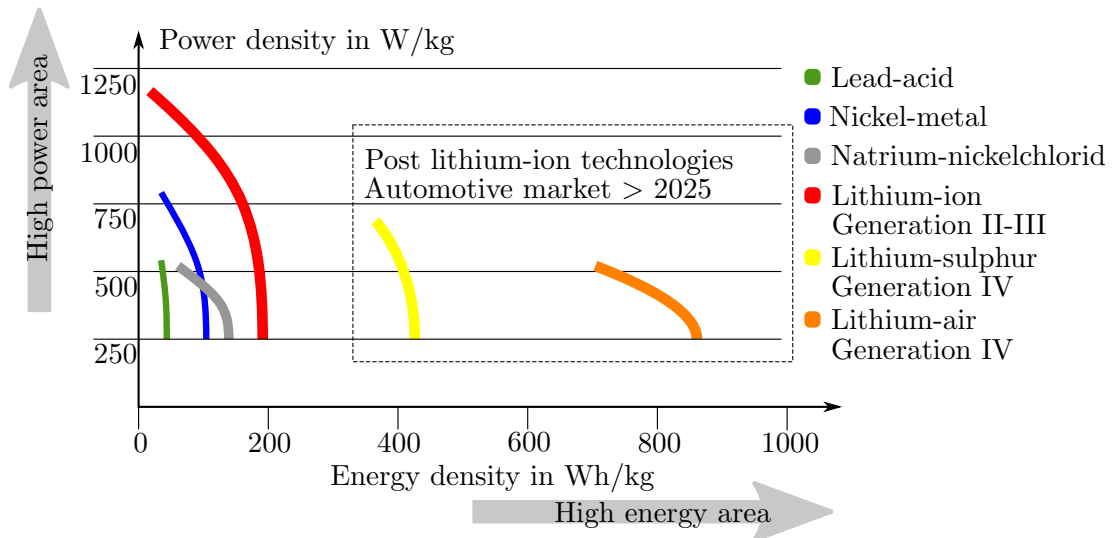


Figure 2.1.: Available battery technologies for vehicle applications based on the energy and power density, adapted from [Wegleiter & Schweighofer, 2017]

### 2.1.2. Lithium-ion technology - state of the art cell type for automotive applications

To guarantee the steady growth of electrified vehicles within the automotive market, battery cells have to fulfil a wide list of requirements. Therefore, the previous subsection has shown that main battery chemistry have changed from lead-acid to nickel-metal in the past, to lithium-ion technologies nowadays and will be go through new chemical compositions like lithium-sulphur or lithium-air in the future.

In addition to the expected high energy densities of future technologies, state of the art lithium-ion batteries already bring a lot of advantages. Besides the internal different chemical compositions to fulfil the wide range of needed energy and power density, further properties are presented and summarised in Table 2.2.

Table 2.2.: Advantages and disadvantages of lithium-ion battery cells, adapted from [Vetter, 2018] and [Batteryforum, 2019]

| | **Advantages** |
|---|---|
| + | Very high energy densities; about four times higher than lead-acid batteries |
| + | High cell voltage: up to $3.7\,V$ nominal power; a lithium-ion cell can replace three NiCd or NiMH cells that only deliver $1.2\,V$. Hence, high cell voltages mean that fewer cells and less connections between cells and electronics are needed to make high voltage batteries. This makes the battery lighter and less vulnerable |
| + | Can be optimised for specific capacity or performance requirements |
| + | Tolerate high discharge currents; can be discharged up to rates of $40\,C$. This allows automotive applications, such as cold starters or hybrid vehicle drives to be equipped with lower battery capacities |
| + | Batteries can be almost completely drained without affecting the cycle time, lifespan or high current output |
| + | Very low self-discharge rate; 3 to $5\,\%$ per month, can store electricity for up to ten years |
| + | Very high coulombic efficiency; discharge and charge capacity almost $100\,\%$ |
| + | Almost no memory effect; no refurbishment or complete unloading and loading necessary to maintain the life cycle |
| + | Variations in basic cell chemistry is possible; for example, the various anode and cathode materials allow refinement of performance characteristics to accommodate particular applications |
| + | Also very small battery sizes are available |

| | **Disadvantages** |
|---|---|
| − | Sensitivity to total discharge and overcharging |
| − | Relatively high sensitivity to high or low temperatures; the ideal operating temperature is between 10 and $35\,°C$. Especially at low temperatures below freezing, the performance of the lithium-ion battery drops sharply |

In summary, lithium-ion technologies are well suitable for portable applications like in automotive vehicles. Furthermore, properties presented in Table 2.2 can be rated based on combinations of anode and cathode materials depending on application cases. Therefore, detailed properties of major and widely used lithium-ion technologies are presented in the description below, based on [Wegleiter & Schweighofer, 2017], [Batteryforum, 2019] and [Battery University, 2019].

**Lithium-cobalt-oxide (LCO) LiCoO$_2$** This type of cell consists of a cobalt-oxide cathode and a graphite-carbon anode. The cathode has a layered structure and during discharge, lithium ions move from the anode to the cathode. LCOs ensure a high energy density but a relatively short number of life cycles and limited load capabilities. Furthermore, their cathodes are not as resistant to high temperatures like other types of lithium-ion cathodes and therefore, danger to burn when misused. For example, applying high voltages or damaging the cell can quickly cause the battery to melt or even burn. In this case, this type of cathode is not suitable especially for electric vehicles that require a particularly large number of cells. Another disadvantage is the limited capacity (specific power). In addition to this, they should not be charged or discharged with currents higher than 1 C-rate, as this may cause overheating as well.

In summary, LCO excels on high specific energy but offers only moderate performance power, safety and life span.

**Lithium-manganese-oxide (LMO) LiMn$_2$O$_4$** The architecture of LMOs forms a three dimensional spinel structure that improves ion flow on the electrode, this results in lower internal resistance and improved current handling for both, charging and discharging. Furthermore, the cathodes provide higher cell voltage than cobalt based materials. This leads to better overall performance especially at high outside temperatures and additionally to better thermal stability, which means enhanced safety. Disadvantages are named by energy density, which are quite lower than LCOs furthermore, number of cycles and lifespan is limited. LMOs are used for power applications, like medical instruments as well as hybrid and electric vehicles. Hence, LMO batteries are blended often with *lithium-nickel-manganese-cobalt-oxide* (NMC) to improve the specific energy and prolong the life span in automotive applications. Examples can be named such as *Nissan Leaf, Chevy Volt* and *BMW i3*.

In summary, LMOs have a sophisticated overall performance specially in energy and power, but offer improvements in performance, safety and life span. Nevertheless, often mix with NMCs is used to improve performance.

**Lithium-nickel-manganese-cobalt-oxide (NMC) LiNiMnCoO$_2$** Lithium-nickel cathodes offer a good compromise between overall electrochemical performance, high energy densities and costs. The specific energy density is higher than from lithium-manganese and lithium-cobalt. Furthermore, a higher discharge rate in comparison to LCOs is given as well. Advantages are given due to the combination of nickel and manganese. Nickel brings the high specific energy density into the material,

but is also responsible for a rather unstable electrode structure. Manganese, has the property of forming stable, so called spinel structures, and ensures low internal resistance. However, poor specific energy densities lead to be the disadvantage of this chemical combination. To create new cathode materials with even higher energy densities, introduce more nickel into the NMC material is tried as one opportunity.

In summary, NMCs have good overall performance and excels on specific energy. Furthermore, due to its low self-heating rate, this type of battery is often used for electrified vehicles.

**Lithium-iron-phosphate (LFP) LiFePO$_4$** Main feature of lithium-iron is given in better thermal and chemical stabilities than other lithium-ion cathode materials, what makes them very safe. Furthermore, they are fireproof in case of overcharge and more resistant in case of short circuit. In the case of misuse, this cathode material does not emit oxygen, does not burn and is accordingly insensitive to heat. In addition, lithium-iron phosphate cells also have a longer life span of 1000 up to 2500 cycles. However, they have a lower energy density than many other cathode materials such as NMCs or NCAs, due to their low rated voltage of 3.2 V. Another disadvantage is the higher self-discharge rate in comparison to other types. But LFP cathodes support higher voltages and correspondingly higher currents, which makes them suitable for use in fast-charge applications. In addition, cold temperature reduces performance of lithium-ion and this could affect the cranking ability in extreme cases.

In summary, LFPs have excellent safety and long lifespan properties but moderate specific energy and elevated self-discharge behaviour.

**Lithium-nickel-cobalt-aluminum-oxide (NCA) LiNiCoAlO$_2$** Lithium-nickel-cobalt-aluminum-oxide have been available as a cathode material since about 1999, at least for special applications. Like NMCs, they have a high specific energy density, good performance and long lifespan behaviour. Disadvantages are given in high costs and safety. Because of their properties they are widely used for automotive applications, for example Panasonic and Tesla.

In summary, NCAs have good overall performance and excels on specific energy. Furthermore, due to its low self-heating rate, this type of battery is quite common for electrified vehicles.

**Lithium-titanate (LTO) Li$_2$TiO$_3$** Lithium-titanate anodes provide a higher discharge and performance rate than graphite at different operating temperatures. Compared to graphite anodes, these are even more reliable because of their high potential and built-in overcharge protection as well as they have a long lifespan. However, LTO anodes tend to have a slightly lower energy density and are more expensive than graphite anodes. In addition, they are compatible with most cathodes and therefore often used in conjunction with manganese-based high voltage materials because of their high potential for lithium. LTOs have a rated voltage of about 2,4 V, and are able to handle fast charging discharged rates of about 10 C. LTOs

are a very safe material, have excellent discharge characteristics, especially at low temperatures. Furthermore, LTO electrodes still use 80 % of their capacity, which is much more than other materials.

In summary, LTOs excel in safety, low-temperature performance and lifespan. Efforts are being made to improve the specific energy and lower cost.

Finally, this description shows that a wide range of state of art applications is already available at the market and used for different use cases. Furthermore, by comparing and validating the presented types of lithium-ion technologies two major points were obvious. First, lithium-ion cell technologies are able to handle energy as well as power based applications, like already presented in Figure 2.1. This means they can be used for high energy as well as power application cases and furthermore combined as well. Second, no battery type is as diverse as lithium-ion batteries. This means, various chemical composition have different properties in kind of specific energy, specific power, safety, performance and life span. In summary, a defined type can be selected according to the requirements and availability. Figure 2.2 concludes the key features of discussed lithium-ion technologies graphically, based on safety, performance, lifespan, costs, specific energy and specific power.

**Types of lithium-ion battery cells**



Figure 2.2.: Property comparison of different types of lithium-ion battery cells, adapted from [Battery University, 2019]
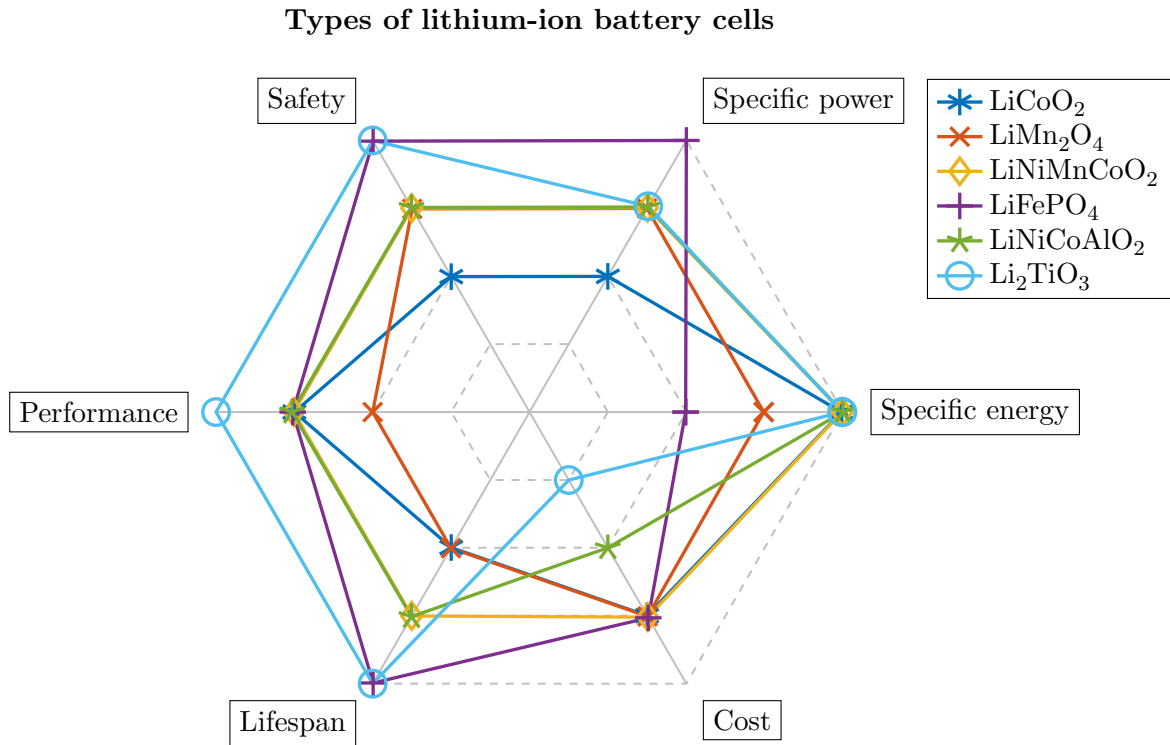
At this point, the battery requirements, technology roadmap and state of the art approaches were presented and discussed. It was shown, that various lithium-ion technologies are available and furthermore different types suitable for state of the art automotive applications. To evaluate and define a model approach which is able to handle almost all chemical types, a short basic overview about functionality of a lithium-ion cell will be presented in the next subsection. This functional knowledge should serve as basis to validate and evaluate different cell model approaches in Section 2.2.

### 2.1.3. Working principle of lithium-ion battery cells

The following subsection deals with the theoretic background of lithium-ion cells. The discussion only includes those aspects which are necessary for the modelling structure decision and process approach. This means, the design and working principle of lithium-ion cells. The theoretical background is referred to [Buller, 2003], [Kölbel, 2019], [Rahimzei et al., 2015] and [Wegleiter & Schweighofer, 2017].

Overall, each lithium-ion cell initially consists of two different electrodes, a negative electrode also named anode and a positive electrode also named cathode. These electrodes consist of a current arrester each and an active material applied to it. Between the two electrodes the ion-conducting electrolyte solution, which acts as a process mediator in the cell, and the separator, which ensures the electronic separation of the electrodes, are placed. For a schematic representation of a lithium-ion cell, see Figure 2.3.

The negative electrode of the cell consists of a copper foil and a layer of graphite or lithium alloy material. During charging, the positively charged lithium ions, required for power supply, are stored in it. Graphite anodes are currently the most common choice because they have a low electrode potential and low volume expansion when positively charged lithium ions $Li^+$ are stored. As mentioned above, lithium-titanate offers an interesting alternative for high performance and safety requirements particularly, but disadvantages include low energy densities and high costs. In general, the positive electrode of a lithium-ion cell consists of the described materials like lithium-cobalt-oxide $LiCoO_2$, lithium-manganese-oxide $LiMn_2O_4$, lithium-nickel-manganese-cobalt-oxide $LiNiCoAlO_2$ or a hybrid material comprised thereof.

During the chemical process, the electrolyte solution acts as a mediator between the reactions at the electrodes and guarantees the transport of lithium ions. Among other things, it must currently behave stably in a voltage range from 0 to 4.5 V and guarantee high conductivity over a wide temperature range from -40 °C to +80 °C. Therefore, non-aqueous solvents with high dielectric constants such as propylene or ethylene carbonate comprising lithium-containing salts, like $LiPF_6$, $LIBF_4$ or $LiClO_4$, are used. However, these electrolytes generally have very high viscosity. Thus, to increase ionic conductivity, in practical systems solvents with lower viscosity are mixed.
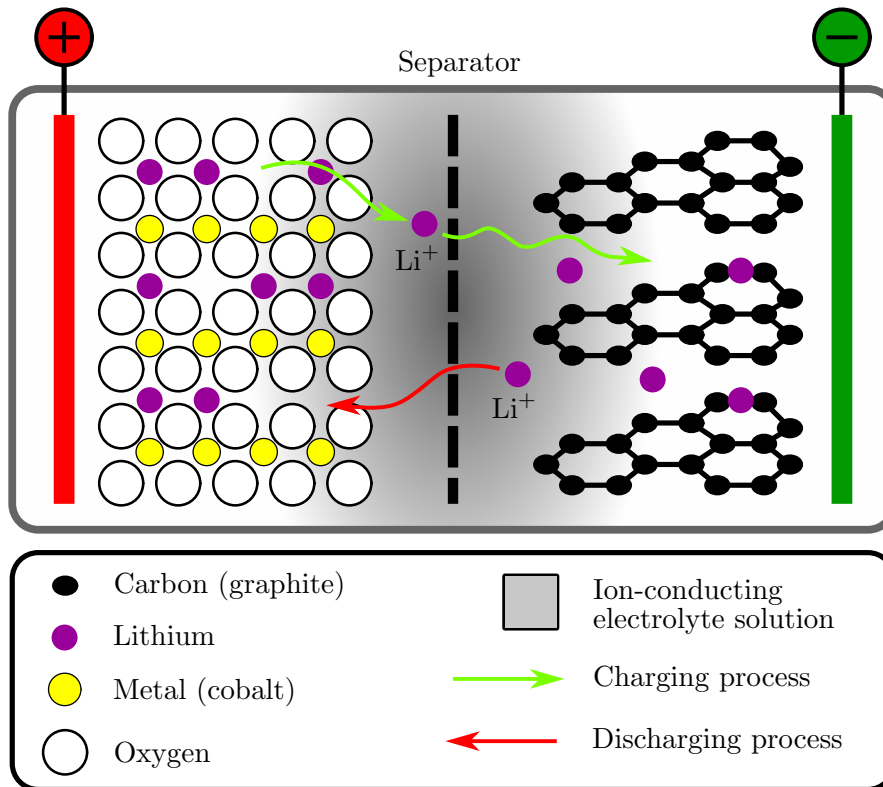
Figure 2.3.: Schematic representation and working principle of a lithium-ion cell, adapted from [Kölbel, 2019]

In suitable electrolyte solutions, a coating insulating electron forms on the anode the so-called *solid electrolyte interphase* (SEI), which protects the anode from the corrosive electrolyte solution and is permeable to lithium ions at the same time. This layer is essential for the use of lithium ion storage compounds in secondary cells. In this context, the positive electrode is rather referred to as a conductive interphase. The performance and ageing of a cell depends on the stability of the SEI. The charge and discharge processes increase the layer and thus the resistance in the cell. This is associated with a loss of lithium ions or cathode material and electrolyte and a corresponding reduction in cell voltage and charge quantity. To avoid this, an excess of electrolyte and cathode material is usually used in the cell.

The separator separates the two electrodes from each other to prevent a short circuit resulting from direct contact. Correspondingly high demands are placed on this component. In most cells, the separator prevents ions from moving further from the anode to the cathode in the event of a failure. The permeability for the ion flow is thus lost. However, the mechanical stability remains. This prevents overheating and subsequent firing of the cell. Polymer membranes are sometimes used as materials. However, these have the disadvantage that their low melting temperature (approx. 165 °C) compared to

ceramic separators makes them less reliable. The latter have more advantageous properties than separators due to their heat resistance. In addition, non-woven fabric and glass fiber separators are frequently used.

To explain the chemical working process depicted in Figure 2.3 and based on the mentioned components, the following equations describe the charging reaction of a battery consisting of a lithium-cobalt-oxide cathode and a carbon anode during discharging:

$$\text{Negative electrode:} \quad \text{Li}_x\,\text{C}_n \longrightarrow n\,\text{C} + x\,\text{Li}^+ + x\,\text{e}^- \tag{2.1}$$

$$\text{Positive electrode:} \quad \text{Li}_{1-x}\,\text{Mn}_2\text{O}_4 + x\,\text{Li}^+ + x\,\text{e}^- \longrightarrow \text{LiMn}_2\text{O}_4 \tag{2.2}$$

$$\text{Cell reaction:} \quad \text{Li}_{1-x}\,\text{Mn}_2\text{O}_4 + \text{Li}_x\,\text{C}_n \longrightarrow \text{LiMn}_2\text{O}_4 + n\,\text{C} \tag{2.3}$$
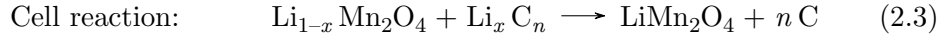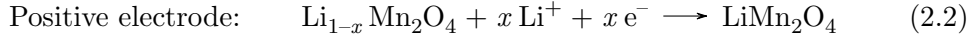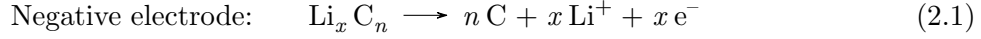
The Equations (2.1) to (2.3) indicate that the cell reaction is the migration of lithium ions between positive and negative electrodes. In detail, during discharging lithium ions are removing from the anode and are intercalating into the cathode due to the electrolyte. At the same time, the same number of electrons moving via the external circuit by generating a current flow from the anode to the cathode. This external electron flow is necessary to balance the lithium ion flow during charging and discharging, to keep the electrodes electrical neutral. While charging, this process runs vice versa.

Nevertheless, since the lithium is not ionised at the negative electrode, it would be optimal to construct the negative electrode from lithium metal. However, this is problematic in practice. Due to the formation of the top layer, lithium is not deposited as a compact metal but dendritically. This finely distributed lithium sponge is highly reactive. In addition, dendrites can perforate the separator, grow through to the positive electrode and thus short-circuit the cell. Therefore, the relatively small lithium atoms are embedded in a different substance, usually graphite, where they are intercalated between the graphite planes. While this chemical process is called intercalation by $\text{Li}_x\,n\,\text{C}$ reaction. The main goal of this intercalation is the generation of a protective layer on the negative electrode, which is permeable for the small $\text{Li}^+$ ions but impermeable for the solvent molecules. If the top layer is insufficiently formed, $\text{Li}^+$ ions are interacting with the solvent molecules and irreversibly destroying the graphite electrode.

Finally, the presented overview about the theoretical background, including investigations into main components as well as the reaction process of a lithium-ion cell, shows two main facts. First, chemical charge and discharge progress of lithium-ion cell including elaborate reaction where focus on save and efficient processes has to be spend. As a second fact, already by discussing this short overview, major information about the modelling process can be defined:

**Voltage versus state of charge** Major part of the cell modelling is characterised by knowing an accurate state of the reaction between full and empty cell. Based on most use cases this means knowing the current voltage over the state of charge level. Anyhow, this part is mostly split into a steady-state component, *open circuit voltage* (OCV) versus *state of charge* (SOC), and a dynamic modelling part

**Internal resistance** The mentioned chemical reaction as well as the electrons moving process via external circuit, generating losses which should be taken into account within the modelling process

**Double layer capacitance** Based on the different layers of the electrodes and the separator a capacitive behaviour is assumed in some case

**Passivation film** If a passivation film exists, this so-called solid/electrolyte interface (EIS) is observed as a high-frequency semi-circle in the impedance spectrum, [Buller, 2003]

**Diffusion process** Based on chemical processes, a diffusion process will be expected in a certain way

In summary, based on the theoretical background of the investigated cell technology, a listing of expected reaction and processes was possible. These mentioned physical and chemical effects should be implemented into a battery model which is able to handle these effects under different environmental conditions. Therefore, a comparison of various literature based model approaches is presented and evaluated in the next Section 2.2.

## 2.2. Battery cell model approaches for automotive application

Based on Section 2.1 which described the requirements and functionality of battery cells, the state of the art cell types and the working principle of lithium-ion batteries, this section focuses on different cell modelling approaches for automotive application. Goal of this part is to evaluate widespread used model approaches based on the properties and information gained in the previous sections. Therefore, three widely applied types of model applications are found based on a literature study and investigated in detail:

1. Electrochemical models

2. Equivalent electric circuit modelling

3. Neuronal networks and black-box models

In this context, information based on the literature listed in Table 2.3 is used and referenced for detail information. Note that in some literature mathematical models are count as a separate group. Because these relate to chemical equations in most approaches, no separate subdivision is used in this thesis.

### 2.2.1. Electrochemical models

Modelling the battery cell behaviour as electrochemical system by furthermore using physics-based equations is defined as the most obvious method. *Electrochemical* (ECH) battery models can provide full information on the internal electrochemical dynamics of

the battery by consisting a set of coupled *partial differential equation*s (PDEs). These equations explain how the cell's potential is produced and affected by the electrochemical reaction, which are taking place inside the cell. As an example, Fick's law of diffusion to describe solid concentrations at each electrode and electrolyte concentration, or Ohm's law to calculate potential of electrolyte and electrode can be named at this point.

Hence, as electrochemical cell models describe key behaviours of battery at the microscopic scale, based on the chemical reactions occurring inside the battery. This type is the most accurate among the group of battery models. For this reason, this type can be used to complement experimental data for evaluation of other models or allowing virtual measurements of quantities that cannot be measured in practice. A further advantage is named with the possibility to model the cell behaviour arbitrarily accurate by using detailed PDEs. Nevertheless, using a higher modelling order can increase the overall model accuracy but also leads to the main disadvantage, namely the computation effort and is therefore not directly applicable to our intended automotive engineering application.

Table 2.3.: Battery cell model approaches - literature overview

| Model principles | Abbreviation | Source |
|---|---|---|
| Electrochemical models | ECH | [Amiribavandpour et al., 2013] [Ashwin et al., 2017] [Han et al., 2015a] [Han et al., 2015b] [Smith et al., 2010] [Sung et al., 2016] [Sung & Shin, 2015] |
| Equivalent electric circuit modelling | EC | [Andre et al., 2011a] [Andre et al., 2011b] [Buller, 2003] [Huang & Chow, 2016] [Farmann & Sauer, 2018] [Jiang et al., 2017] [Karden et al., 2000] [Kollmeyer et al., 2017] [Mousavi G. & Nikdel, 2014] [Westerhoff et al., 2016] |
| Neuronal networks & black-box systems | NN & BX | [Chemali et al., 2018] [He et al., 2014] [Hussein, 2019] [Tao et al., 2017] [Yang et al., 2017] |

Nonetheless, also in types of electrochemical model approaches simplifications, defined as order reduction, are common in the literature, see for example [Han et al., 2015a], [Han et al., 2015b] or [Smith et al., 2010]. In detail, by way of an example, [Smith et al., 2010] demonstrates a simple schematic of a lithium-ion cell containing different parts which are negative and positive electrodes, electrolyte, separator and current collectors. Based on a coordinate direction from the negative to the positive electrode, see Figure 2.3, the one dimensional electrochemical model consists of four PDEs. These equations describing the conservation of lithium in the solid phase (written for a spherical active material particle with reaction current $j^{\mathrm{Li}}$ from the surface) by

$$\frac{\partial c_s}{\partial t} = \frac{D_s}{r^2} \frac{\partial}{\partial r} \left( r^2 \frac{\partial c_s}{\partial r} \right) \quad \text{with} \quad D_s \left. \frac{\partial c_s}{\partial r} \right|_{r=R_s} = \frac{-j^{\mathrm{Li}}}{a_s\,F}\,, \tag{2.4}$$

conservation of lithium in the electrolyte phase by

$$\frac{\partial\,(\epsilon_e\,c_e)}{\partial t} = \frac{\partial}{\partial x} \left( D_e \frac{\partial}{\partial x} c_e \right) + \frac{1 - t^0}{F} j^{\mathrm{Li}} \quad \text{with} \quad \left. \frac{\partial c_e}{\partial x} \right|_{x=0} = \left. \frac{\partial c_e}{\partial x} \right|_{x=L} = 0\,, \tag{2.5}$$

conservation of charge $e^-$ in the solid phase (active material particle/binder matrix) by

$$\frac{\partial}{\partial x} \left( \sigma \frac{\partial}{\partial x} \phi_s \right) - j^{\mathrm{Li}} = 0 \quad \text{with} \quad \left. \sigma \frac{\partial \phi_s}{\partial x} \right|_{x=0} = \left. \sigma \frac{\partial \phi_s}{\partial x} \right|_{x=L} = \frac{I(t)}{A} \tag{2.6}$$

and conservation of charge in the electrolyte phase

$$\frac{\partial}{\partial x} \left( \kappa \frac{\partial}{\partial x} \phi_e \right) + \frac{\partial}{\partial x} \left( \kappa_D \frac{\partial \ln(c_e)}{\partial x} \right) + j^{\mathrm{Li}} = 0 \quad \text{with} \quad \left. \frac{\partial \phi_e}{\partial x} \right|_{x=0} = \left. \frac{\partial \phi_e}{\partial x} \right|_{x=L} = 0\,, \tag{2.7}$$

where the state variable defined as coordinate direction $x$, particle radius $r$ and the time $t$. Based on the constant values reference is given to [Smith et al., 2010]. In addition, Equations (2.4) to (2.7) are coupled by the *Buttler Volmer* (BV) equation describing the reaction current at the solid/electrolyte interface. In addition to the chemical description, thermal equations can also be coupled to electrochemical equation. In [Amiribavandpour et al., 2013] for example, a thermal-electrochemical model is developed for a lithium-ion battery pack.

Hence, already with this simple example the complexity of such electrochemical models is recognisable. This means in detail, models of this type can be very accurate and be used for application cases where detailed information of the chemical process is needed. By contrast, models of this complexity can only be solved using powerful computational tools and methods as *Compuational Fluid Dynamics* (CFD) frameworks. In summary, based on the automotive requirements, these models can only be used within limited extent, see for example [Sung & Shin, 2015], [Sung et al., 2016].

### 2.2.2. Equivalent electric circuit modelling

Because of the complexity of the electrochemical models as well as the limitation of computational power in the past, a further approach, so called *equivalent electric circuit* (EC) modelling, has become quite common nowadays. Because it is necessary for many applications to find a balance between model accuracy, computational effort and parameterability, for example for integration in microprocessors, this type of model has become quite important for real time application as they are used in online automotive applications.

To describe the behaviour of a battery cell, the EC models are constructed by putting resistors, capacitors, inductivities and OCV in an electric model circuit, see for example [Andre et al., 2011a], [Andre et al., 2011b] or [Jiang et al., 2017]. Depending on the model requirements, the circuit contains a number of different elements, as seen for example in Figure 2.4. The simplest form, called *internal resistance model*, consists of an ideal voltage source OCV, which is dependent on the SOC level, and a resistance $R_0$, see Figure 2.4 a.). Within this approach as well as for further extensions, the battery terminal voltage is defined with $U_a$ and the load current with $I_a$.

A first extension is given by adding one RC-network to the internal resistance model, see Figure 2.4 b.) and named *Thevenin model* in the literature, [Huang & Chow, 2016]. This can increase the accuracy by considering the charge transfer characteristics of the model approach by adding an equivalent resistance $R_{ct}$ and the double layer capacity $C_{dl}$ respectively. Hence, by adding more RC-networks to the battery model, an increase in accuracy is possible but also leads to higher computational effort.
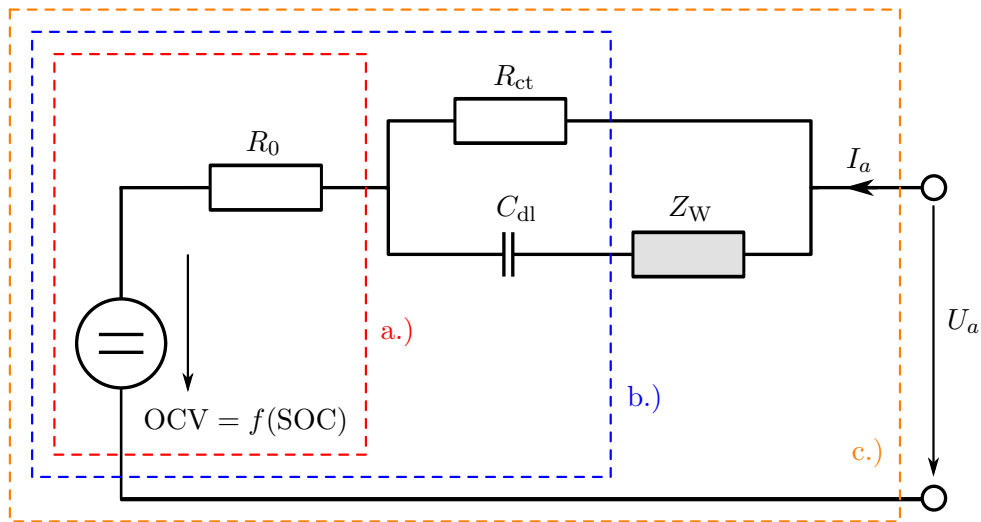


Figure 2.4.: Equivalent electric circuit model applications, based on application requirements; with increasing complexity, following models are shown: a.) *internal resistance model*, b.) *Thevenin model* and c.) *Randles circuit*

A further model extension brings the implementation of the diffusion process by adding a Warburg impedance $Z_W$, see Figure 2.4 c.) and named *Randles circuit* based on [Randles, 1947]. With this extension the model is able to handle very smooth diffusion processes within low frequency ranges.

Nevertheless, as for electrochemical models, a trade-off between model accuracy, computational effort and parameterability has to be solved, dependent on the profile of requirements. Therefore, a wide range of different equivalent electric circuit models within various levels of complexity are already on the market and compared based on different use cases, see for example [Farmann & Sauer, 2018], [Mousavi G. & Nikdel, 2014] or [Kollmeyer et al., 2017]. This means in detail that a model definition has to be defined based on the problem to solve.

A further property which should be named when discussing about EC modelling is the parameterisation process. This means in detail that two methods are quite common on the market. The first one is based on pulse charge and discharge manoeuvres, see for example [Schweighofer et al., 2012], [Schweighofer et al., 2013]. The advantage of this method is the clear definition of the manoeuvre which leads to an easy parameterisation process. In most cases the model parameters are defined by minimising the error between simulation and measurement data with an optimisation tool. The main disadvantage of pulse manoeuvres is that only a small frequency spectrum can be used for the parameterisation process. In addition, this spectrum is depending on the sample ratio of the measurement equipment.

The second method uses an *electrical impedance spectroscopy* (EIS) to parameterise the model parameters, see for example [Karden et al., 2000] or [Westerhoff et al., 2016]. Within this method, an expression for the equivalent impedance of the circuit model is obtained in the frequency domain theoretically. Then, related to measurement data, the electrochemical impedance is the response of a system to an applied potential. Therefore, an *alternating current* (AC) is practised to the system and the voltage is measured in order to calculate the impedance at that frequency. During this manoeuvre the frequency varies slowly from very small to large values and the impedance spectrum can be calculated and plotted as a function of the frequency. Within this plot the parameterisation process can be done from the technical point of view by comparing the simulated and measured characteristics, but also using an optimisation tool. This process can be repeated within different SOC and/or temperature conditions. This brings the advantage that all network parameters can be defined within a wide range of frequency as well as under SOC and/or temperature conditions. Nevertheless, this measuring procedure requires special measurement equipment. That fact, as well as the more complicated parameterisation process, is the disadvantage of parameterising the model by EIS data.

In summary, EC modelling has become a common method to model the cell behaviour during these days. The main advantage brings the accuracy to computational effort ratio and the model parameters with physical meaning. Both possibilities to parameterise the model bring some drawbacks each, but the flexibility for the parameterisation process can count as an advantage.

### 2.2.3. Neuronal networks and black-box models

The third method which is quite common to model the cell behaviour is based on *neuronal network*s (NNs), or also named as black-box models. While this approach has become quite famous, especially during the last years, the goal is to describe a system behaviour with biological neuronal networks in a highly simplified way. Anyhow, describing and modelling of system behaviour based on NNs definitely did not start with battery modelling, it rather has a long history already. In the early 1943 first investigations were done by [McCulloch & Pitts, 1943], to understand how the brain could produce highly complex pattern by using many basic cells which are connected together and named as the well-known neurons. This concept of connecting neurons served as foundation to the development of artificial NNs.

Based on these investigations, next major development in NNs was the concept of a perceptron which was introduced by *Frank Rosenblatt* in 1958. As the name suggests, a perceptron was intended to be a pattern recognition device, and the association units correspond to feature or pattern detectors. Thus, this shows that similar inputs should be able to reproduce identical outputs again. The next milestone for NNs was given by [Rumelhart & McClelland, 1987] which presented a back propagation method to train a pre-defined NNs based on data. Because of these theoretical foundations and the fact that computational effort has became cheaper during the last years, the usage of NNs is becoming more and more popular in a wide field of technical application.

Due to the fact that large neural networks can be used for a wide range of applications, they are also very popular in the field of automotive industry, like estimating the SOC or *state of health* (SOH) of a battery cell, see for example [Chemali et al., 2018], [He et al., 2014] or [Yang et al., 2017]. For a better fundamental understanding, an overview about the functionality of NN based on SOC calculation is given as next step based on the schematic representation in Figure 2.5.
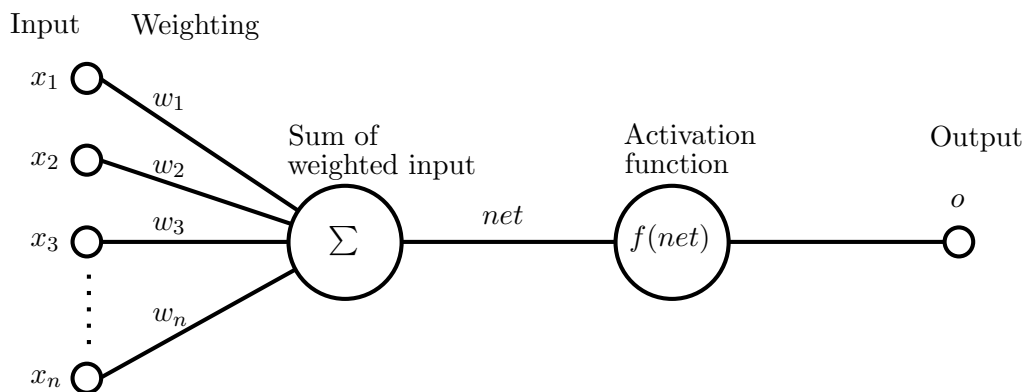


Figure 2.5.: Schematic representation of an artificial neuronal network, based on [Frölich, 2006]

Goal of the NN schematic is do define the SOC as output $o$, depending on various inputs $x_1 \ldots x_n$. Inputs which are needed to calculate the SOC for the next time step $t_{i+1} = t_i + \Delta t$ could be the C-rate (discharge or charge current), overall health situations of the cell but as well as the SOC state at the present time step $t_i$ via a feedback loop. Because, various input parameters influencing the output in a different way, these values are weighted with weighting factors $w_1 \ldots w_n$. Using the scaled input parameters, all effects which are influencing the SOC were added to a sum factor *net* and the output calculated via activation function by $o = f(net)$. By adding more layers, one after the other, more accurate results are possible, but also more weighting parameters are needed. Using measurement data to find or optimise the best factors $w_i$ so that real and simulated SOC delivers the smallest deviation is named as training the NN.

In summary, a larger NN with a lot of neuron and layers brings the possibility for a very accurate model description. As the literature presented above, already a lot of research based on SOC and SOH estimation was published during the last years. Furthermore, also results to model the overall power behaviour of a cell in a very accurate way seems also be possible already, see [Hussein, 2019]. Nevertheless, using NN needs a lot of computational effort and time, which equally means costs, to train the network. Furthermore, proving the correctness and stability of the NN model approach seems to be a technical challenge.

### 2.2.4. Comparative conclusion of the investigated model approaches

In the last subsections, three different types of models to mathematically describe a battery cell behaviour were presented and evaluated. The first type was named electrochemical models where the cell characteristic is described by electrochemical partial differential equations. These equations explain how the cell's potential is produced and affected by the electrochemical reactions. This property makes this method as the most obvious one because direct influence on chemical behaviour is given. Furthermore, very detailed and accurate characteristics can be modelled and simulated. Nevertheless, the possibilities that PDEs bring with, also lead to the main disadvantage. For this model type high computational effort is needed to solve the equations but as well as to parameterise the model.

The second model presented is based on equivalent electric circuit and has become quite common during these days. Within this method the behaviour of a battery cell is constructed by putting resistors, capacitors, inductivities and the OCV in an electric model circuit. Model accuracy can be influenced by adding more elements based on the problem requirements. This simplified model structure brings the disadvantage that physical effects can only be modelled within a certain accuracy. Nevertheless, this type of model approach is defined as very user friendly, where a skilled engineer with physical background is able to understand the basic behaviour. Furthermore, computational effort is low and parameterability is given from the technical point of view.

The third method presented, describes the cell behaviour based on neuronal network or black-box systems. Goal of this approach is to use biological oriented neuronal networks in a highly simplified way. This brings the advantage that existing model structures, already evaluated in a wide technical field, can be used for modelling the cell behaviour. This means in detail, more or less complex model structures with different numbers of layers can be used with focus on the accuracy and complexity needed, based on the problem requirements. Anyhow, to parameterise the weighting factors, or other named train the NN, a lot of measurement data are needed. This makes the whole parameterisation process very time and cost consuming. In addition, large NN have very complex structures and parameters which do not have physical meaning, this means only experts are able to understand properties and behaviour in detail.

This summary shows again that all methods could be used for modelling the cell behaviour in a certain way. But also all three methods have advantages and disadvantages. Before a final decision is presented which type of model is used for further project investigations, a short description about major requirements in automotive industry, based on [Schweighofer et al., 2013], is presented.

In summary a battery model has to be found which fulfils the following requirements:

- The overall battery cell model should be easy to use and practical to parametrise

- A high model accuracy versus a low model complexity is sought; keyword: Monte-Carlos analysis

- A precise description of current and voltage behaviour on various SOC states and various C-rates is needed

- Able to integrate the model into hardware; real-time capability is necessary

- All major parameter affecting the behaviour of the battery should be able to taken into account; state of charge, cell temperature and charge/discharge current

- Long term effects like ageing is neglected in this project but should be taken into account for further investigations

Finally, by comparing the properties of the type of models with the requirements presented above, the decision was made to use **equivalent electric circuit** for further investigations. The most decisive point for this decision were the usage and parameterability from the technical point of view, as well as the accuracy due computational effort ratio.

## 2.3. Comparative conclusion on battery cell modelling

The introduction from Chapter 1 has shown that modelling and simulation has become an important tool to reduce time and save cost in the development process in automotive engineering. Based on the goal to reduce greenhouse gases the trend goes towards electrified and electric vehicles. Thus, the increasing demands on electrified and electric drivetrain models, is the result of these two factors. Taking this one step further, increasing interest on battery and cell modelling is given during these days. Nevertheless, before the modelling process starts, focus has to be held on system understanding.

Therefore, this chapter has dealt with the requirements and functionalities of battery cells, as fundamental knowledge for the modelling process, in the first part. Based on the power and energy density needed for automotive cell applications, lithium-ion technologies have proven to be a good choice during these days. Based on this result, deeper focus on advantages and disadvantages of lithium-ion technologies including their different chemical compositions was given. It was presented that already a lot of types of these technologies are available on the market. Based on the system requirement, different types can be used for various applications.

Based on a fundamental functionality presentation of a lithium-ion cell, first information about modelling cell effects were gained as introduction to the second part of the chapter. Within this part, three common battery cell model applications were presented, based on a literature study. Detailed focus was spent on electrochemical models, equivalent electric circuit modelling and neuronal networks. It was discussed that electrochemical models and neuronal networks bring the possibility to model cell behaviour in a quite accurate way. But while electrochemical models need a lot of computational effort due to the PDEs, neuronal networks need a lot of measurement date for training the model. Therefore, the decision was made to focus on **equivalent electric circuit** modelling within this project because this type brings the best overall accuracy to computational effort and parameterability ratio.

Based on this decision, the next two chapters deal with the modelling and parameterisation process of an equivalent electric circuit model approach based on automotive requirements. Thus, focus on steady-state open circuit voltage versus state of charge modelling, including the needed measurement equipment, is part of Chapter 3. Following, Chapter 4 deals with modelling and parameterising the transient cell behaviour, including an overall validation process using wide range of measurement data.

# 3

# Open circuit voltage as basis for equivalent electric circuit based cell modelling

In the comparative conclusion of Chapter 2, it was shown that cell modelling based on *equivalent electric circuit*s (ECs) is a sophisticated possibility to describe the cell behaviour in a technical way. Within this method, modelling the current cell voltage dependent on *state of charge* (SOC), discharge or charge rate (C-rate) as well as the temperature, is defined as the main overall goal. To achieve this goal, a separation into two modelling parts is used in nearly all literature based approaches. For this reason, explaining and discussing the fundamentals behind this deliberation, is the goal of the first part of this chapter. It will be demonstrated that the subdivision into a steady-state part and a transient part turns out to be a good choice. In this case, the steady-state part is implemented as *open circuit voltage* (OCV) versus the *state of charge* (SOC) by using a lookup table or mathematical description. Meanwhile, the transient part describes the changes in charge or discharge current and temperatures.

After defining the subdivision strategy including the modelling process, the test equipment as well as the test cell for further practical realisation is presented. Hence, key facts and boundary conditions are given, based on the information from the data sheet.

The second part of the chapter deals with the determination of the before mentioned model part, by generating the OCV versus SOC characteristics. Nevertheless, this SOC dependent behaviour can only be generated by charging or discharging the battery. This means further, that transient effects occur. Thus, measuring an ideal OCV versus SOC characteristics without transient effects is only possible theoretically. Thus, to minimising this dynamic influences by using a practical duration of measurement time, two different methods have become very popular nowadays. The first one uses very small charge and discharge currents, while the second one uses pulse manoeuvres including pauses for bringing the cell back to the equilibrium state.

Hence, within both approaches accuracy can be increased by increasing the overall measurement time. Thus, the question arises, what is the best trade of between accuracy and measurement time, which equally means costs. Nevertheless, goal of this chapter is to compare both methods and give a final statement based on practical usage. Finally, the generated OCV versus SOC characteristics is defined and serves as foundation for the transient circuit in Chapter 4.

## 3.1. Basic considerations on the voltage potential of a battery cell

Before the second part of the chapter focuses on OCV versus SOC characteristics generation, basic considerations on the voltage potential of a battery cell is presented. Thus, the working principles of a lithium-ion cell from Section 2.1, presented in Figure 2.3, serves as basis for these considerations. As already explained, lithium ions as well as electrons moving from one to the other electrode as soon as an external load is applied or the battery is charged.

Nevertheless, to know how many ions are currently located at the anode respectively at the cathode the parameter SOC is defined. If all ions are located at the anode, the SOC is defined by SOC = 100 % and the battery cell is fully charged. Vice versa, if all ions are located at the cathode, the battery cell is empty and the SOC is defined with SOC = 0 %. Thus, the current state can be determined mathematically, based on [Weber, 2018], by

$$\text{SOC} = \frac{Q}{Q^{\text{N}}} \cdot 100\,\% \,, \tag{3.1}$$

where $Q$ describes the current electric charge at the anode and $Q^{\text{N}}$ the overall electric cell charge in coulomb. Thereby, a coulomb is defined by the electric charge, transported through the cross-section of a wire by an electric current of 1 ampere for 1 second. Note that an alternative form can be defined by using the same data with the *depth of discharge* (DOD), which is the inverse of the SOC.

Beside the SOC state from Equation (3.1), the OCV is also defined by considering the electric potential of the anode $\Phi_{\text{a}}$ and cathode $\Phi_{\text{c}}$ by

$$\text{OCV} = \Phi_{\text{c}} - \Phi_{\text{a}} \,. \tag{3.2}$$

However, both potentials show a strong dependency based on the number of ions located on the electrodes, which equally means that both are SOC dependent. Furthermore, for both electrodes, anode and cathode, potential behaviour strongly changes by using a different material, see Figure 3.1 on the left and right side. In summary, because a lot of material compositions are used for different fields of applications, remember Figure 2.2, the OCV versus SOC characteristic is given by a strongly non-linear behaviour, depending on the chemical components of the electrodes.

The merged representation of the OCV versus SOC behaviour is given in the middle of Figure 3.1, whereby the non-linearity is clearly visible. Since the implementation of an accurate open circuit voltage is essential for a sophisticated overall model behaviour, this characteristic is directly implemented as a lookup table in nearly all model applications. Also fitting the measured data by a polynomial higher order seems possible but not recommended, due to the high accuracy needed at this point.
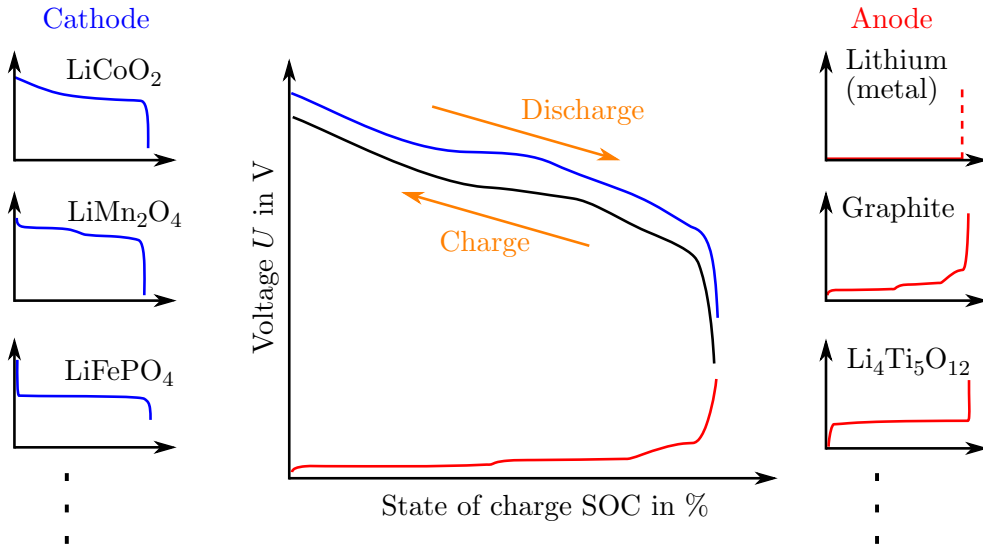
Figure 3.1.: Schematic representation of the open circuit voltage versus state of charge characteristic, generated by the potential differences from the cathode and anode, based on the electrode material, adapted from [Weber, 2018]

Hence, to generate the OCV versus SOC characteristic based on measurement data, charging and discharging the battery cell in some way is unavoidable. This leads to transport processes and lossy reactions inside the cell, which influence the cell output voltage. This means that under load the battery voltage drops from the OCV to a working, or so called output, voltage $U_a$ of the cell. This difference $OCV - U_a$ is called load voltage and is caused by internal loss processes. In the case of a load, this load voltage ensures that the final discharge voltage $U_{min}$ is reached earlier, and leads to a reduction in discharge capacity in addition.

By describing this process from an equivalent circuit point of view, losses generated during charging and discharging the cell, are summarised in a impedance $Z_a$ and related to the charge or discharge current, see Figure 3.2. In this way, the output voltage $U_a$ can be mathematically calculated with

$$U_a(I_a) = \text{OCV} - \sum_k U_{l,k} = \text{OCV} - I_a \cdot Z_a \,, \tag{3.3}$$

where $U_{l,k}$ defines the different losses during the charging or discharging process under current $I_a$ and is summarised in the resistance $Z_a$. This contemplation leads once again to the point that using an EC, seems to be a sophisticated possibility to model the behaviour of a battery cell.
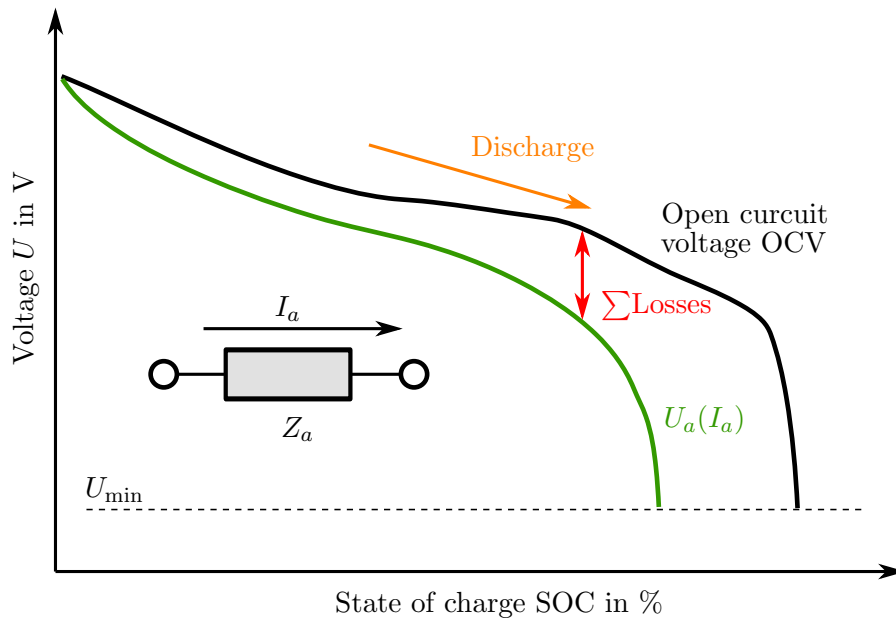
Figure 3.2.: Generated output voltage $U_a$ of a battery cell, composed out of the *open circuit voltage* (OCV) and the sum of the losses $\sum_k U_{l,k}$ during charging and discharging, adapted from [Weber, 2018]

In summary, the SOC dependent OCV characteristic forms the foundation for modelling the cell behaviour, based on an EC. In addition, internal losses occurring during added load or charging the cell, can be modelled by electric elements which are summarised into a resistance respectively into a complex impedance. Furthermore, these electric components change their behaviour dependent on the SOC, current rate and cell temperature in addition. Thus, to guarantee an accurate model behaviour, this behaviour should be implemented as well.

This consideration summarised Figure 3.2, confirm the idea to split the battery modelling process in two main parts. First, generating an accurate OCV characteristic, which is the final goal of this chapter. Second, find an EC, which is able to model the transient cell behaviour as well as handle various SOC, C-rate and temperature changes. This second part, as well as an experimental validation and evaluation process of the combined overall model is presented in Chapter 4.

Nevertheless, before measurements can be done to model, parameterise and validate a cell model, measurement equipment including a test cell is needed. Therefore, an overview about the used components is given in the next Section 3.2.

## 3.2. Measurement setup and cell information

After defining the modelling strategy by dividing it into a first part, with focus on the OCV versus SOC characteristic and a second part, with focus on the transient electric circuit, measurement equipment is needed to be able to handle both of it. Therefore, measurements were done at the Institute of Electric Measurement and Measurement Signal Processing at Graz University of Technology.

The test setup, presented in Figure 3.3, consists of a real-time system, running at a sample frequency up to $f_s = 5\,\text{kHz}$ which is sufficient for most applications. The used power amplifier is able to provide up to $20\,\text{A}$ charge and discharge current. With an *analog to digital converter* (ADC) the resulting battery voltage and current is fed back to the controlling system. To perform different temperatures, the cell is located in a temperature controlled environment. During this project, two different temperatures $T_1 = 40\,^\circ\text{C}$ and $T_2 = 0\,^\circ\text{C}$ were used, but can be arbitrarily expandable.
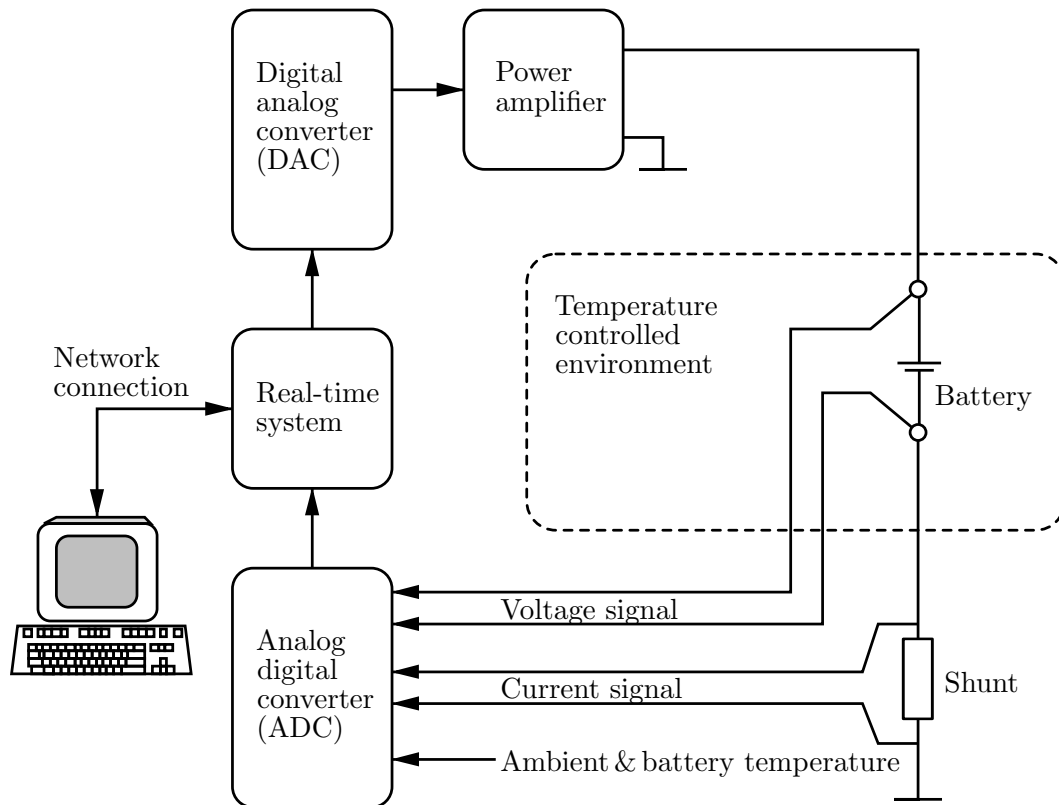


Figure 3.3.: Block diagram of the used measurement setup, including a network connection to a personal computer which logs and saves the generated data as well as a temperature controlled environment for investigations within different temperatures, adapted from [Schweighofer et al., 2012]

The investigated cell is a cylindrical 3500 mAh LiNiCoAlO$_2$ from Samsung type INR18650-35E (Pink), with a nominal voltage of $U_\mathrm{N} = 3.6$ V and a minimum discharge voltage of $U_{min} = 2.65$ V, see [Samsung INR18650-35E, 2019]. Major key facts are summarised in Table 3.1. Note that investigations were done with two different numbers of the same type of cell. Because just very small deviations were realised, only results from one cell are presented in this thesis.

Finally, after defining the model strategy and presenting the used test bench setup as well as the test cell, focus on generating the OCV versus the SOC is presented in the second part of this chapter.

Table 3.1.: Official battery cell specifications of the used test cell of type Samsung INR18650-35E (Pink); source: [Samsung INR18650-35E, 2019]

| Specification | Value | Unit |
| --- | --- | --- |
| Nominal capacity | 3500 | mAh |
| Minimum capacity | 3350 | mAh |
| Nominal voltage | 3.6 - 3.7 | V |
| Charging voltage | 4.2 | V |
| Discharge current | 8 | A |
| Maximum discharge current | 13 | A |
| Charge current | 0.6 | C |
| Discharge minimum voltage | 2.65 | V |
| Pluspol | FlatTop | - |
| Chemistry | LiNiCoAlO$_2$ | - |
| Diameter | $18.55 \pm 0.1$ | mm |
| Height | $65.25 \pm 0.15$ | mm |
| Weight | $48 \pm 1$ | g |

## 3.3. Generation of the open circuit voltage based on the state of charge

While the parameterisation strategy as well as the test bench setup was presented in the Sections 3.1 and 3.2, the third part of the chapter focuses on generating the OCV versus SOC characteristic. Because this behaviour deals as foundation for the overall model concept, a well accurate model behaviour is desired. This means further, an inaccuracy within the OCV model, directly leads to inaccuracies in the overall battery model.

Hence, to define a strategy to generate OCV versus SOC characteristic, the two plots in Figure 3.1 and Figure 3.2 as well as Equation (3.3) form the basis for the OCV generation. Therefore, two major statements can already be named out of the presented fundamentals from Section 3.1. First, by considering Figure 3.1, the behaviour does not depend on the charge direction but on the charge state respectively. This means that each state of charge value should measured, because of the high non-linearity.

Second, by considering Figure 3.2 and Equation (3.3), it is obvious that the load voltage influences the OCV determination, when adding a charge or discharge current to the cell. By comparing charging $-I_a$ and discharging $+I_a$ influences with focus on load voltage, deviations with different signatures to the OCV characteristic occur. If both, charge and discharge processes are considered, a kind of hysteresis effect is generated. Hence, this behaviour is definite undesirable for defining the OCV characteristic but practically inevitable anyway.

Concluding, these two considerations lead to the two well-known methods, generating the OCV versus SOC characteristic, based on literature like [Petzl & Danzer, 2013] or [Somakettarin & Funaki, 2017], by

**Constant charging and discharging** The first method is based on using a small current rate, C-rate, and going through the charging and discharging process. This has the advantage that for all SOC states a defined voltage can be measured. Nevertheless, because always a current is applied to the cell, a load voltage is additionally added as well. Hence, the amount of the undesirable load voltage is defined by the order of magnitude of the current. Thus, lower current rates decrease the load voltage but also bring the disadvantage of an increasing measurement time.

**Puls charging and discharging** The second method is defined by charging or discharging the cell through different SOC states by waiting an idle time before measuring the cell voltage. This brings the advantage that cell voltage is measured without an additional load voltage. Nevertheless, after adding a load, (very) long pauses are needed until the cell comes back to an equilibrium state. Like within the constant charging and discharging strategy, higher accuracy can be generated by a longer idle time, which additionally leads to increasing measurement time and costs.

In summary, both methods include more or less the compromise between accuracy and measurement time. Nevertheless, to compare these strategies based on practical usage, measurements were done for both methods and evaluated in the next two subsections.

Note that during OCV investigations a constant ambient temperature of $T_\mathrm{a} = 40\,^\circ\mathrm{C}$ was used. The reason of this value was defined, because a linear dependency exists between temperature of the battery and relaxation time needed until the battery is in equilibrium state, [Farmann & Sauer, 2017]. This means, with even lower temperature, the hysteresis effect as well as measurement time increases significantly. Furthermore, temperature influences on OCV characteristic is a current research topic, see for example [Farmann & Sauer, 2017] or [Barai et al., 2016]. However, due to the long relaxation time, a detailed examination of this topic requires a huge amount of measurement time. This is the reason why focus in this work was held on $T_\mathrm{a} = 40\,^\circ\mathrm{C}$. A brief insight can already be given with the idle investigations later in this chapter.

### 3.3.1. OCV generation based on the constant current method

The first method presented and evaluated in detail, is generating the OCV versus SOC characteristic, based on a constant charge and discharge current. Thus, a fully charged battery forms the initial state. Afterwards, a defined discharge current, based on the mentioned trade-off between accuracy and measurement, is applied to the cell. This discharge process is carried out until the cell voltage reaches the minimum value of about $U_\mathrm{min} = 2.65\,\mathrm{V}$, see Table 3.1. After a short break, the battery cell is charged with the same charge current until the maximum voltage of $V_\mathrm{max} = 4.2\,\mathrm{V}$ is entered.

This measurement procedure was also carried out with our test cell, where the results are presented in Figure 3.4. On the upper left plot, the discharge current over the manoeuvre time $t$ is presented. It is feasible that a current of $I_a = 150\,\mathrm{mA}$ was used for discharging as well as charging the battery cell. Hence, this value represents an approximate C-rate of $0.043\,\mathrm{C}$. Furhtermore, this leads to an overall duration of the measurement procedure of $t \approx 46$ hours. Corresponding thereto, the measured cell voltage $U_a$ over the time $t$ is presented in the upper right plot. In both upper plots it is clearly visible that a very short resting time between discharging and charging the cell was used. The reason therefore, the used minimum voltage $U'_\mathrm{min} = 2.50\,\mathrm{V}$ was chosen with a smaller value which is recommended in the data sheet with $U_\mathrm{min} = 2.65\,\mathrm{V}$ and the cell should not keep a long time at such small levels. Nevertheless, quite common voltage behaviour properties are seen on the upper right plot. On one side, higher voltage drops are given within very close to full charged and empty cell levels. This behaviour is quite common for various types of cells. On the other side, discharging and charging behaviour is not equally symmetric. This can be traced back to the internal non-linear processes.

In addition, the well known determined OCV versus SOC characteristic is presented in the bottom plot of Figure 3.4. Thereby, the measured voltages during discharging $u_{a,\mathrm{discharge}}$, in dash-dotted orange, and while charging $u_{a,\mathrm{charge}}$, in dotted orange, are directly plotted. Furthermore, to compensate the positive and negative lead voltage, the average behaviour $u_{a,\mathrm{avg}}$ is calculated by the mean out of the two others and plotted as black solid line.
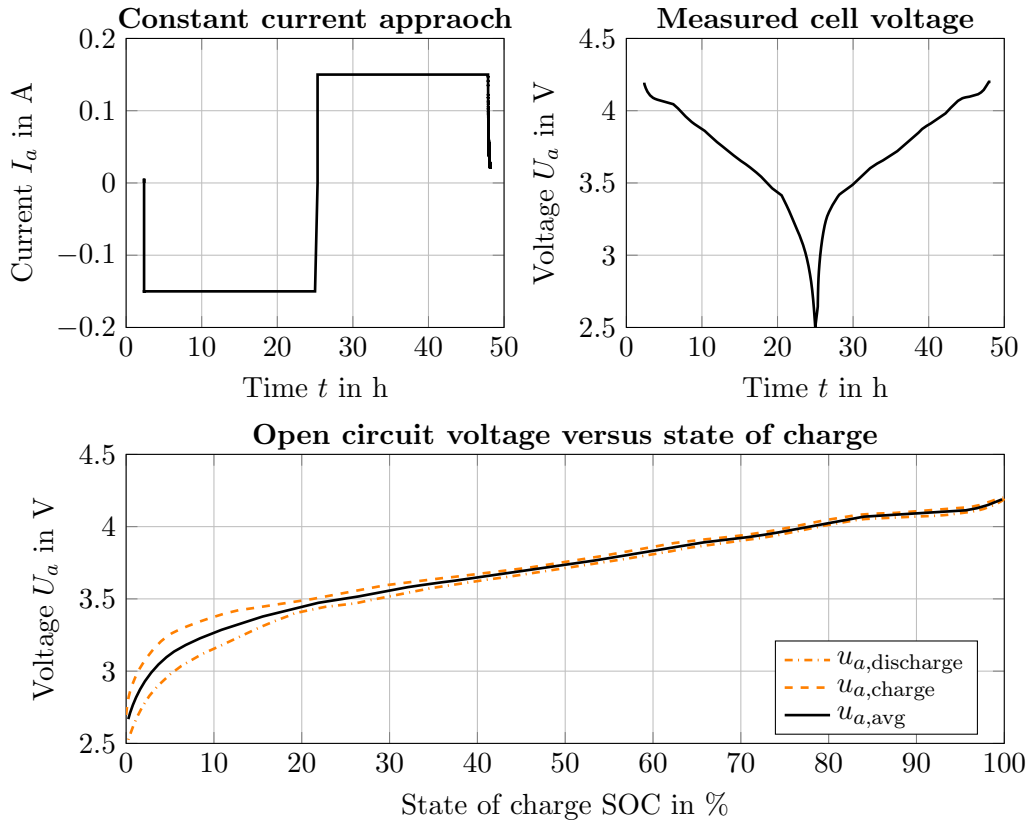
Figure 3.4.: Experimental determination of open circuit voltage versus state of charge characteristic, based on the constant current method; upper left, discharge and charge target value of $I_a = 150\,\mathrm{mA}$; upper right, measured cell voltage; bottom, the measured open circuit voltage versus state of charge characteristic measured during discharging and charging the cell as well as the average value calculated out of both

By validating the two measured and the generated average characteristics, a very small hysteresis effect is given, especially at SOC levels higher than 20 %. This leads to the statement that using a current value of $I_a = 150\,\mathrm{mA}$ seems a good trade-off. Also the non-linearities within SOC levels smaller than 20 %, which lead to a larger hysteresis effect, are clearly visible within this illustration.

In summary, averaging the discharge and charge voltages which are generated by using small current values, seems to be a good possibility from the first glance. Especially within widely used SOC working area of 20 % < SOC < 85 %. Hence, an even smaller current could be used but will effect the measurement time significantly. A detailed investigation in the size of the hysteresis is given within the comparison between this and the pulse method in Subsection 3.3.3.

### 3.3.2. OCV generation based on the pulse method

The second approach, which is quite common nowadays, deals with generating the OCV versus SOC characteristic based on discharge and charge pulse currents, including pauses in between. Also within this method, initial condition is a fully charged battery. Starting by a discharge current applied to the cell until a predefined SOC level is reached. Subsequently, the charging current is set to zero, so that load voltage is able to decrease to the equilibrium state of the cell. Because this is a non-linear process and further depends on different influences like cell chemistry, SOC level, temperature and many more, this process takes a long time. Nevertheless, the already mentioned trade-off between accuracy and measurement time is given within this time. In detail, using longer rest time, load voltage decreases stronger and a more accurate voltage can be measured. A detailed investigation in voltage change in relation to relaxation time is given in Subsection 3.3.4.

At the end of the relaxation time, the present voltage state and the current SOC value is measured. Afterwards, the same procedure is repeated until the cell reached the minimum cell voltage $U_{\min}$. Also within this method, the same procedure is repeated for the charging process until the maximum voltage of $U_{\max} = 4.2\,\text{V}$ has been entered.

This measurement procedure was carried out with our test cell too and the results are presented in Figure 3.5. As in the previous consideration, the upper left plot presents the current target $I_a$ and the upper right the measured cell voltage $U_a$, both versus the measurement time $t$. Also within this method, a pulse current of $I_a = 150\,\text{mA}$ was used for discharging and charging the cell to the defined SOC levels. The upper right figure shows that the voltage drops during discharging and subsequently the relaxation phases are visible. As within the previous investigations, quite larger drops are given at SOC $<$ 20 %. Hence, this means that behaviour is independent on the method and depending on the cell characteristic itself. For this application, twelve SOC levels were used, which leads to a measurement time of about $t \approx 163$ hours. Hence, this value was attributed from a point of experience. But once again, a higher number of operation points lead to a higher accuracy but also to a longer measurement time.

The bottom plot in Figure 3.5 presents the fully measured OCV versus SOC characteristic. Normally only points after the relaxation time are measured and plotted, but by using this representation a better cell voltage behaviour within this method can be seen. This means, also here a very small hysteresis effect is seen at SOC $>$ 20 % and a wider one at SOC $<$ 20 %. Also within this representation a very close behaviour is presented in comparison to the first approach. This leads to the statement that both methods provide very similar results in general. A detailed comparison between both is presented in the next Subsection 3.3.3.
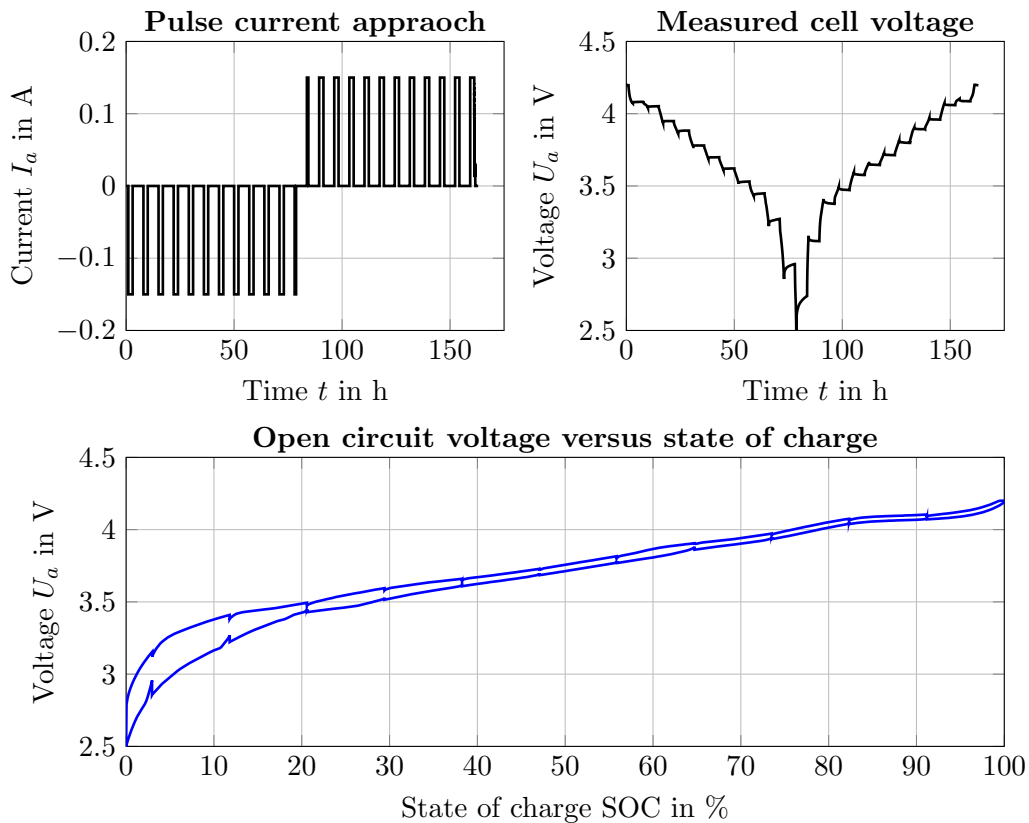
Figure 3.5.: Experimental determination of open circuit voltage versus state of charge characteristic, based on the pulse current method; upper left, discharge and charge pulses with a target amplitude of $I_a = 150\,\text{mA}$; upper right, measured cell voltage; bottom, the generated open circuit voltage versus state of charge characteristic

### 3.3.3. Comparison of constant and pulse current approach

While an overview of the two different methods to generate the OCV versus SOC characteristic shows quite similar results overall, focus on a detailed comparison is given in this subsection. To evaluate influences of the pause durations as well as magnitude values of the pulse current, an additional setup of the pulse method is added. This means in detail that the general pulse method stays the same but with a larger current magnitude value of $I_a = 350\,\text{mA}$ and a shorter pause duration of only 1 hour instead of 5 hours, presented in Figure 3.5. With this additional pulse method setting, influences in current magnitudes and pause durations can be investigated additionally.

The overall comparative presentation of both methods, within the two mentioned setups of the pulse method, is presented in the upper plot of Figure 3.6. In the four plots below, detailed cut outs on different SOC levels are shown.
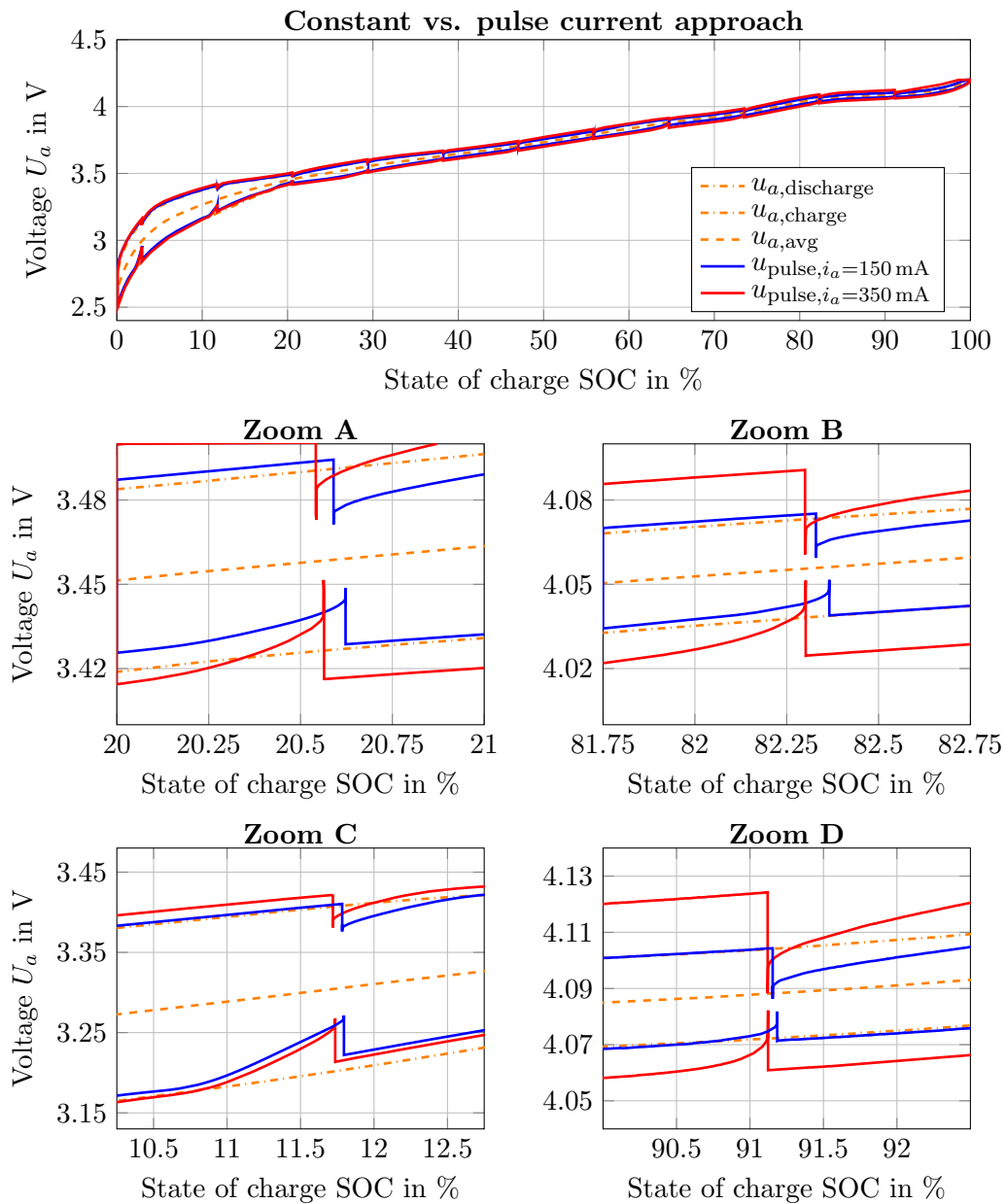
Figure 3.6.: Experimental validation of different methods to generate the open circuit voltage versus state of charge behaviour; on the top; overall results of both methods with different setups are presented; the four plots bellow show detailed cut outs of the overall characteristics for enhanced investigations

As already presented separately, the upper plot of Figure 3.6 shows the overall comparison. It is obvious that all three setups are providing quite similar results. Therefore, detailed cut outs are shown in the four plots below. For all four plots, the orange dash-dotted line presents the discharge and charge behaviour of the constant current method from Subsection 3.3.1. Belonging to these two lines, the average of both is calculated. Furthermore, the two setups generated from the pulse method; as blue solid line the values used in Subsection 3.3.2 with $I_a = 150\,\mathrm{mA}$ and rest time $t_\mathrm{r} = 5$ hours each, and as red solid line with $I_a = 350\,\mathrm{mA}$ and rest time $t_\mathrm{r} = 1$ hours; are presented.

The two plots in the middle (Zoom A and Zoom B) present cut outs of typical SOC levels which are used in most applications. On the left, a SOC area of around 20 % and on the right an area of around 82 % are presented. Thus, writing down a few properties $p_i$ and the related declaration $c_i$ for a detailed evaluation:

$p_1$) The solid blue and the dash-dotted orange curves are overlapping very close while positive and negative pulse periods

$c_1$) Because within both approaches, same currents and temperatures are applied on the cell and consequently both methods should deliver the same results. Because this is given in both plots, the two methods can be directly compared

$p_2$) The total equilibrium have not reached because there is still a gap between the discharging and charging pause voltage

$c_2$) Thus, the question arises, how long should be waited? More on that, later in this section. Hence, it seems that also within this method, respectively long relaxation time, no final SOC value is reached. Concluding, do define the OCV also an average calculation of the discharging and charging value needs to be done

$p_3$) By comparing the calculated mean value of the discharging and charging voltage pulses of $u_{\mathrm{pulse},i_a=150\,\mathrm{mA}}$ with the $u_{a,\mathrm{avg}}$, it is visible that they are very close. It seems the voltage $u_{a,\mathrm{avg}}$ is situated in the middle of the $u_{\mathrm{pulse},i_a=150\,\mathrm{mA}}$ pulses

$c_3$) By calculating the mean values in detail, only a deviation of about $\Delta u_a \approx 1\,\mathrm{mV}$ is given. This leads to the statement that both methods bring nearly the same OCV results

$p_4$) Comparing the two pulse setups, red with $I_a = 150\,\mathrm{mA}$ and blue with $I_a = 350\,\mathrm{mA}$, by calculating the mean OCV values, only small differences at SOC $= 20.5$ % and nearly no differences at SOC $= 82.25$ % are given

$c_4$) These results show that within operating points between $20\,\% < \mathrm{SOC} < 85\,\%$ also a setup with a higher current as well as shorter pauses generate accurate results. Thus, this setup is preferable from the economic point of view

In summary, both methods, within both setups, deliver very similar OCV results by calculating the average values. Furthermore, also by resting duration of $t_\mathrm{r} = 5\,\mathrm{h}$ the equilibrium have not reached. This means, exact results could not be determined yet. Therefore, detailed investigations on resting time is given in the next Subsection 3.3.4.

But first, further method comparisons are done at close to empty and fully charged SOC levels (Zoom C and Zoom D). Thus, the two bottom plots of Figure 3.6 show the method comparison at a SOC area around 11.5 % on the left and around 91.25 % on the right. Also here, a closer inspection on the following properties is given:

**p₅)** Again, total equilibriums have not been reached yet at this SOC states. But it seams at very high SOC level it is getting quite close

**c₅)** Especially on a very low level is clearly visible that a high hysteresis effect is given even after the longer duration. This confirms the assumption that a high non-linearity behaviour inside the cell is given at very low SOC levels. On the contrary this effect is definitive quite smaller on SOC > 20 %

**p₆)** Dropping behaviour are different for charging and discharging

**c₆)** Hence, a different behaviour at charging and discharging, especially at very small and high SOC level is seen at all. This concludes that the SOC area has an influence on OCV generation. This behaviour is directly seen in the left plot because $u_{a,\mathrm{avg}}$ is not in the middle. In detail, a difference of $\Delta u_a \approx 20\,\mathrm{mV}$ occurs between both methods. In addition on the right plot, the characteristics already intersects the behaviour within a deviation of $\Delta u_a \approx 5\,\mathrm{mV}$

In summary, a small deviation of both methods are given outside typical operation areas of $20\,\% < \mathrm{SOC} < 85\,\%$. Due to the high non-linearity effects especially at very small SOC levels, a deviation of $\Delta u_a \approx 20\,\mathrm{mV}$ occurs. Hence, if a high accuracy at these limits is needed the pulse method seems to be the better choice. Nevertheless, the pulse approach loses overall accuracy at all because measurement cannot be done at all SOC states. In detail, this leads to an interpolation error at all. Remedial actions can be done by using a high number of SOC states which leads to higher measurement time and costs. Nevertheless, in all four zooms the rest time was chosen too short to exactly define the OCV value. Therefore, the question about the preferable rest time has to be investigated in the next subsection.

### 3.3.4. Investigation on relaxation time based on the pulse method

During detailed investigations within different SOC levels in Figure 3.6, it is obvious that in all four states the equilibrium is not yet reached. Therefore, to exclude measurement errors and gain more experience about influences of the duration of the relaxation time, two more experiments were done and presented in Figure 3.7. Within this manoeuvres, a fully charged battery is discharged until defined SOC levels are reached, and a very long relaxation time was applied afterwards.

To do so, the two different SOC levels used are plotted separately as well as in comparison in the three bottomed plots in Figure 3.7. Thereby, the first SOC resting level at around 56 % is given with a relaxation duration of $t_{\mathrm{r,A}} = 209\,\mathrm{hours}$. In addition, the second SOC resting level at around 29.5 % is given with a relaxation time of $t_{\mathrm{r,B}} = 72\,\mathrm{hours}$.
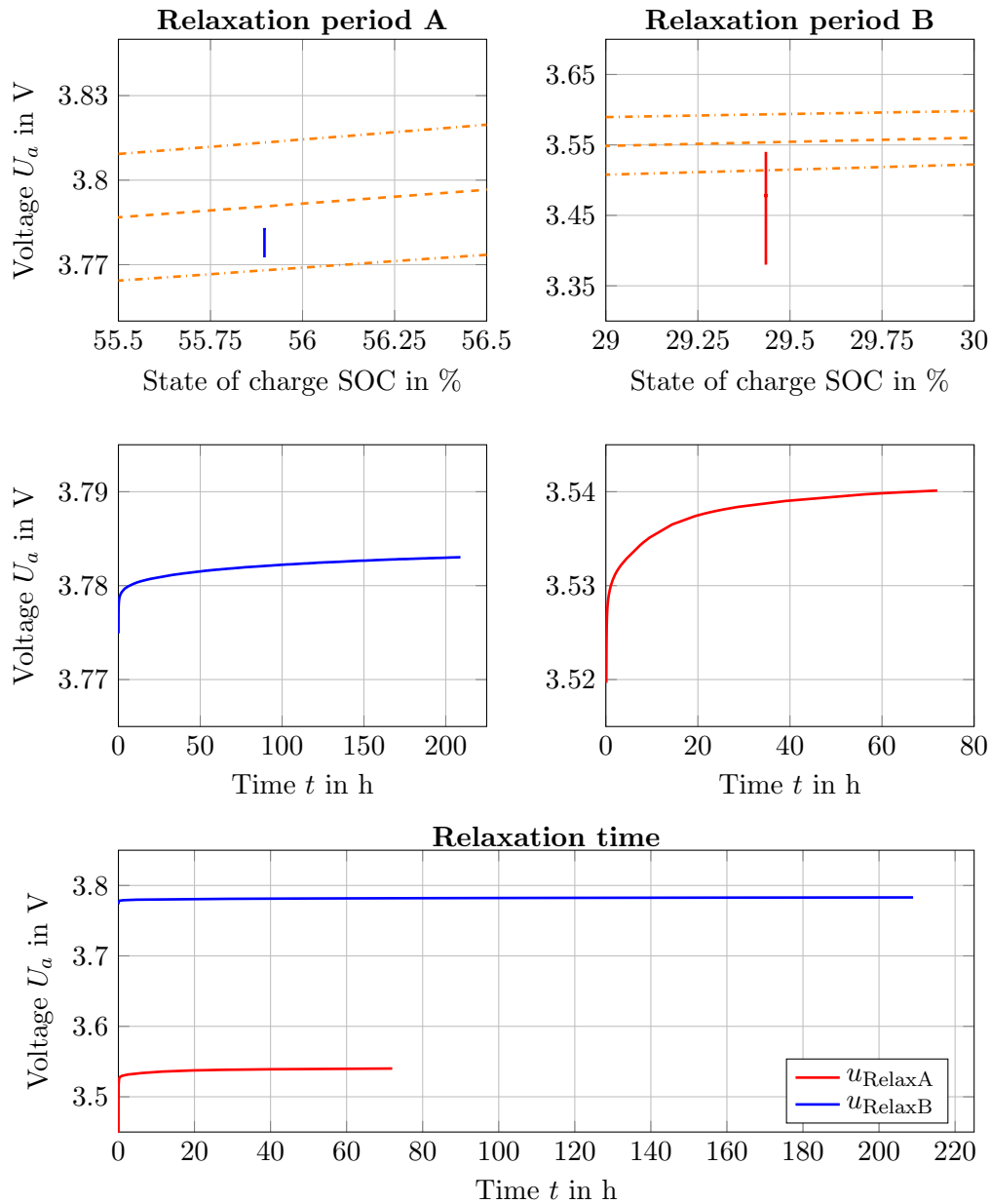
Figure 3.7.: Extended investigations on the relaxation time based on the pulse method to generate the open circuit voltage versus state of charge characteristic; on the three bottomed plots the relaxation voltage versus the time is given within two different SOC levels; on the top, the comparison between the constant current method and the voltage changes during the resting duration is shown

In addition, the voltage changes during the relaxation time, in comparison to the constant current method, is given in the two upper plots of Figure 3.7. Thus, in both upper plots it is feasible that the voltage at the end of the resting time $u_{\mathrm{Relax},i}$ does not match the average value from the constant current method $u_{a,\mathrm{avg}}$. To validate this effect, the voltage behaviour versus the time in the two plots in the middle can be used. It seems that also after such a long relaxation time of $t_{\mathrm{r,B}} = 72$ hours respectively $t_{\mathrm{r,A}} = 209$ hours there is still a small voltage increase visible, respectively the final equilibrium is not reached already. Hence, it looks like that both curves are intersecting after an even longer relaxation time. But this is still an assumption and can not be proven at this point.

In summary, also with such long resting times it is not possible to measure the OCV characteristic without a hysteresis effect, respectively gaining the behaviour without using averaging education from charging and discharging. Hence, it seems when using an even longer relaxation time, the distance to the average voltage becomes smaller or tends to be zero. But this is just an assumption and can not be proven at this point. Nevertheless, within these investigations, based on the resting time, further knowledge was gained. Hence, such long times are definitive not economical but it seems that the strategy based on the averaging education is quite close to the equilibrium state.

### 3.3.5. Method summary to generate the open circuit voltage

In this section, the generation of the OCV based on the SOC level was presented, evaluated and validated within two different methods, extracted from the literature. The first method was defined by using a small constant discharging and charging current and averaging the measured behaviour finally. It was presented that this practical method is very easy to define and furthermore it generates a suitable and usable characteristic, especially within a practical user range of $20\,\% < \mathrm{SOC} < 85\,\%$. Hence, small uncertainties arise in the range of small SOC areas where non-linear behaviour, based on the cell chemistry, occurs. Furthermore, a trade off between accuracy and measurement time has to be solved, depending on the performance requirements.

The second method named pulse current approach, uses pulses to discharge and charge the cell to define SOC levels and additionally include pauses to minimise the load voltage for measuring the OCV. It was shown by using pauses, the cell voltage moves to an equilibrium state but is not able to reach the final level within an economical timeframe. This leads to the fact, that also with this method some kind of averaging education has to be done. Based on the presented experimental investigations, it seems that this method is more accurate at small and very high SOC areas. Additionally, short relaxation times already generate sophisticated results, especially within a practical user range of $20\,\% < \mathrm{SOC} < 85\,\%$. Hence, because only a predefined number of SOC states is measured with this methods and interpolation errors can not be excluded.

In summary, both methods are suitable for practical usage. Thus, the preferable approach is mostly defined on the mentioned trade off's as well as the performance requirements.

## 3.4. Comparative consideration based on generating the open circuit voltage

Modelling and simulation of the battery cell behaviour, by using ECs, represents a common method nowadays. Overall goal therefore is the mathematical reproduction of the cell voltage, based on different discharge and charge currents (C-rates) and temperatures for all SOC stages. To achieve this goal, a separation into two modelling parts was decided, based on the literature study from Chapter 2. To confirm this idea, basis considerations on the voltage potential of a battery cell was done in the first part of this chapter.

Thus, the fundamentals on material dependent potential behaviour of the anode and cathode electrode has shown that cell voltage occurs non-linear and is dependent on the SOC. Furthermore, by summarising all losses appearing during discharging and charging the cell, into a resistance respectively into a complex impedance shows transient effects of the voltage behaviour. These considerations confirmed the gained knowledge from the literature study, to separate the modelling process into a steady-state and a transient part. After the definition of the subdivision strategy, including the modelling process, the used test equipment as well as the test cell was presented. Overview of the functionality as well as the key information of the test cell were noted.

The second part of the chapter focused on the first main part of the overall cell model. This steady-state cell behaviour is described by the *open circuit voltage* (OCV) versus *state of charge* (SOC) characteristic. Because the accuracy of this characteristic is of major importance for the overall model accuracy, the two well-known literature based methods, to generate this behaviour, were investigated in detail. The first method was defined by using a small constant discharge and charge current and OCV was generated by averaging both. This method worked quite well, especially within a practical SOC range. Small uncertainties occurred in the range of small SOC areas.

The second method relied to a pulse current approach including pauses in between. It was presented that during the pauses the cell voltage moves to an equilibrium state but was not able to reach the final level within not even with long relaxation time durations. This leads to the fact that also with this method, some kind of averaging education has to be done. Furthermore, this method showed higher accuracy at smaller SOC areas but also includes an interpolation error.

In summary, both methods are well suitable for practical usage, where just small deviations between both were seen, especially at small and very high SOC areas. Finally, accuracy can be increased by higher measurement time in both cases. Thus, the generation is mostly defined on this trade-off as well as on the performance requirements.

# 4

# Modelling of the transient battery cell behaviour

After theoretical investigations on cell requirements and the work principles of lithium-ion cells in Chapter 2, followed by the steady-state behaviour implemented as *open circuit voltage* (OCV) versus *state of charge* (SOC) characteristic in Chapter 3, modelling of the transient cell behaviour is the topic of this chapter. Thus, based on the fundamental investigations presented in Section 3.1, understanding and modelling the transient processes inside the cell, is defined as next step. This means in detail that the properties behind the summarised resistance, respectively the complex impedance, need to be worked up.

To do so, processes based on the work principles of lithium-ion cells are summarised with detailed focus on time response. It will be shown that the chemical processes are working within a very wide time range and therefore, they also have different time constants. Thus, this fact of course has an influence into modelling, parameterisation and measurement process of a cell. Therefore, beside working in the time domain, a further method called *electrical impedance spectroscopy* (EIS) has become quite common nowadays.

Based on the fundamental idea behind, to transform the cell behaviour into the frequency domain, an overview about the EIS concept is presented first. Goal is to understand the basic idea behind as well as present the method output, which is used for further parameterisation and validation processes. Out of it, an extended semi-physical model approach, based on literature, is presented. Electrical component behaviour as well as the already discussed chemical processes inside the cell, serve as major foundation for this explanation.

Afterwards, this elaborated extended approach is revised based on the thesis requirements and the behaviour of the cell used. Thus, goal is to find a sophisticated model approach, based on the *Monte-Carlos analysis*. This means in detail that a trade-off between maximum accuracy but with less computational effort and a low number of model parameters has to be worked out. Following, the elaborated semi-physical model approach will be validated based on external influences, like different SOC levels, temperatures and load currents, in Chapter 5.

Finally, this chapter ends with a summary of the model finding process and a comparative conclusion.

## 4.1. Basic considerations on transient cell modelling

To define a suitable model approach, which is able to mathematically describe the transient cell process, a basic understanding about the internal dynamic effects is needed. This means, knowledge about the procedure but also about the time duration of the internal processes are needed. Therefore, investigations of the time period of the cell are done first. In addition, it turned out that there is a second opportunity besides the investigation in the time domain, called EIS, and presented in detail. Finally, these two outcomes are used to build an extended literature based equivalent circuit model approach, which serves as basis for further experimental investigations.

### 4.1.1. System dynamics of lithium-ion battery cells

The foundation of the system dynamics forms the fundamental working principle of lithium-ion cells, presented in Section 2.1 respectively Figure 2.3. Already within an understanding of these basic descriptions it was clearly visible that a lot of different processes within wide time periods occur. Thus, for a detailed discussion, a schematic overview about the time durations is presented in Figure 4.1. It is obvious that chemical processes are given between a few micro seconds up to about ten thousand hours.
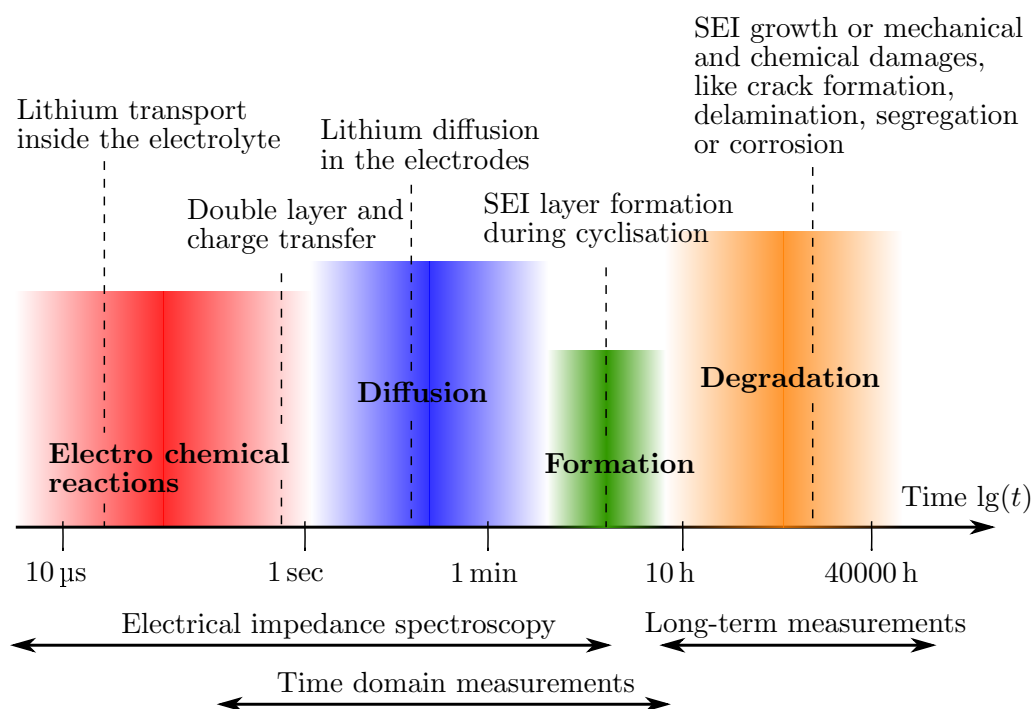


Figure 4.1.: System dynamics of lithium-ion battery cells based on the chemical processes, adapted from [Weber, 2018]

Thus, processes starting from electro chemical reaction within a few micro seconds, like the lithium transport inside the electrolytes, going through the diffusion process in the electrodes via a few seconds or minutes, and finally ends up in the degradation process, which includes mechanical and chemical damages, like crack formation, delamination, segregation or corrosion. Furthermore, also the *solid electrolyte interphase* (SEI) formation, which occurs during first cyclisation, is shown in Figure 4.1. In summary, this shows the already expected wide time duration of the cell chemistry.

Hence, implementing all these effects within one battery model, becomes a complex task in modelling but even more in measuring, respectively measurement time. Since this project focuses on modelling the cell voltage during driving conditions, long-time processes, like degradation and damage impacts are not examined in detail and therefore neglected for further investigations. Additionally, major part of the solid electrolyte interphase layer formation happens only at the very beginning of a cell's lifespan. This means, that this effect is also neglectable for general investigations. In summary, modelling the electro chemical reactions as well as the diffusion processes represent the main tasks for automotive applications. Nevertheless, by only modelling these two effects, also a wide time range occurs.

To investigate and validate cell behaviour or even parametrise battery cells in such a wide time domain becomes difficult. Therefore, an alternative approach has become quite common nowadays, the so called *electrical impedance spectroscopy* (EIS) method. Goal of this approach is to transform the battery behaviour from the time into the frequency domain. This brings the main advantage that the cell behaviour within a wide time respectively frequency range can be represented, further investigated and evaluated within one plot. This makes investigations quite easier.

Hence, a fundamental description about the basics of this, state of the art, approach is given in the next subsection. Since this method is also mainly used for further investigations in this thesis. Nevertheless, property comparison between EIS and parameterising within the time domain, is worked out at the end of Chapter 5.

### 4.1.2. Fundamentals of the electrical impedance spectroscopy (EIS)

Because chemical processes have such a wide time range, investigations, parameterisation and validation processes within an EIS have become a very common method in the area of battery cells. As already mentioned, the main goal is to transform the cell behaviour from the time into the frequency domain and then, examine the cell behaviour within one defined representation.

Thus, this method is based on the assumption that the cell can be defined as *linear time invariant system* (LTI system) for a fixed operating point. This means further that the properties of a causal, linear and time invariant system can be used. Following, a symmetrical load current applied, generates a symmetrical voltage behaviour on the cell. This can be further used to calculate the magnitude and phase response of the system, see Figure 4.2.
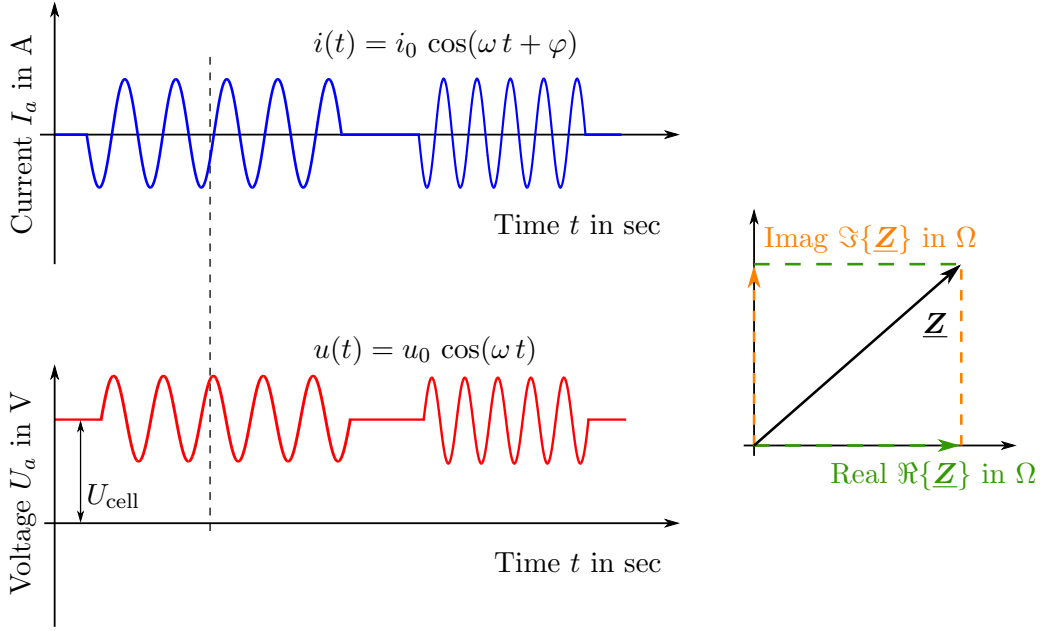
Figure 4.2.: Strategy behind the functionality of an *electrical impedance spectroscopy* (EIS) methode; left, cell target currents $i(t)$ and measured voltages $u(t)$; right, representative input and output signals, transformed into frequency domain

On the upper left diagram of Figure 4.2, a schematic representation of the sinusoidal current target $i(t)$ for two different frequencies $\omega$ are given. In addition on the bottom left, the cell voltage $U_a = U_{\text{cell}} + u(t)$ is given as a result. Thus, $U_{\text{cell}}$ is defined as SOC dependent steady state voltage and $u(t)$ as result of the input current. Based on this input and output behaviour, a complex characteristic $\underline{Z}$ can be defined out of the real part $\Re\{\underline{Z}\}$ and the imaginary part $\Im\{\underline{Z}\}$ for each frequency, like on the right side of Figure 4.2.

Mathematically, this behaviour can be defined as follows

$$\underline{Z} = \frac{\underline{u}(t)}{\underline{i}(t)} = \frac{u_0}{i_0}\, \mathrm{e}^{\mathrm{j}\,\varphi} = \Re\{\underline{Z}\} + \mathrm{j}\,\Im\{\underline{Z}\}\,. \tag{4.1}$$

The real and imaginary part of the complex impedance are defined with

$$\Re\{\underline{Z}\} = \frac{u_0}{i_0}\,\cos\varphi \quad \text{and} \quad \Im\{\underline{Z}\} = \frac{u_0}{i_0}\,\sin\varphi\,, \tag{4.2}$$

where $i_0$ and $u_0$ are defined as the amplitude of the target current and the measured voltage and $\varphi$ as the time delay between both. Finally, this calculation can be done for a wide frequency range and each point plotted into a so called *Nyquist plot*, like in Figure 4.3.
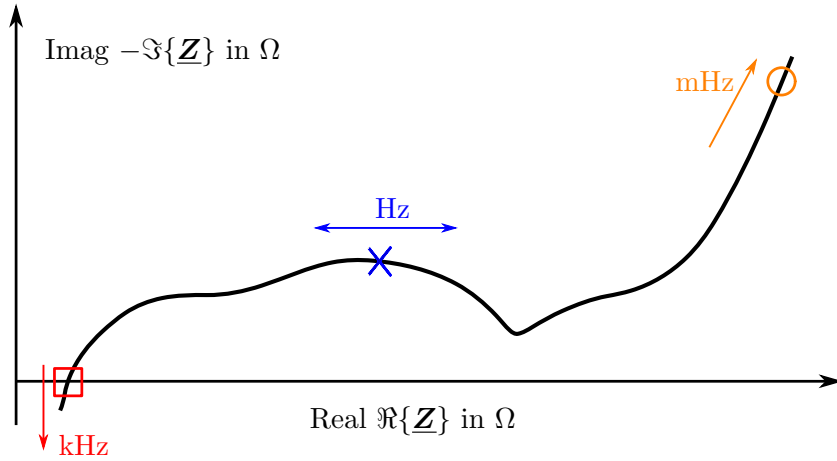
Figure 4.3.: Schematic representation of an EIS result for a lithium-ion battery cell; the marked red rectangle, blue cross and orange circle represent major frequency areas where the solid line shows the overall behaviour generated out of infinitesimal small frequency steps for SOC = const and $T$ = const

Within this representation of the *Nyquist plot* in Figure 4.3, three major frequency areas are shown representatively; the red rectangle for very high frequency areas $f \geq 1\,\text{kHz}$, the blue cross for frequencies around $f \approx 1\,\text{Hz}$ and the orange circuit for very small frequencies $f \leq 10\,\text{mHz}$. By using this strategy, applied on a large number of frequency points, the black solid line can be generated and it represents the behaviour of a lithium-ion battery cell for infinitesimal frequency steps.

As already noted, battery behaviour is depending on various external influences, like SOC level, temperature or C-rate. So, changing one or more of the mentioned influences, this also effects the behaviour of the cell and therefore the results in the *Nyquist plot*. In summary, the presented characteristic in Figure 4.3 is only valid for one SOC level, one temperature and one C-rate. Of course, influences by changing these values can be investigated in this plot quite well. Reference is made to the second part of the chapter.

Finally, a short note about the current target amplitude $i_0$ should be given at this point. Thus, a trade-off between very small and high values is given here as well. While large current amplitudes bring well defined voltage changes, which are easy to measure and transformable into the frequency domain, the disadvantage brings changes in the SOC level during a period. In contrast, while charging and discharging with high currents, temperature changes inside the cell occur. Nevertheless, very small currents bring properties vice versa. Ideally, different values are tried and compared before the main investigation started, like in [Andre et al., 2011a], [Andre et al., 2011b]. They compared current amplitudes from $I_a = 0.1 \ldots 1\,\text{A}$ and recommended to use $I_a \approx 0.5\,\text{A}$ finally.

### 4.1.3. Electric circuit modelling based on chemical processes

After studying the system dynamics of the chemical processes inside the lithium-ion battery cell and discussing fundamentals of the EIS, the knowledge of both parts are now combined in this subsection. This means in detail that based on the generated results out of the EIS, shown in Figure 4.3, an *equivalent electric circuit* (EC) has to be defined which is able to model this dynamic behaviour.

To do so, frequency segments out of the EIS characteristic are sub-divided, described by an equivalent electric element, like a resistor, capacity, inductivity or a combination out of those, and lined up together to an electric circuit. As a first step, the three frequency areas defined in Figure 4.3 are discussed as a fundamental example. Thus, knowledge of how these elements perform within the frequency domain respectively the *Nyquist plot* serves as basis. Nevertheless, the properties are summarised in Appendix A for the purpose of completeness.

**Area kHz** A closer look at the red rectangular area shows that the characteristics cross the real axis at a value $\Re\{\underline{Z}\} > 0$. This means that at one frequency, only an ohmic resistance behaviour is given. Furthermore, the line moves towards an area $\Im\{\underline{Z}\} > 0$ which can only be modelled by an inductance. In summary, an ohmic resistance as well as an inductance is needed in the electric circuit in some way.

**Area Hz** The area around the blue cross correspondents to one or more semicircular behaviours. From the theory, a semicircle in the *Nyquist plot* can be modelled within one or more RC-elements. Note that RC-elements are quite common for EC based cell modelling, but for a detailed description an extension is used. For details, see later.

**Area mHz** The diffusion area shows an increasing behaviour at very small frequency areas. Thus, this can be modelled by using a capacity in some way. For a smoother transition from small to very small frequencies, a so called *Warburg impedance* can be used in addition to the capacity.

In summary, this exemplary description shows how an EC can be defined by using basic electrotechnical knowledge, based on the information from Appendix A. The same strategy is also used in most literature approaches, only with a few more or less elements. Finally, by modelling this behaviour quite in detail, an extended model approach can be created, see Figure 4.4, based on [Andre et al., 2011a], [Andre et al., 2011b] and [Weber, 2018].

Like in the description above, a combination of an ohmic resistance and an inductance modelling the area at very large frequencies. Furthermore, a capacity and a *Warburg impedance* describing the area at very small frequencies. The only differences are the three *Zarc*-elements which are replacing the mentioned one more RC-elements. Thus, the main advantage of a *Zarc*-element is the possibility to depress the semicircular behaviour within a depression factor. Which means the possibility to fit the wavy behaviour in a more accurate way. A detailed mathematical description as well as a comparison to a RC-element based on measurement data is given in the next Section 4.2.
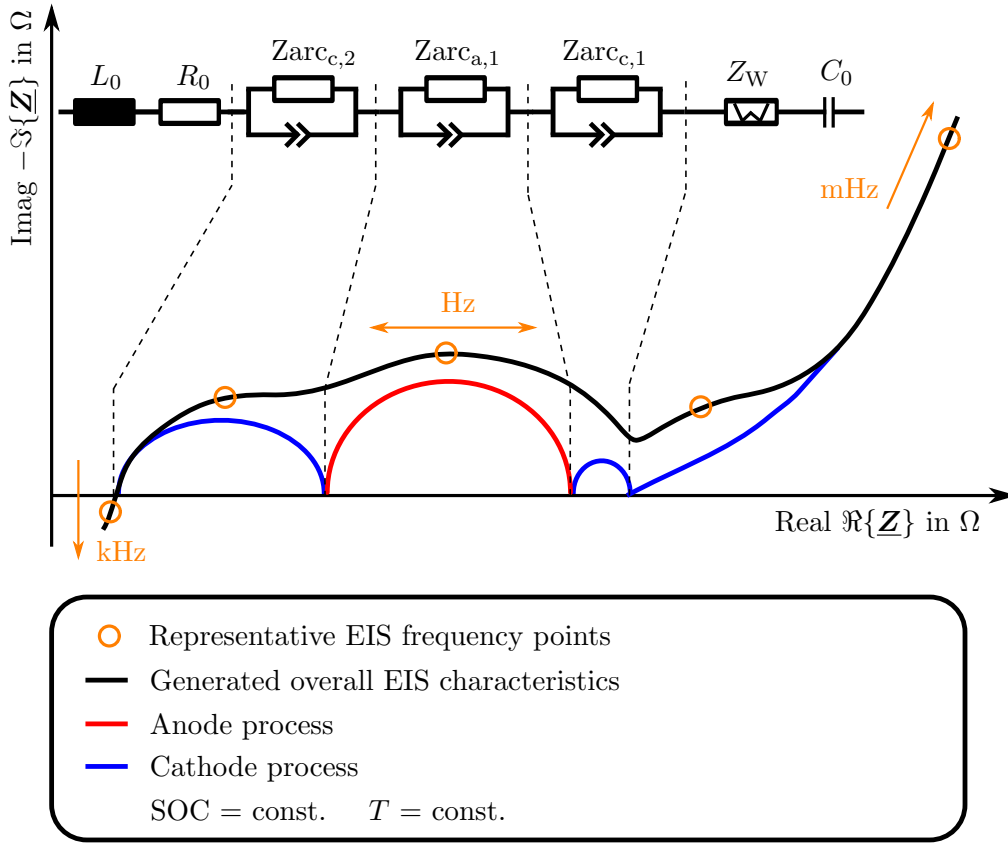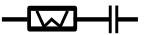
Figure 4.4.: Equivalent electric circuit model based on the loss processes of a battery cell and broken down into their frequency ranges, adapted from [Weber, 2018]

Additionally, in Figure 4.4 a detailed representation about the working areas of the different elements is presented. Started with the resistance $R_0$ and the impedance $L_0$ at very high frequencies, followed from the three *Zarc*-elements $\text{Zarc}_{a/c,i}$ for middle frequency ranges and ended with and *Warburg impedance* and a capacity for very low frequency ranges. Thus, the $\text{Zarc}_{a,1}$ is used to model the charge transfer between anode and electrolyte, $\text{Zarc}_{c,1}$ models the charge transfer between the cathode and electrolyte and furthermore $\text{Zarc}_{c,2}$ describes the highly frequent contact resistance in the cathode. In summary, within these elements combined into an extended electric circuit, the electro chemical reactions as well as the diffusion process can be modelled in a sufficient way. A summary, of the modelling responsibilities of each element is given in Table 4.1.

In summary, this section presented a semi-physical model design process, based on electro chemical and diffusion processes. Hence, the presented extended model is able to describe the mentioned processes from the theoretical point of view. Therefore, investigations on practical usage as well as on the possibility to simplify the model and reduce the parameter is the goal of the next section.

Table 4.1.: Physical origin related equivalent electric circuit description, working within different frequency ranges, adapted from [Weber, 2018]

| Equivalent circuit | | Frequency range | Physical origin |
|---|---|---|---|
| $R_0$ | | - | Electrical and ionic conductivity |
| $L_0$ | | $> 1000\,\mathrm{Hz}$ | Inductive current arrester |
| $\mathrm{Zarc_{a,1}}$ | | $10 \ldots 200\,\mathrm{Hz}$ | Charge transfer anode - electrolyte |
| $Z_\mathrm{W} + C_0$ | | $0.001 \ldots 0.1\,\mathrm{Hz}$ | Solid body diffusion |
| $\mathrm{Zarc_{c,1}}$ | | $0.1 \ldots 10\,\mathrm{Hz}$ | Charge transfer cathode - electrolyte |
| $\mathrm{Zarc_{c,2}}$ | | $100 \ldots 1000\,\mathrm{Hz}$ | Contact resistance cathode |

## 4.2. Design process of the equivalent electric circuit

In this section, the design process of the thesis related EC is presented. The discussed basic considerations on transient cell behaviour as well as the elaborated theoretical model from the previous section serves as foundation. Main goal is to find a practical equivalent circuit which is able to handle the cell behaviour in a quite accurate way. Additionally, a low number of parameter, which simplifies the parameterisation process, complexity and practicability, is a further sub goal which should be considered. Furthermore, the possibility to use the designed model online during driving has to be given. This means in detail, the model designed in the frequency domain must be transferable to the time domain.

Note that the final design process of such ECs always depends on the cell chemistry, problem or modelling requirements and application cases. The presented modelling and design process serves as a template for further application cases. If applications are different or frequency areas are of special interest, maybe more or less respectively different simplifications are preferable.

Thus, to start the design process from the practical point of few, measurement data are now used. To do so, three different EIS manoeuvre domains are chosen and used for the thesis modelling design process, see Figure 4.5. The first manoeuvre is presented in the two upper plots of Figure 4.5, where a zoom visualisation is given on the upper right one. Within this manoeuvre, the EIS is done at a SOC level of SOC $= 73.54\,\%$ and an ambient temperature of $T_\mathrm{a} = 40\,°\mathrm{C}$. For the EIS manoeuvre a frequency range of $f = 0.003 \ldots 5000\,\mathrm{Hz}$ is used.
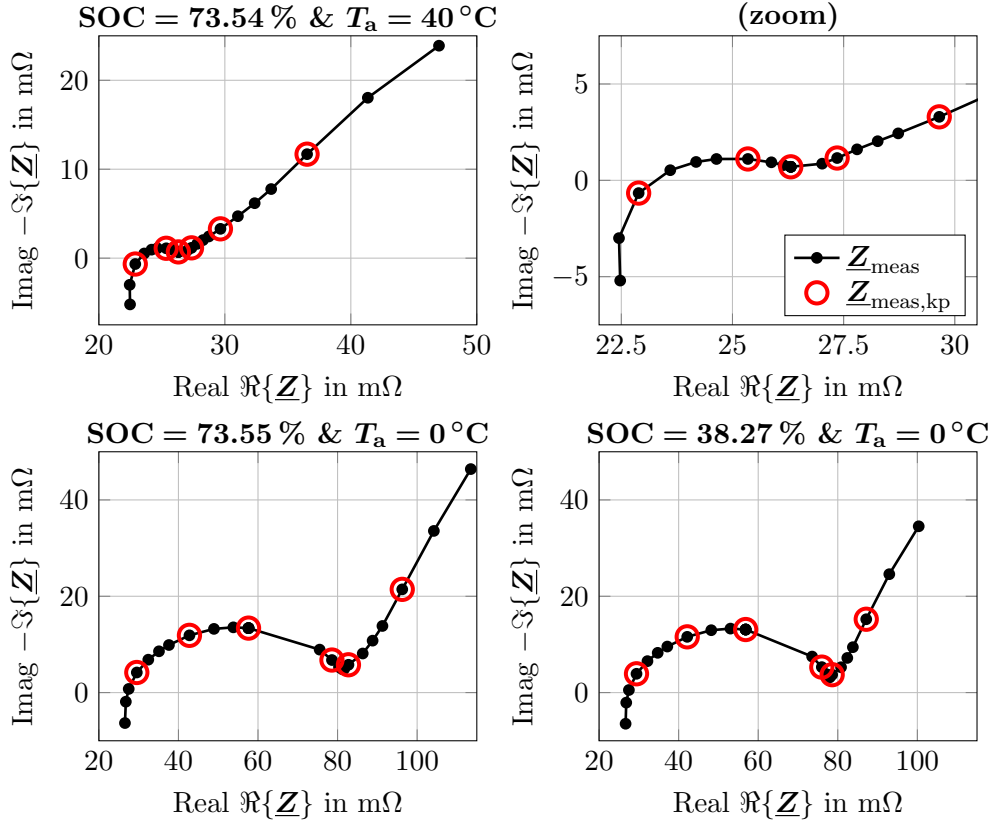
Figure 4.5.: Experimental electrical impedance spectroscopy results $\underline{Z}_{\text{meas}}$ at different SOC levels and ambient temperatures $T_{\text{a}}$; upper two plots, $T_{\text{a}} = 40\,°\text{C}$ and SOC $= 73.54\,\%$; bottom left, $T_{\text{a}} = 0\,°\text{C}$ and SOC $= 73.55\,\%$; bottom right, $T_{\text{a}} = 0\,°\text{C}$ and SOC $= 38.27\,\%$

The results generated out of these frequencies are presented as the small black dots, where the black solid line represents the linear interpolation in between. The red circles marking the key points at $f_{\text{kp}} = \{1000, 100, 10, 1, 0.1, 0.01\}$ Hz additionally. In the two bottom plots of Figure 4.5 two further manoeuvre domains are presented. On the bottom left, the result within nearly the same SOC level of SOC $= 73.55\,\%$ but with a different ambient temperature of $T_{\text{a}} = 0\,°\text{C}$ is presented. On the bottom right, the result with an ambient temperature of $T_{\text{a}} = 0\,°\text{C}$ but a lower SOC level of SOC $= 38.27\,\%$ is given.

By comparing the results with the same SOC level, a clearly different behaviour is evident. This means that ambient temperature has a large impact on the cell behaviour. Thus, the final model should be able to handle both respectively a wide range of temperature. Alternatively, a smaller influence on the cell behaviour is seen by changing the SOC level. Nevertheless, the circuit should be also able to handle this changes.

In summary, the overall behaviour of the EIS results are looking quite similar, also by comparing the behaviour from the literature in Figure 4.3 and Figure 4.4. However, large differences are visible in the scaling of the characteristics. This means that one model can be used for different external and environmental situations but the parameters depend on it. Therefore, an equivalent circuit has to be designed which is able to handle the behaviour within different situations first. Afterwards, influences of these external effects on model parameters are investigated in detail in the next Chapter 5.

Starting with the model design process, the main frequency areas including the representing sub models are investigated separately. To do so, the areas are sub divided like in Figure 4.3 and Figure 4.4.

### 4.2.1. EC modelling - large frequency area

The first area which is investigated in detail, is generated by inductive current arresters and the electrical and ionic conductivities, respectively modelled by the inductance and the ohmic resistance, and located at very high frequency values by $f > 500\,\mathrm{Hz}$. Like in the theoretical representation, in all three different setups zero crossing of the real axis is given at a value $\Re\{\underline{Z}\} > 0$. Furthermore, also characteristics move towards an area $\Im\{\underline{Z}\} > 0$ within all three setups. Thus, using the elaborated inductance and the ohmic resistance looks very practically in a first consideration.

But looking into detail with respect to the frequency values, a different modelling situation can occur from the engineering point of view. Thus, in the upper right plot it is clearly visible that the cell characteristics cross the real axis within a frequency in between of $f = 1000\,\mathrm{Hz}$ (see the first key point) and $f = 500\,\mathrm{Hz}$. Alternatively, looking at the same details within the results at ambient temperature of $T_\mathrm{a} = 0\,^\circ\mathrm{C}$ zero crossing is given at around $f \approx 2000 - 3000\,\mathrm{Hz}$. Based on the *Nyquist-Shannon sampling theorem* this means, we need a practical sampling frequency $f_\mathrm{s}$ which is minimum two times higher than the manoeuvre frequency, by $f_\mathrm{s} \geq 2\,f$. This means further, sampling frequency should be minimum around $f_\mathrm{s} \geq 2000\,\mathrm{Hz}$ at $T_\mathrm{a} = 40\,^\circ\mathrm{C}$ respectively $f_\mathrm{s} \geq 6000\,\mathrm{Hz}$ at $T_\mathrm{a} = 0\,^\circ\mathrm{C}$. Hence, these are theoretical boundaries, for practical usage an even higher sample frequency than two times higher is recommended.

In summary, such high sample frequencies are only used in special and exceptional practical cases and therefore, not used under general requirements. Concerning the *Monte-Carlos analysis* method, which means minimising the number of parameters, the inductive behaviour is neglected for further practical investigations. Thus, by only using a resistance to model this frequency area means, a reduction of the number of parameter by fifty percent.

### 4.2.2. EC modelling - small frequency area

The second area which is investigated in detail, is generated by the solid body diffusion and proposed as a series connection of a capacity and the so called *Warburg impedance* and properties are located at very small frequency values of $f < 0.01\,\mathrm{Hz}$. By considering this area in Figure 4.4, the diffusion process starts where the influences of the *Zarc* elements end. At this point a crossover into a nearly constant slight increase can be seen. Following by a kink, the behaviour ends up within a greater slope. Hence, the kink and increasing slope are not seen within the measurement data from Figure 4.5, but they are definitely there at smaller SOC levels.

To mathematically describe the crossover to the diffusion process, the *Warburg impedance* has become quite common. Due to the literature research, small deviations in the definition respectively within the modelling process were found but the principle is similar in nearly all cases. Thus, different possibilities to implement this behaviour are presented and evaluated in a next step.

A widely applied method to describe the *Warburg impedance* based on the electrical engineering point of view is with

$$\underline{Z}_{\mathrm{W}} = R\,\frac{\tanh\left(\sqrt{\mathrm{j}\,\omega\,\Theta}\right)}{\sqrt{\mathrm{j}\,\omega\,\Theta}} \tag{4.3}$$

where the resistance $R$ and the generalised capacity $\Theta$ represent the two *Warburg* constants and $\omega$ the frequency. This impedance presented in Equation (4.3) represents a linear slope with an angle of $45°$ and changes into a semicircle behaviour, see the solid black line in both plots of Figure 4.6.

Thus, by comparing the simulated design with the Nyquist plots in Figure 4.5, a good correlation between the measured data seems to be possible. Nevertheless, a different problem occurs by using this modelling approach from Equation (4.3). As already mentioned, model approaches are often used online within automotive applications. This means further that the designed models should also work in the time domain. Thus, a transformation of Equation (4.3) from frequency into the time domain is not possible.

Hence, instead of using totally different modelling approaches, approximations have become established. Two approximations based on electric elements, adapted from [Handschuh, 2007], are presented in Figure 4.6 and compared with the ideal *Warburg* element. The first approximation left, is a simple way to approximate the behaviour within a series connection of a resistor $R_1$ and a RC-element ($R_2$ and $C_2$), were the impedance for this approach is mathematically defined with

$$\underline{Z}_{\mathrm{appr,R+RC}} = R_1 + \frac{1}{1/R_2 + \mathrm{j}\,\omega\,C_2}\,. \tag{4.4}$$

For the definition of the parameters $R_1$, $R_2$, $C_2$ and the frequency $\omega_0$, where the spectrum reaches its minimum value, is required.
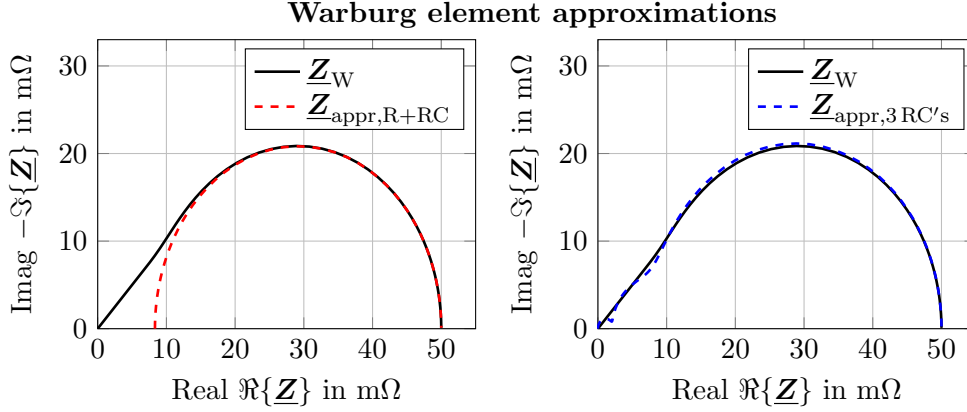
**Warburg element approximations**



Figure 4.6.: Nyquist plot of a *Warburg* element including two possible approximations; the black solid line represents the ideal element from Equation (4.3) with $R = 50\,\text{m}\Omega$ and $\Theta = 1000\,\text{F}$; left, an approximation with a resistance and a RC-element based on Equation (4.4); right, an approximation with three RC-elements based on Equation (4.5)

[Handschuh, 2007] showed that the value of $\omega_0$ is independent of $R$ and can be approximated well by $\omega_0 = 2.53/\Theta$. Furthermore, it was shown that the minimum value is only depending on the resistance. Finally, the parameters for the first approximation in Equation (4.4) can be defined with $R_1 = 1/6\,R$, $R_2 = 5/6\,R$ and $C_2 = 1/(\omega_0\,R_2)$.

By showing this approximation, it is clearly visible that the concordance at high frequencies is given very well but large discrepancies are given on the linear slope. Therefore, a second approximation is presented in [Handschuh, 2007]. To get a better approximation of the $45°$ slope, the resistance $R_1$ has to be separated in two additional RC-elements by

$$\underline{Z}_{\text{appr},3\,\text{RC's}} = \frac{1}{1/R_{1,1} + \text{j}\,\omega\,C_{1,1}} + \frac{1}{1/R_{1,2} + \text{j}\,\omega\,C_{1,2}} + \frac{1}{1/R_2 + \text{j}\,\omega\,C_2}\,, \qquad (4.5)$$

with the values $R_{1,1} = 1/24\,R$, $R_{1,2} = 3/24\,R$, $C_{1,1} = 1/100\,C_2$ and $C_{1,2} = 1/3\,C_2$. By comparing the second approximation with the ideal *Warburg* element in Figure 4.6 right, a sophisticated correlation in all frequency areas is given.

In summary, both methods developed from [Handschuh, 2007] can be used as an approximation of the *Warburg* element and are also transformable from the frequency into the time domain. Especially with the second method, a sophisticated correlation in all frequency areas is possible. Nevertheless, improving potential is given in the number of the parameters. Because, three parameters respectively six parameters and a sophisticated correlation seems not to be a satisfactory trade-off in the area of semi-physical modelling. However, the second approach turns out to be somehow more promising.

An alternative approach is based on the fundamental description from [Barsoukov & Macdonald, 2005]. Within their investigation, the *Warburg* element is defined with a more chemical based definition with

$$\underline{Z}_{\mathrm{W}} = \frac{c}{\sqrt{\mathrm{j}\,\omega\,D}}\,\tanh\left(\frac{l}{\sqrt{D}}\,\sqrt{\mathrm{j}\,\omega}\right)\,, \tag{4.6}$$

where the angular frequency $\omega$, diffusion coefficient $D$, diffusion length $l$ and some additional constant $c$ is used. Nevertheless, also this equation can not be transformed into the time domain. Anyway, [Mauracher & Karden, 1997] also tried to approximate Equation (4.6) by using RC-elements. Alternative to [Handschuh, 2007], *Mauracher etal.* transformed the equation in a way that first, a various number of RC-elements can be used and second, all RC-element parameter depends only on two main values. From the mathematical point of view, this correlation is given with

$$R_i \quad = \quad \omega_i\,\frac{c\,l}{D} = \omega_i\,R_\omega\,, \tag{4.7}$$

$$C_i \quad = \quad \frac{l}{2\,c} = C_\omega \quad \text{and} \tag{4.8}$$

$$\omega_i \quad = \quad \frac{8}{(2\,n-1)^2\,\pi^2}\,. \tag{4.9}$$

For a detailed derivation of these equations, reference to [Mauracher & Karden, 1997] is given. Finally, by using Equation (4.7) to (4.9) with various numbers of RC-elements $n$, the approximation of this method is presented in Figure 4.7.
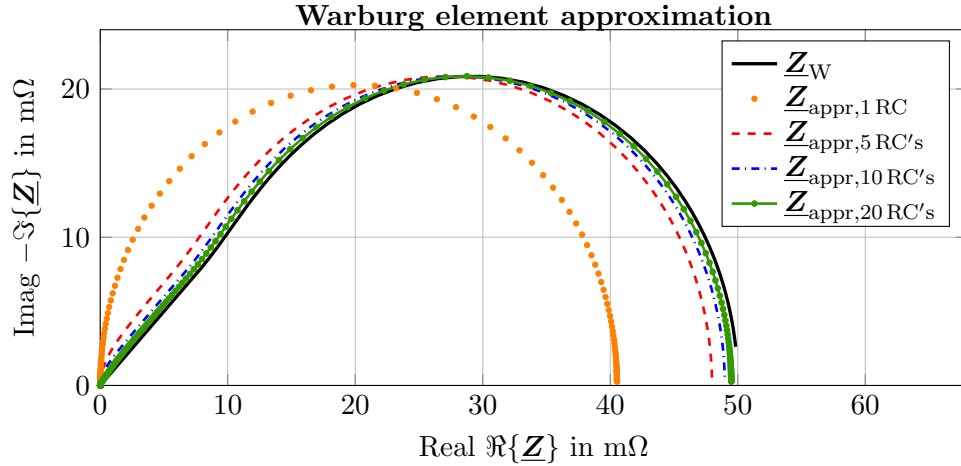


Figure 4.7.: Nyquist plot of a *Warburg* element including its approximation based on [Mauracher & Karden, 1997]. Within this approach a various number of RC-elements can be used; parameter defined with $R_\omega = 50\,\mathrm{m\Omega}$ and $C_\omega = 2500\,\mathrm{F}$

In Figure 4.7 the ideal *Warburg impedance*, black solid line, is compared with different approximations setups from 1 up to 20 RC-elements, coloured lines. It is clearly visible that with the increasing number of RC-elements less deviation occurs. Finally, the preferable number of elements always depends on the trade-off between calculation time and accuracy, respectively the problem requirements. Based on the recommendations form [Schweighofer et al., 2012] a good trade-off is given by using 10 RC-elements, which also correlates with the results from Figure 4.7.

In summary, this approach represents a sophisticated possibility to model the *Warburg impedance*. It was demonstrated that with the small number of only two parameters, the behaviour can be modelled quite well. Therefore, this approach is also used for further investigations.

Thus, comparing the model behaviour presented in Figure 4.7 with the experimental results from Figure 4.5, the two characteristics already match well at first glance. Nevertheless, by comparing the model characteristic with the theoretical results from Figure 4.4, only the behaviour until the kink can be modelled quite well. Furthermore, also during measurements at a very small SOC level, this behaviour is given with the used test cell. Therefore, also the second part must be considered when accuracy within a wide SOC range is desired.

To do so, by modelling this increasing characteristics with an electrical component, a capacity in series to the *Warburg impedance* is the first and also quite well choice, by remembering the element behaviour from Figure A.1. This means that the differential cell capacitance is modelled with a capacitor in addition. But instead of using an additional parameter, an implementation is quite common in the literature, can be used instead, see for example [Wegleiter & Schweighofer, 2017] or [Weber, 2018]. Because the internal differential capacitance depends also on the current SOC this information can be used in some kind. In detail, with the physical definition of the capacity by

$$C_0 = \frac{\mathrm{d}Q}{\mathrm{d}U} \tag{4.10}$$

where $\mathrm{d}Q$ is the electric charge and $\mathrm{d}U$ the voltage changes, where both caused by load current. Based on the knowledge that such a physical association is already defined, the OCV versus SOC characteristic can directly be used, see Figure 4.8. Thus, the SOC dependent capacity can be directly calculated and the behaviour is implemented without using an additional parameter. This implementation brings theoretical improvements because also the second part can be modelled but also show accuracy improvements during experimental investigations.

In summary, investigations to model the solid body diffusion processes inside the cell show that using a *Warburg impedance*, in series to a capacity, proves to be a good possibility. Thus, implementing the impedance within a model approach, based on [Mauracher & Karden, 1997], brings the advantage that various numbers of RC-elements can be used which relate only on two parameters. This leads to an accurate model behaviour including a practical parameterisation process.
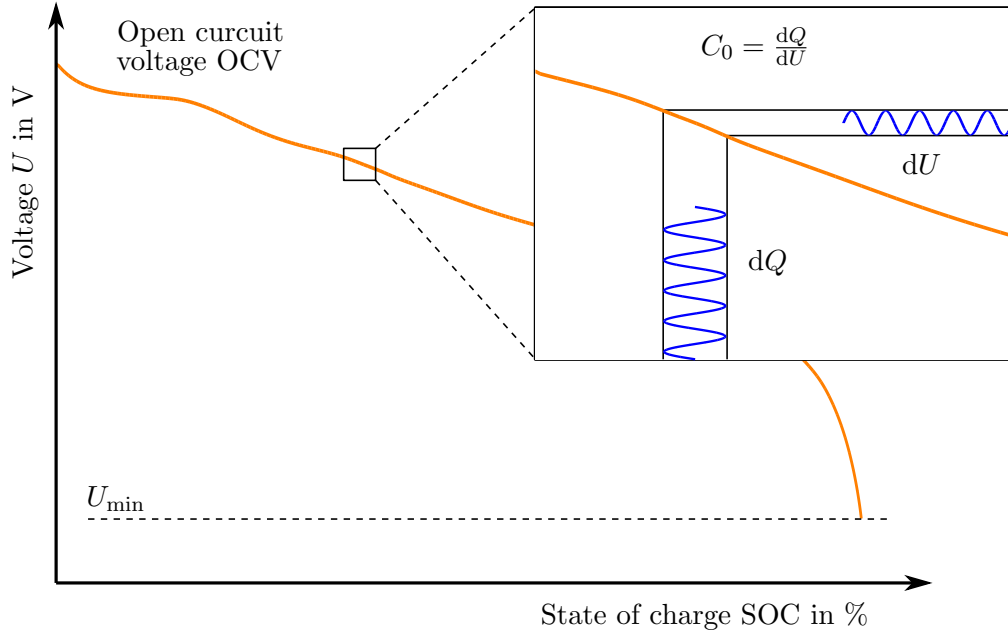
Figure 4.8.: Modelling of the differential capacitance based on the SOC charac-
teristic; the detailed zoom shows how the capacity is defined based
on the previously generated OCV versus SOC behaviour

Furthermore, the OCV versus SOC dependent capacity also brings model improvements
without an additional set of parameters. While such an effect is always preferable in
the area of semi-physical modelling. Thus, how well this model approach fits to the
measurement data is shown during the discussion about the last frequency range in the
next subsection.

### 4.2.3. EC modelling - middle frequency area

The third and last part is generated from the charge transfers in cathode and anode
as well as from the contact resistance in the cathode. The frequency range of these
processes is between $0.01 < f < 500\,\text{Hz}$ and therefore, in between the two frequency
areas presented in previous subsections. To model this effects, three *Zarc* elements have
been elaborated in the previous investigations, based on literature review.

*Zarc* elements are a parallel connection of a resistor $R$ and a *constant phase element*
(CPE), [Barsoukov & Macdonald, 2005]. CPEs considering a generalised capacity $\Theta$
and a depression factor $\psi$ and are mathematically defined by

$$\underline{Z}_{\text{CPE}} = \frac{1}{(\text{j}\,\omega)^{\psi}\,\Theta}\,, \tag{4.11}$$

and in parallel with the resistor $R$ it leads to the *Zarc* element by

$$\underline{Z}_{\mathrm{Zarc}} = \frac{1}{1/R + (\mathrm{j}\,\omega)^{\psi}\,\Theta}\,.$$ (4.12)

As already mentioned and also visible from Equation (4.12), the *Zarc* element is an extension of the RC-element by the depression factor $\psi$. This factor is valid between 0 and 1 and describes the depression of the semi circles in the Nyquist plot, see Figure 4.5. While for the boundaries $\psi = 1$, the *Zarc* element becomes a RC-element and by contrast $\psi = 0$, it becomes an ohmic resistance. Because especially lithium-ion cells have such depressions of the semi circles these properties are the main advantages of such *Zarc* elements. Thus, a more accurate model possibility can be achieved by using it. Nevertheless, the main disadvantage is given in the non-transferability into the time domain. So, an approximation is also needed if a *Zarc* element is used.

In summary, an easier to use approach is given with one or more RC-elements but higher accuracy can be achieved by using *Zarc* elements. Thus, do find the best choice for practical usage, model comparison based on the cell properties is recommended at this point. For the purpose of completeness it is mentioned that also literature does not agree either. Various publications are found with different configurations; just representing a few examples with **1 RC** [Huria et al., 2012], [Schweighofer et al., 2012]; **2 RC's** [Petzl & Danzer, 2013], [Somakettarin & Funaki, 2017] or [Kollmeyer et al., 2017]; and with one or more ***Zarc's*** [Andre et al., 2011b], [Buller, 2003] or [Weber, 2018].

Nevertheless, model selection and parameter reduction from the technical point in advance is always recommended. Thus, by looking at the measurement results from Figure 4.5 already a few main facts are seen to simplify the model selection:

- Charge transfer between cathode and electrolyte as well as anode and electrolyte are not very pronounced. This means that these two effects can be summarised to one *Zarc* element anyway

- Only one semicircle is visible at all. Which means, maybe one RC-element or one *Zarc* element is enough for the model application

- For all three setups a strong depression behaviour is evident. This means, a *Zarc* element or two RC-elements are preferable

Summarising, by looking at the measurement results from the technical point of view, three model structures should be finally validated based on model accuracy. A RC-element, a RCRC-model and a *Zarc* approach. Thus, based on the fact that the behaviour from $\mathrm{SOC} = 73.55\,\%$ and $\mathrm{SOC} = 38.27\,\%$ at temperature $T_{\mathrm{a}} = 0\,^{\circ}\mathrm{C}$ have a very close behaviour, only the first one is used. So, the model validation of the three model approaches elaborated, combined with the model elements defined previously, are applied on the two measurement setups with the different temperatures and presented in Figure 4.9 and Figure 4.10.
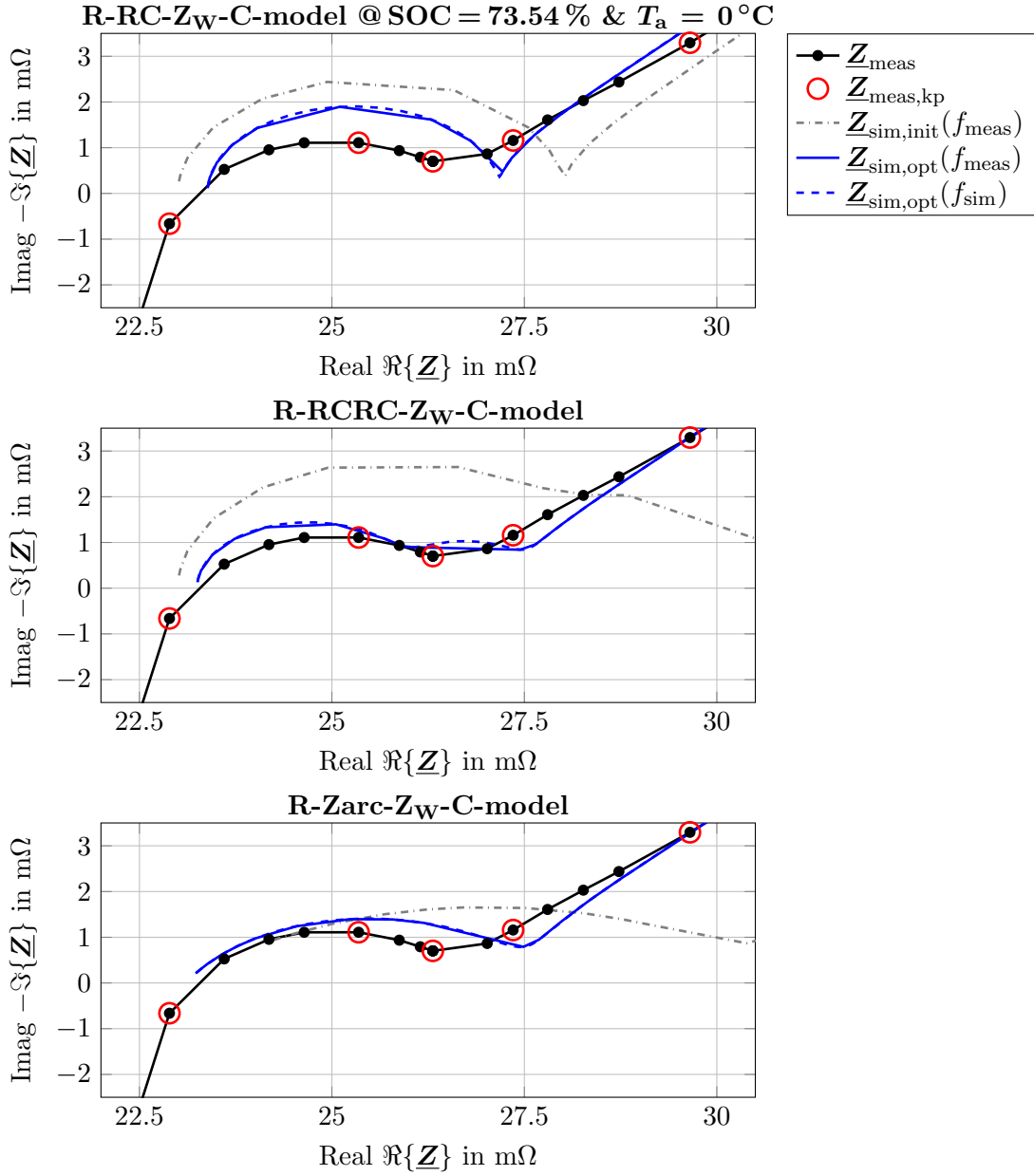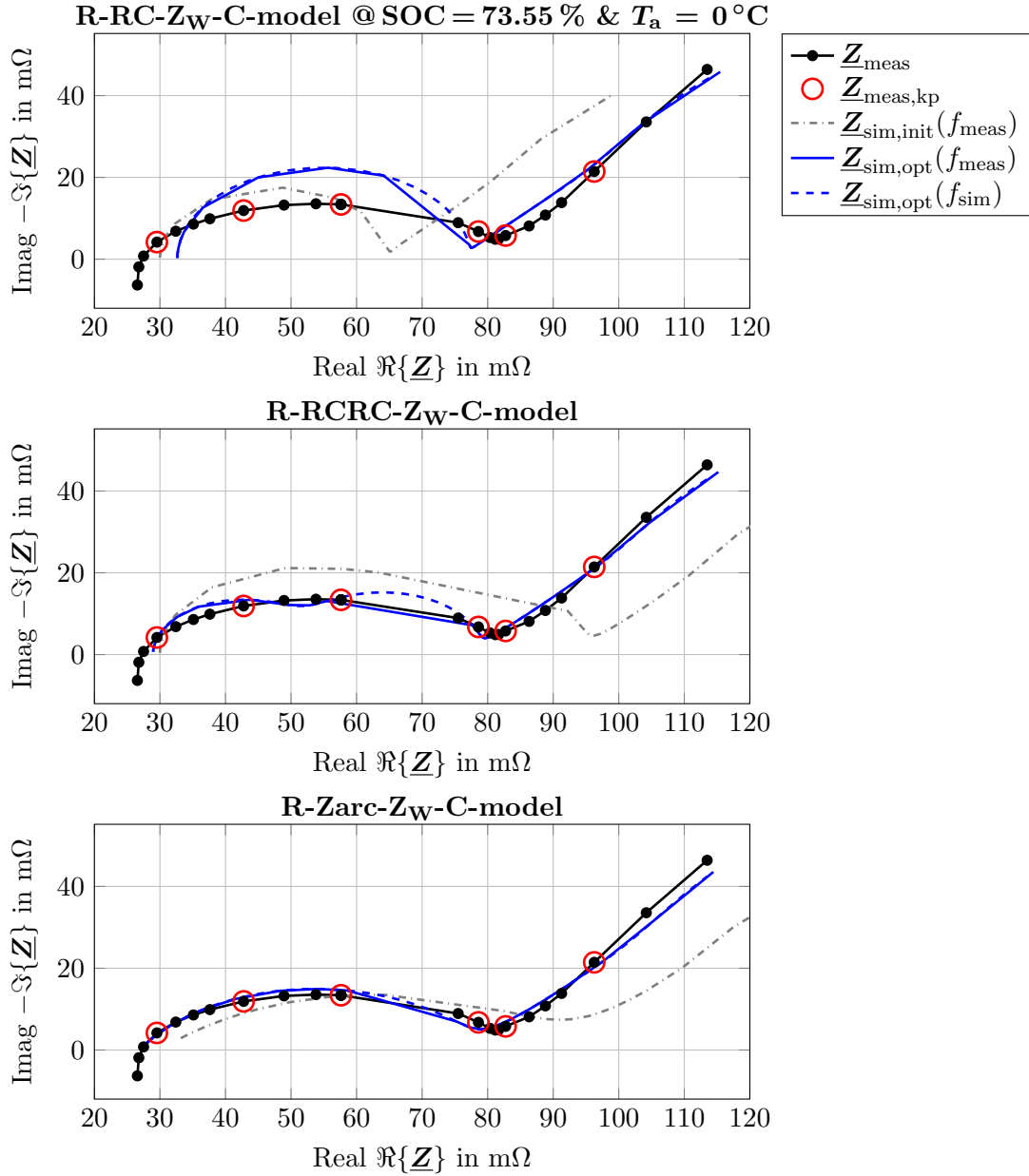
Figure 4.9.: Experimental investigations of various EC approaches within the Nyquist plot under temperature condition $T_a = 40\,°C$ and SOC $= 73.54\,\%$. For all approaches, measurement data $\underline{Z}_{meas}$ in black solid including marked key frequencies $\underline{Z}_{meas,kp}$ in red circuits, model behaviour with initial values $\underline{Z}_{sim,init}(f_{meas})$ in dash-dotted grey as well as the optimised model $\underline{Z}_{sim,opt}$ at the measured $f_{meas}$ and simulated $f_{sim}$ frequency range are presented. Thus, on top, a R-RC-$Z_W$-C model, in the middle R-RCRC-$Z_W$-C model and on the bottom a R-Zarc-$Z_W$-C model is compared with the measurement data

Figure 4.10.: Experimental investigations of various EC approaches within the Nyquist plot under temperature condition $T_{\mathrm{a}} = 0\,^{\circ}\mathrm{C}$ and SOC $= 73.55\,\%$. For all approaches, measurement data $\underline{Z}_{\mathrm{meas}}$ in black solid including marked key frequencies $\underline{Z}_{\mathrm{meas,kp}}$ in red circuits, model behaviour with initial values $\underline{Z}_{\mathrm{sim,init}}(f_{\mathrm{meas}})$ in dash-dotted grey as well as the optimised model $\underline{Z}_{\mathrm{sim,opt}}$ at the measured $f_{\mathrm{meas}}$ and simulated $f_{\mathrm{sim}}$ frequency range are presented. Thus, on top, a R-RC-$Z_{\mathrm{W}}$-C model, in the middle R-RCRC-$Z_{\mathrm{W}}$-C model and on the bottom a R-Zarc-$Z_{\mathrm{W}}$-C model is compared with the measurement data

The results of both temperature setups is given equally for Figure 4.9 and Figure 4.10. For all approaches, measurement data $\underline{\mathbf{Z}}_{\text{meas}}$ in black solid, including marked key frequencies $\underline{\mathbf{Z}}_{\text{meas,kp}}$ in red circuits, model behaviour with initial values $\underline{\mathbf{Z}}_{\text{sim,init}}(f_{\text{meas}})$ in dash-dotted grey as well as the optimised model $\underline{\mathbf{Z}}_{\text{sim,opt}}$ at the measured $f_{\text{meas}}$ and additionally simulated $f_{\text{sim}}$ frequency range are presented. Thus, on top, a R-RC-Z$_{\text{W}}$-C model, in the middle R-RCRC-Z$_{\text{W}}$-C model and on the bottom a R-Zarc-Z$_{\text{W}}$-C model is compared with the measurement data.

For both temperature levels the model including only one RC-element is not able to model the measurement behaviour sophisticated. As already discussed, lithium-ion cells have a high depression behaviour, which the RC-element can not handle for any parameter combination. In contrast to the first approach both others are able to handle model description better. While, within in the centre plot, it is clearly visible that the model approach with the two RC elements tries to use smaller semicircles to handle the depression. Nevertheless, the *Zarc* element shows best match to the measurement data, especially at the lower temperature in Figure 4.10. A further advantage at this approach is seen because also a good model accuracy is given at very low and high frequencies, which indicates a good general model behaviour as well.

In summary, all three model approaches have advantages and disadvantages within their approaches. While one RC-element is easy to handle but brings inaccuracy in comparison to the measurement data. On the opposite, the *Zarc* element brings a high accuracy but higher number of parameters and additional effort on transformation into the time domain. Finally, the *Zarc* element has been chosen for further investigations. Main advantages are the high accuracy at main frequency areas and the lower number of parameters in comparison to two RC-elements. Nevertheless, the transformation behaviour has to be discussed next, to confirm this decision.

**Approximation of the Zarc element**

To model the semicircles behaviour within the Nyquist plot, one *Zarc* element has been proven to be a good solution for the used test cell. Nevertheless, in contracts to the positive modelling properties, the non-transferability into the time domain is definitive a disadvantage. Therefore, like for the *Warburg impedance*, an approximation is needed as well. Thus, approximations by using one or more RC-elements is the most common approach found in the literature. So, three different model approaches are presented, compared and evaluated for further usage. For detailed information, reference to [Buller, 2003] is given.

Thus, the depression behaviour of the semicircle of the *Zarc* element is preferably modelled by an uneven number of RC-elements. For the first approach, five RC circuits (A . . . E) are chosen. Thereby, the characteristic of the main semicircle in the middle (index C) is chosen with the same characteristic of the *Zarc* element. So, the diameter

of the semicircle C is calculated by

$$R_\mathrm{C} = f_1(\psi)\, R\, \frac{\sin\left(\frac{\pi}{2}\,\psi\right)}{1 + \cos\left(\frac{\pi}{2}\,\psi\right)}\,, \tag{4.13}$$

where $R$ and $\psi$ are the resistance and depression factor of the *Zarc* element, respectively. In addition, the term $f_1(\psi)$ is defined as an amplitude factor, depending on the depression and has been defined offline. Belonging to the resistance, the capacitance $C_\mathrm{C}$ of the semicircle C is calculated by

$$C_\mathrm{C} = \frac{1}{\omega_{0,Zarc}\, R_\mathrm{C}}\,, \tag{4.14}$$

where $\omega_{0,\mathrm{Zarc}}$ is defined out of the *Zarc* parameter with

$$\omega_{0,\mathrm{Zarc}} = \left(\frac{1}{R\,\Theta}\right)^{\frac{1}{\psi}}\,. \tag{4.15}$$

Due to symmetry reasons, the diameters of the two RC elements neighbouring (B and D) are chosen equally. Thus, the resistances $R_\mathrm{B}$ and $R_\mathrm{D}$ are calculated with

$$R_\mathrm{B} = R_\mathrm{D} = f_2(\psi)\, \frac{R - R_\mathrm{C}}{2}\,, \tag{4.16}$$

where $f_2(\psi)$ is defined as the second optimisation factor. Following, the associated capacitances of the semicircles B and D are given with

$$C_\mathrm{B} = \frac{1}{\omega_{0,\mathrm{Zarc}}\, f_3(\psi)\, R_\mathrm{B}} \quad \text{and} \quad C_\mathrm{D} = \frac{1}{\omega_{0,\mathrm{Zarc}}\, \frac{1}{f_3(\psi)}\, R_\mathrm{D}}\,, \tag{4.17}$$

where $f_3(\psi)$ is the third optimisation factor. Finally, the parameters of the two remaining semicircles A and E are defined in a way that the boundary condition with $R = R_\mathrm{A} + R_\mathrm{B} + R_\mathrm{C} + R_\mathrm{D} + R_\mathrm{E}$ is fulfilled. This leads to the mathematical definition for the resistances

$$R_\mathrm{A} = R_\mathrm{E} = \frac{R - R_\mathrm{C} - R_\mathrm{B} - R_\mathrm{D}}{2}\,, \tag{4.18}$$

and the capacitances

$$C_\mathrm{A} = \frac{1}{\omega_{0,\mathrm{Zarc}}\, f_3(\psi)^2\, R_\mathrm{B}} \quad \text{and} \quad C_\mathrm{D} = \frac{1}{\omega_{0,\mathrm{Zarc}}\, \frac{1}{f_3(\psi)^2}\, R_\mathrm{D}}\,. \tag{4.19}$$

In summary, after parameterising the *Zarc* element in the Nyquist plot, like in Figure 4.10, the three optimisation parameters $f_1(\psi)$, $f_2(\psi)$ and $f_3(\psi)$ need to be defined. To do so and using Equation (4.13) to Equation (4.19), this implementation is presented in Figure 4.11 representatively.
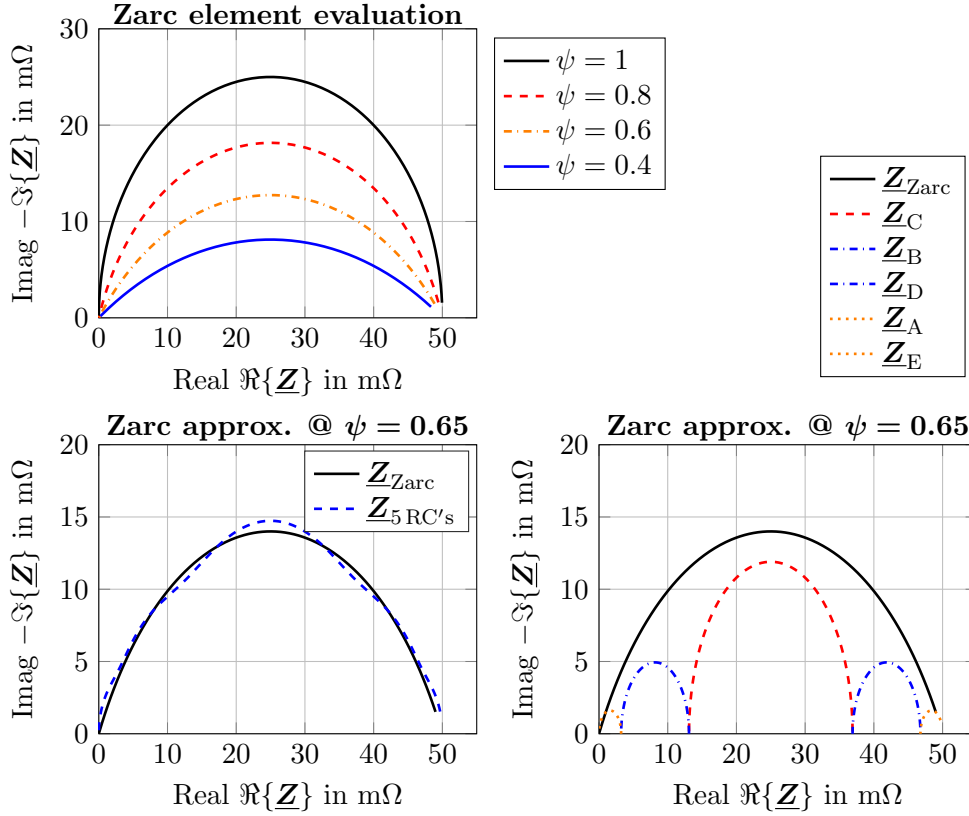
Figure 4.11.: Approximation of the *Zarc* element by means of five RC-elements; upper left, depression factor $\psi$ definition respectively; bottom right, the calculated RC-elements using Equation (4.13) to Equation (4.19); bottom left, comparison of the ideal *Zarc* element $\underline{Z}_{\text{Zarc}}$ with the approximated approach based on five RC-elements $\underline{Z}_{5\,\text{RC}'\text{s}}$

In the upper plot of Figure 4.11 the *Zarc* behaviour, based on different depression values $\psi$, is given. Following, by parameterising the *Zarc* with measurement data, a value with $\psi = 0.65$ is defined representatively. Next, the five RC-elements can be calculated by using Equation (4.13) to Equation (4.19) separately, see the bottom right plot. By putting all five circuits in series, the depressed semicircle from the *Zarc* element can be modelled quite well, see bottom left plot. In summary, this shows that using five RC-elements in series, parameterised out of the *Zarc* values and the three optimisation parameters, the *Zarc* can be modelled sophisticated.

Nevertheless, two simplified approaches are presented and validated in addition. Thus, the most obvious simplification is to reduce the number of employed RC circuits from five to three, as a second approach. Hence, this reduces the number of parameters from 3 to 2 but further reduction is still possible.

The two approximation procedures so far, propose a large central semicircle and at least two smaller neighbouring RC circuits with higher or lower characteristic frequencies. Thus, the basic idea behind the next simplification is to model the *Zarc* by means of three RC-elements of equal diameter. This means further that also one parameter set is needed for the parameterisation. Hence, to define the resistance with one third of the *Zarc* diameter each value can be defined with

$$R_{\mathrm{A}} = R_{\mathrm{B}} = R_{\mathrm{C}} = \frac{R}{3} \, . \tag{4.20}$$

In addition, the corresponding capacitances are calculated with

$$C_{\mathrm{B}} = \frac{1}{\omega_{0,\mathrm{Zarc}} \, \frac{R}{3}} \quad , \quad C_{\mathrm{A}} = \frac{C_{\mathrm{B}}}{f(\psi)} \quad \text{and} \quad C_{\mathrm{C}} = C_{\mathrm{B}} \, f(\psi) \, , \tag{4.21}$$

where $f(\psi)$ represents the optimisation factor based on the depression. With this application a less accurate adaptation is possible, but only one parameter has to be defined offline. Thus, to validate the three approaches, based on model performance, a comparison is presented in Figure 4.12. On the upper left plot, the already presented approximation with $5$ RC-elements is given as a benchmark. As first simplification, the approach based on $3$ RC-elements is given in the upper right plot. It is seen that a lower accuracy is given with this approach overall. The third setup with the three constant RC-elements is presented in the bottom left plot. Also with this approach, accuracy is lost by using less numbers of RC-elements. On the fourth plot, the overall comparison is given for the purpose of completeness. It is clearly visible that the approach, based on five RC circuits brings the best model performance. Nevertheless, accuracies of the two others are good as well.

In summary, three approaches are presented to model the *Zarc* element within a various number of RC-element. Like in the two frequency areas discussed previously, a trade-off between accuracy and number of parameters is given. Thus, also at this point a decision has to be made for further usage. The decision for the third approach, using three constant RC-elements, has been made. Hence, implementation from the practical point of view is easy and the accuracy is sophisticated.

Finally, with the definition of the model approach for this frequency area, the model process is finished. Before, the defined model approach is evaluated, based on different influences, like SOC levels, temperatures and load currents, major outcomes are summarised and the final model is presented in the next subsection.
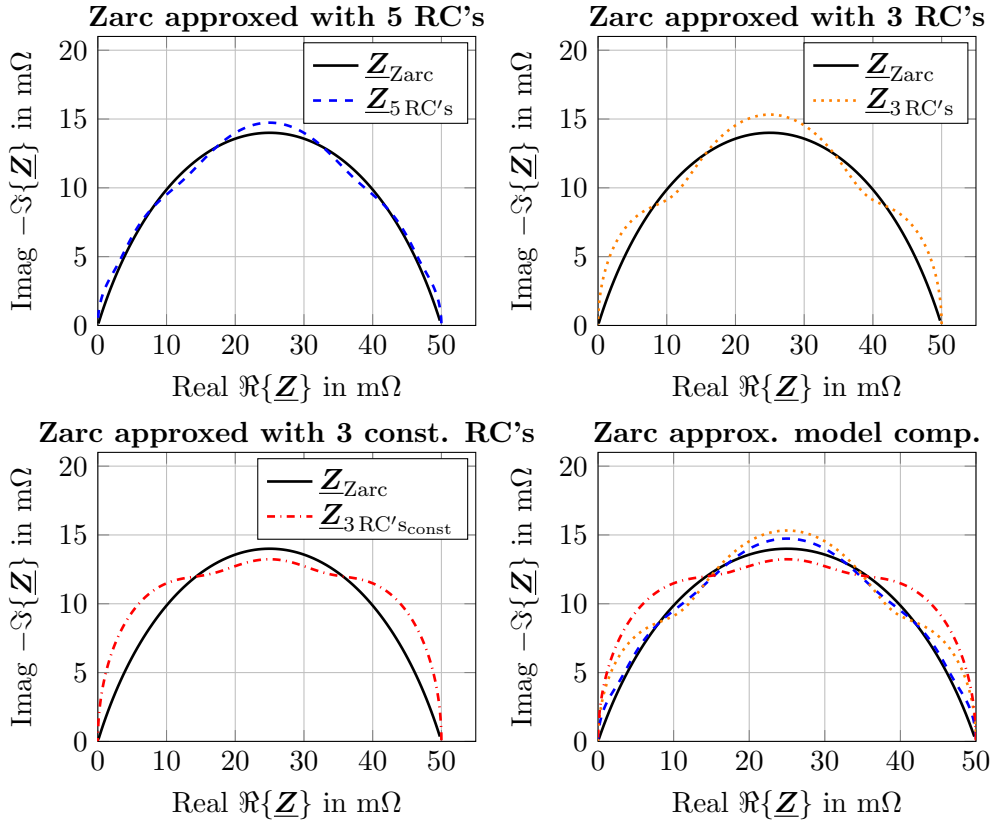
Figure 4.12.: Approximation of the *Zarc* element by different approaches; upper two plots, the applications based on five (left) respectively three (right) RC-elements are presented; bottom left, an application on three RC-elements with constant parameters is given; bottom right, comparison of all three approaches are shown

### 4.2.4. Conclusion of equivalent electric circuit modelling process

After the discussion and definition of the three frequency areas, the overall equivalent electric circuit can be merged together, see Figure 4.13. The fundamental of this model forms the steady-state OCV versus SOC characteristic from Chapter 3. Out of their behaviour also the internal differential capacitance $C_0$ is defined without using an additional parameter to parameterise.

Following, the steady-state characteristics, the additional electric circuit elements are set in series to model the transient behaviour of the battery cell. The first element is defined by an electric resistance $R_0$ and describes the electrical and ionic conductivities. In addition, a so called *Zarc* element $\underline{Z}_{\mathrm{Zarc}}$ is used, which defines the cell behaviour in mid size frequency areas. This *Zarc* element is defined by a resistance $R_{\mathrm{Zarc}}$, a generalised capacity $\Theta$ and a depression factor $\psi$.
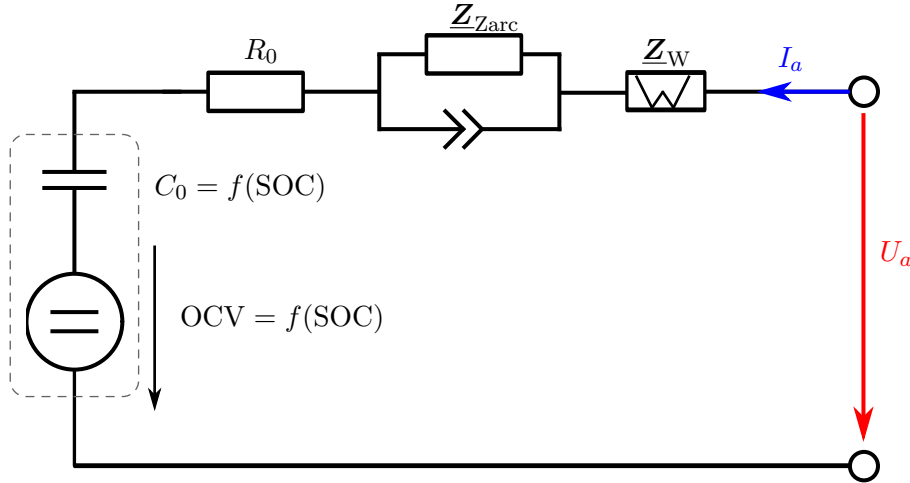
Figure 4.13.: Elaborated equivalent electric circuit for the used test cell of type Samsung INR18650-35E (Pink). Finally the circle is defined by a resistor $R_0$, one *Zarc* element $\underline{\mathbf{Z}}_{\text{Zarc}}$ and a *Warburg impedance* $\underline{\mathbf{Z}}_{\text{W}}$

After defining this three parameters in the Nyquist plot, an optimisation factor, respectively a depression factor, dependent characteristic $f(\psi)$ has to be defined offline to be able to transform the *Zarc* element into the time domain. In addition, the diffusion process is modelled by a *Warburg impedance* $\underline{\mathbf{Z}}_{\text{W}}$. The approximation in this work is done by a series connection of ten RC-elements, where the values of these elements depend on the two parameters, namely the *Warburg* resistance $R_{\text{W}}$ and *Warburg* capacity $C_{\text{W}}$. Finally, the needed set of parameters is summarised in Table 4.2.

In the next chapter, this elaborated EC is used and validated based on different SOC levels, temperatures and load currents. Thus, influences of these effects on the parameters as well an overall validation is given.

Table 4.2.: Parameter description for the elaborated equivalent electric circuit worked out for the used test cell of type Samsung INR18650-35E (Pink)

| Circuit element | Number of parameters | Parameter description |
|---|---|---|
| Resistance $R_0$ | 1 | Electrical resistance $R_0$ |
| *Zarc* element $\underline{\mathbf{Z}}_{\text{Zarc}}$ | 3 | *Zarc* resistance $R_{\text{Zarc}}$ |
| | | Generalised capacity $\Theta$ |
| | | Depression factor $\psi$ |
| *Warburg impedance* $\underline{\mathbf{Z}}_{\text{W}}$ | 2 | *Warburg* resistance $R_{\text{W}}$ |
| | | *Warburg* capacity $C_{\text{W}}$ |

## 4.3. Comparative conclusion of the transient modelling process

To model an accurate battery cell behaviour, two main parts are needed. First, a well defined OCV versus SOC characteristic, which was done in Chapter 3. Second, an equivalent electric circuit is needed which is able to model the transient battery cell behaviour which was the goal of this chapter. Thus, before modelling started, focus on system dynamics of internal processes was given. This evaluation has shown that behaviour inside the cell is given with a wide time range from a few micro seconds up to ten thousand of hours. During this description, decision was made to focus on electro chemical reactions as well as on diffusion processes based on applications which occur during driving.

Even if only these two processes are considered, a wide time range is needed. Thus, this fact of course has an influence on modelling, parameterisation and measurement processes at all. Therefore, beside working in the time domain, a further method called EIS has become quite common nowadays. Because this approach is also used within this thesis investigation an overview about the EIS concept was presented next. Based on the outcome of this method an extended theoretical model, based on internal chemical processes, was derived.

The second part of this chapter focused on the modelling design of the thesis model approach, related to the requirements and the cell behaviour. Thus the goal was defined to find an accurate model approach but with less complexity as well as a low number of parameters. To do so, three frequency areas were investigated in detail based on measurement data and the model defined finally. The large frequency area has shown that inductive behaviour is existing but modelling not practicable. The small frequency area is modelled within a capacity and a *Warburg* element. Thus, approximating the *Warburg* element with a series connection of various RC-elements which are related to each other and the capacity based on the SOC behaviour, only two parameters are needed. In addition, the third area around middle size frequencies is modelled by only one *Zarc* element. This decision was made by an elaborated comparison within different numbers of RC-elements.

Finally, a semi-physical model approach was presented, based on these three areas. This approach only includes three elements while six parameters for parameterisation are needed. In an next step, different influences, like SOC level, temperature and C-rate are applied on the model. Thus overall model accuracy as well as the influence on the parameters are investigated in detail in Chapter 5.

# 5

# Electric circuit model validation based on external influences

During the last chapters, the stepwise modelling process of an *equivalent electric circuit* (EC) was presented. This started from basic theoretical investigations and requirements in Chapter 2, followed by the generation of the steady-state *open circuit voltage* (OCV) versus *state of charge* (SOC) characteristic in Chapter 3 and ended by modelling the transient cell behaviour by means of electric elements in Chapter 4. Thus, parameterisation and validation of the overall model presented, is focus of this chapter.

Because it is theoretical and practical impossible to keep the SOC constant during charging or discharging, the first section starts with influences of changing SOC levels. To do so, *electrical impedance spectroscopy* (EIS) measurements are done at different SOC levels and behaviour discussed within the Nyquist plot. Furthermore, influences on the parameter setup are presented and discussed. Finally, an analysis about those parameters which could be independent on SOC influences gives an outlook about the possibility to decrease the parameterisation effort. Following, changes in environmental temperature is presented as second influence. Thus the two measured temperatures are used to compare the parameterisation based on the temperature. In addition, outcomes from the SOC changes are evaluated on both temperatures as well.

After discussion, results presentation and model validation by means of different SOC levels and environmental temperatures, changes of the load current are given. It is shown that a model, parameterised by a constant EIS current, is not able to handle various C-rates. Therefore, the influence on current changes, also called *Buttler Volmer* (BV) effect in the literature, has to be investigated in detail. Based on the EIS results, a semi-physical model approach to handle the BV effect is presented. Finally the results are compared with and without the model extension, based on measurement data.

For the purpose of completeness, the model is parameterised and validated by means of a pulse manoeuvre within the time domain in the last part of this chapter. Thus, goal is to compare the results based on parameterising the EC model within the time domain and by using the EIS method. To do so, results are compared in the Nyquist plot as well as within the pulse manoeuvre.

Finally, the chapter ends with an overall conclusion and a recommendation for further research steps.

## 5.1. SOC dependent influences on the model behaviour

First and main influencing behaviour, which will be investigated in detail, are changes on the SOC level. Because it not possible to keep the SOC constant, during charging or discharging, the behaviour has a main influence of the cell characteristics under usage. To investigate this behaviour in detail, the already known EIS procedure will be used and results evaluated for various SOC levels.

To do so, the SOC levels are chosen with $\text{SOC}_{\text{EIS}} = \{91.18, 82.36, 73.54, 64.72, 55.93, 47.09, 38.25, 29.42, 20.59, 11.79, 3.02\}\,\%$ and applied at an ambient temperature of $T_{\text{a}} = 40\,°\text{C}$. Thus, the results are presented in Figure 5.1 where only every second $\text{SOC}_{\{1,3,5,7,9,11\}}$ level is given for a better representation.
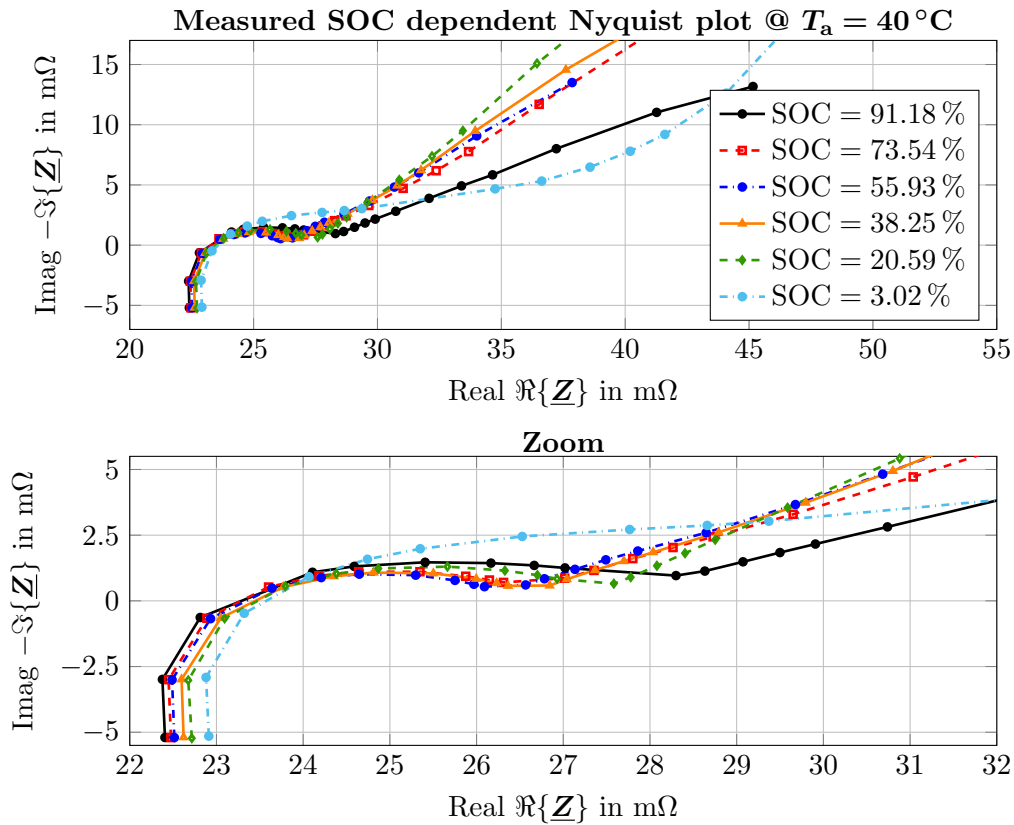


Figure 5.1.: Nyquist plot to evaluate the SOC dependent influence on the cell behaviour at an ambient temperature of $T_{\text{a}} = 40\,°\text{C}$. For a clear representation only every second SOC level measured is presented. The upper plot represents the cell behaviour for the six defined SOC levels. In addition, a detailed view on large and middle frequency ranges is given in the bottom plot

In the upper plot of Figure 5.1 the overall cell behaviour for the various SOC levels is presented. While in the bottom plot, a detailed view for large and middle frequency areas is given. Thus, with the exception of the largest one at $SOC1 = 91.18\,\%$ and the total outlier behaviour at $SOC_{11} = 3.02\,\%$, a very similar behaviour for the whole frequency range is given for all SOC states.

If a closer look at the zero crossing real axis is given, a slightly increasing behaviour within decreasing SOC level is recognisable. This suggests an increasing resistance at smaller SOC level. Furthermore, quite similar depression as well as *Zarc* behaviour is given within the four levels $SOC_{3 \to 9}$. This means, also parameter behaviour should be quite similar in this area. Same characteristic is seen within the diffusion process. Nevertheless, very different behaviour at large and very small SOC levels is given. Thus, this confirms that most cells are only used around $20\,\% < SOC < 90\,\%$ in practice.

In a next step, the elaborated model from Figure 4.13 is parameterised, respectively optimised, for each SOC level separately by minimising the error between measured and simulated behaviour. The comparative results, generated out of the six $SOC_{1:2:11}$ levels, are presented in Figure 5.2. Thus, the comparison at a different SOC levels are given in each plot. The black solid line represents the measured EIS and the red dashed line the behaviour generated by the parameterised model.

It is visible, that the parameterised model is able to handle the measured behaviour satisfactorily, except at $SOC_{11} = 3.02\,\%$. This shows that close to a total empty cell the behaviour is quite different. However, a higher capacity than the one generated out of the OCV characteristic would bring a first and easy to implement remedy. Furthermore, this behaviour of a not perfect match of the diffusion process can already be seen at $SOC_9 = 20.59\,\%$. To summarise, the capacity defined out of the OCV characteristic brings satisfactory model properties at middle and large SOC levels, but for a detailed model behaviour at very low SOC levels, the capacity needs to be re-parameterised.

Nevertheless, beside this deviations at the diffusion around small SOC levels, a good match between measured and simulated data is given for all levels. Especially the decision to use a *Zarc* element seems to be a good choice. According to the simulation validation, the SOC dependent parameters are given in Figure 5.3 for each element.

Starting from the top right, the parameterised resistance $R_0$ for the used $SOC_{EIS}$ levels are presented. Hence, the slightly decreasing behaviour for larger SOC levels confirm the characteristics from Figure 5.1. The top right and the two middle plots representing the three parameters responsible for the *Zarc* element. Especially, for the depression factor $\psi_{Zarc}$ a nearly constant behaviour is given. In addition it seems that the two resistances $R_{Zarc}$ and $R_W$ are not so sensitive by changing SOC, especially at middle levels. Thus, most varying elements are the two capacities $\Theta_{Zarc}$ and $C_W$.

In summary, the elaborated EC is able to handle various SOC levels well. By evaluating Figure 5.3, it seems that especially the resistance $R_0$ and the depression factor $\psi_{Zarc}$ are nearly independent on the SOC, while main influence is given by the two capacities $\Theta_{Zarc}$ and $C_W$. In addition, the further two resistances $R_{Zarc}$ and $R_W$ can also kept constant, if no SOC state close to the boundaries has to be modelled.
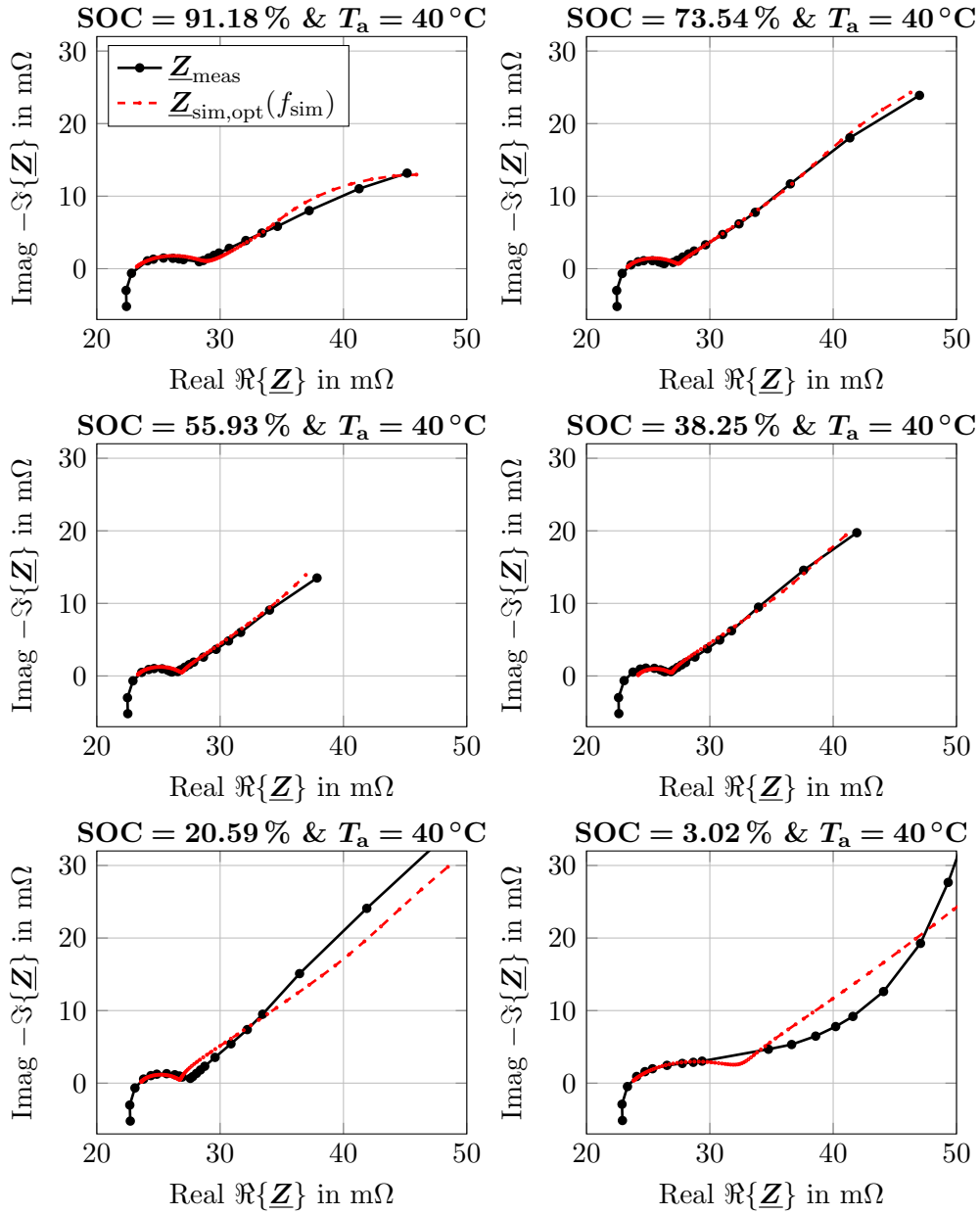
71

Figure 5.2.: Nyquist plot to validate the elaborated EC model dependent on various SOC states at an ambient temperature of $T_\mathrm{a} = 40\,°\mathrm{C}$. The presented six plots present different SOC levels each, while the black solid line represents the measured EIS behaviour $\underline{Z}_\mathrm{meas}$ and the red dashed line the characteristic generated out of the EC $\underline{Z}_\mathrm{sim,opt}(f_\mathrm{sim})$
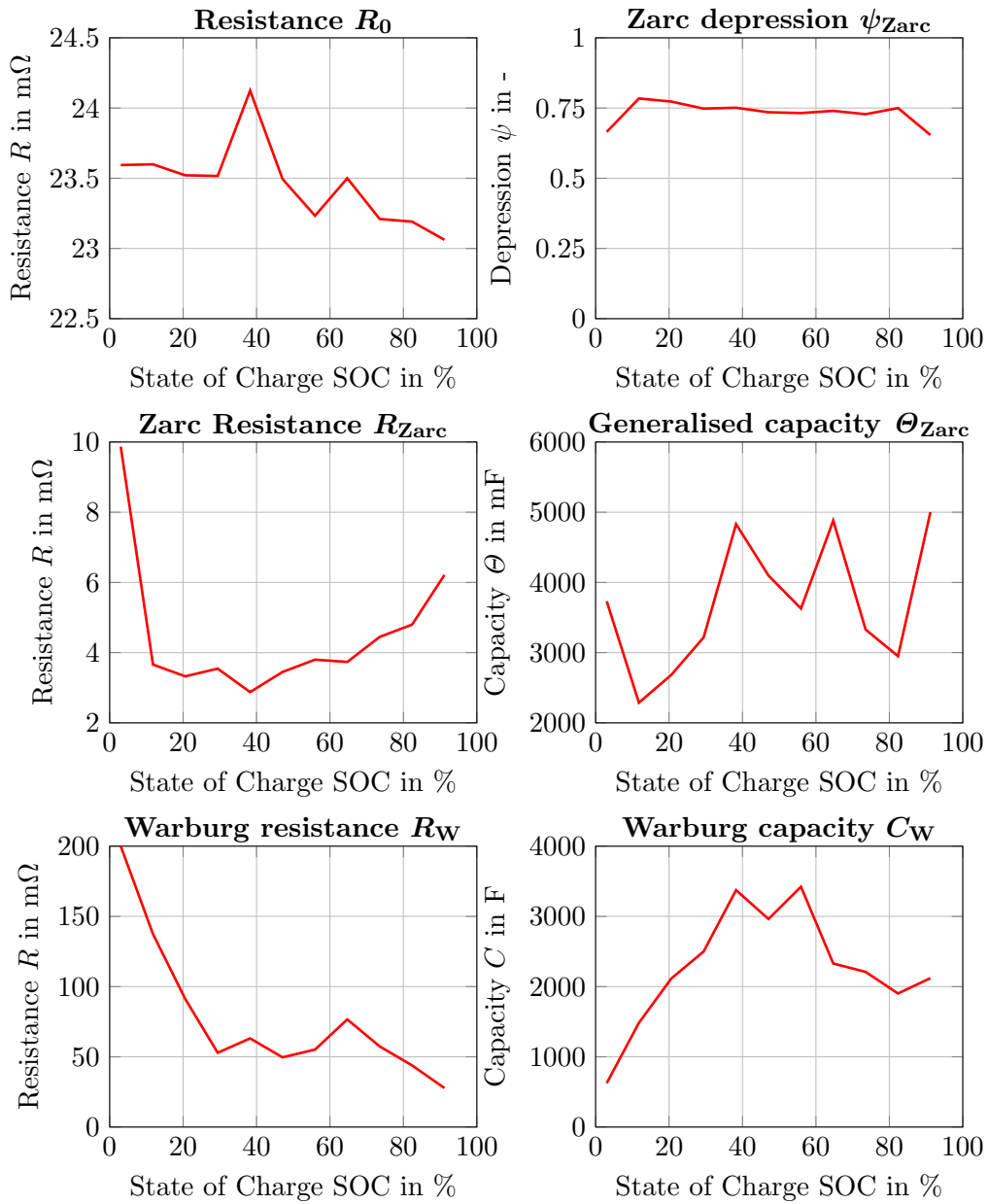
Figure 5.3.: Equivalent electric circuit parameter estimation for various SOC states and an ambient temperature of $T_{\mathrm{a}} = 40\,^{\circ}\mathrm{C}$; top left, behaviour of the resistance $R_0$ is shown; top right and the two middle plots represent the *Zarc* element; the two bottom plots show the behaviour from the *Warburg impedance*

## 5.2. Temperature dependent influences on the model behaviour

The second influence which is investigated in detail is the ambient temperature. Thus, because only two different temperatures are measured during the project, detailed presentation of the parameter behaviour depending on various temperatures is not possible. Therefore, cell behaviour investigations and model validation for the wide $SOC_{EIS}$ range is done, based on the second ambient temperature $T_a = 0\,°C$, like in the previous section. Afterwards, the model parameters gained, are compared with the two different temperatures. To do so, the results for the measured EIS characteristics for the different SOC levels at ambient temperature of $T_a = 0\,°C$ are presented in Figure 5.4.
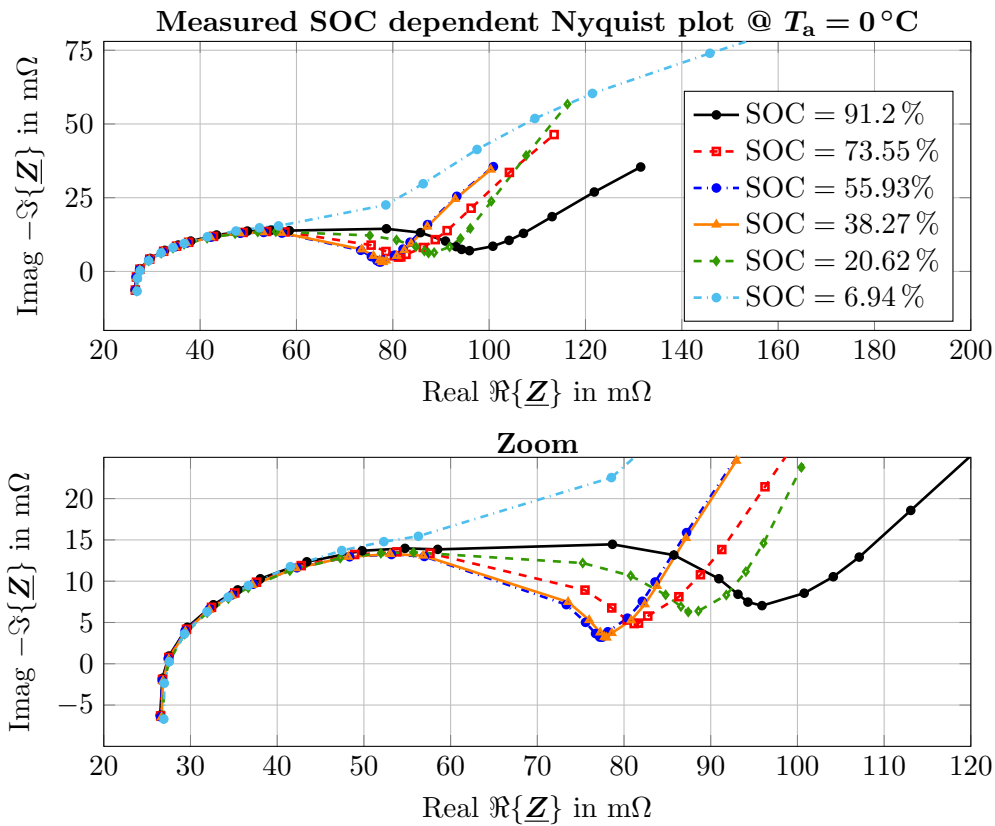


Figure 5.4.: Nyquist plot to evaluate the SOC dependent influence on the cell behaviour at an ambient temperature of $T_a = 0\,°C$. For a clear representation only every second SOC level done is presented. The upper plot represents the cell behaviour for the six defined SOC levels. In addition, a detailed view on large and middle frequency ranges is given in the bottom plot

Overall, a very similar behaviour to the results at $T_a = 40\,°\mathrm{C}$ from Figure 5.1 is evident at the first glance. However, larger differences are given on the axis scaling, on closer inspection. While the scaling of the imaginary axis was only around a few m$\Omega$ at $T_a = 40\,°\mathrm{C}$, at lower temperature around $T_a = 0\,°\mathrm{C}$ it is about ten times larger. Thus, this is definitely a difference to the behaviour at smaller temperatures.

Nevertheless, by investigating the characteristic itself, nearly no influences at high frequencies are given for the different SOC levels. This means in detail, especially the values of the resistance $R_0$ and the *Zarc* element $\underline{\boldsymbol{Z}}_{\mathrm{Zarc}}$ should be quite constant. Furthermore, smaller influences at small SOC levels are presented. In addition, different behaviour is given at the largest level at $\mathrm{SOC}_1 = 91.2\,\%$ and the total outlier behaviour at $\mathrm{SOC}_{11} = 6.94\,\%$. Which is a very similar behaviour to the higher temperature level.

By validating the model results presented in Figure 5.5, a similar behaviour to the higher temperature is seen. Especially for $\mathrm{SOC} > 20\,\%$ a very good match between measured and simulated data is given. In contrast, looking at the lowest SOC level, at the bottom right plot, the model is definitive not able to handle the measured characteristic. Therefore, if a higher model accuracy around this SOC area is needed, a re-work design of the model is recommended.

Finally, the parameters of the modelling process for the two different temperatures are presented in Figure 5.6. It is clearly visible that the temperature has an influence on nearly all model parameters. Only, the depression factor of the *Zarc* element is closer. By comparing the resistance behaviour $R_0$ within the two different temperatures, for both, a nearly SOC independent behaviour is seen. This confirms the previous statement to keep this parameter constant based on the SOC level. By comparing the values of the *Zarc* element, a quite constant parameter behaviour over the SOC level is given as well. Thus, a SOC independent implementation is recommended. Finally, highest influences on SOC are given for the *Warburg* parameter.

In summary, the elaborated EC is also able to handle the behaviour at very low temperatures well. It was also presented, that all model parameters are sensitive to the temperature. This means, if the model should be able to handle a wide range of temperatures, this behaviour should be implemented in all model values. To reduce parameter complexity, it seems the resistance $R_0$ and the *Zarc* parameter can be implemented SOC independent out of this results.
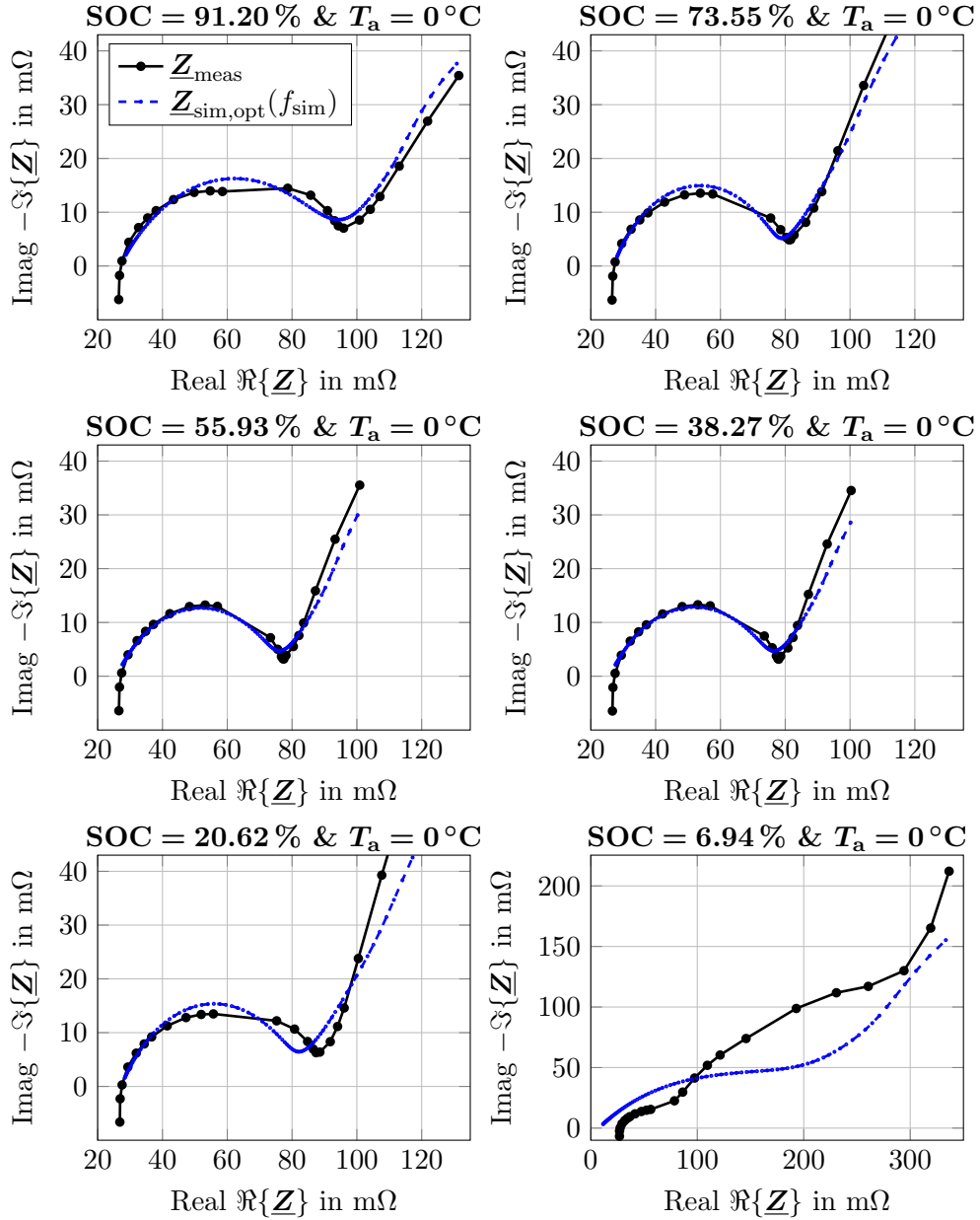
Figure 5.5.: Nyquist plot to validate the elaborated EC model dependent on various SOC states at an ambient temperature of $T_a = 0\,^\circ\text{C}$. The presented six plots present different SOC levels each, while the black solid line represents the measured EIS behaviour $\underline{Z}_\text{meas}$ and the blue dashed line the characteristic generated out of the EC $\underline{Z}_\text{sim,opt}(f_\text{sim})$
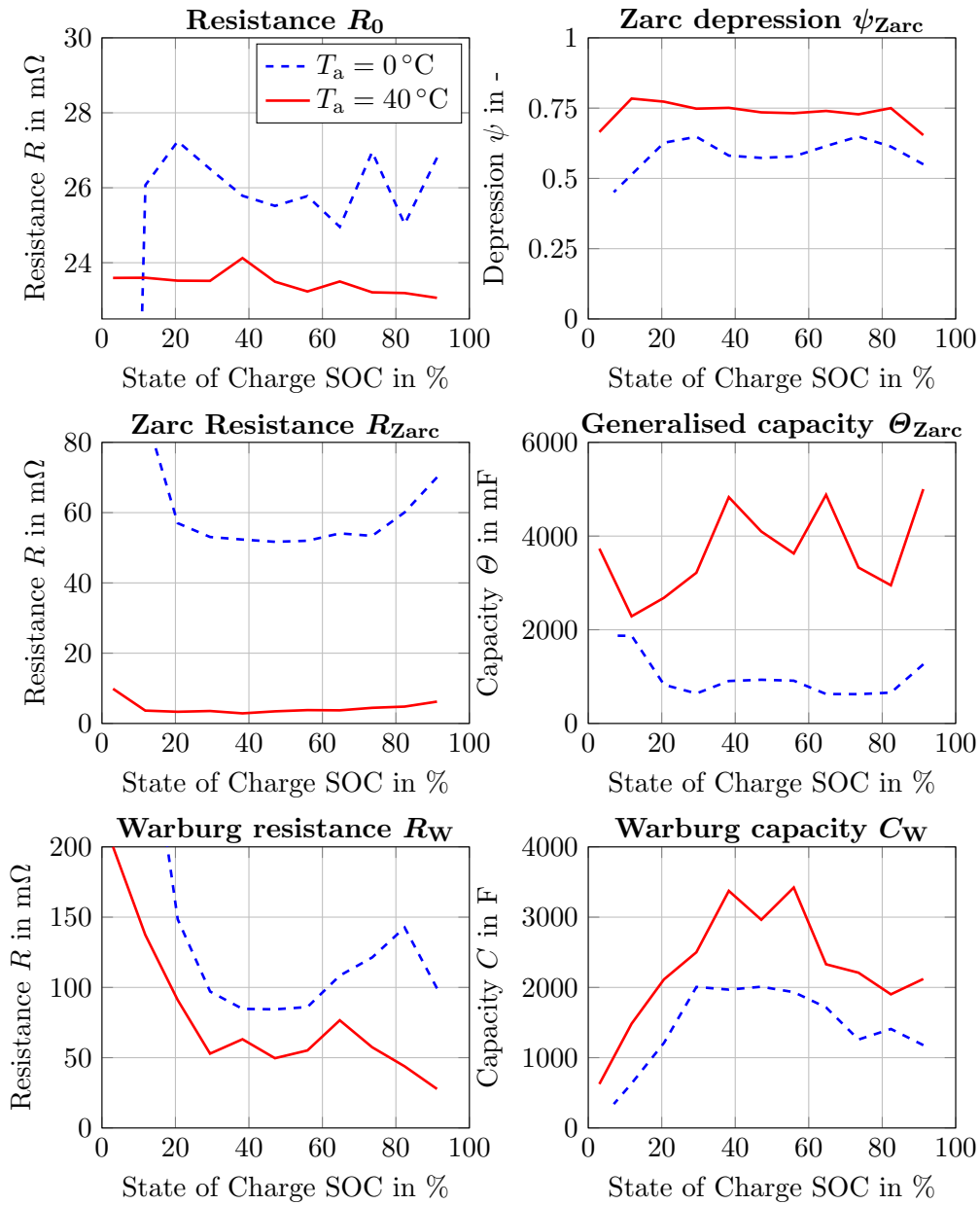
Figure 5.6.: Equivalent electric circuit parameter estimation for various SOC states and an ambient temperature of $T_a = 0\,^{\circ}\mathrm{C}$; top left, behaviour of the resistance $R_0$ is shown; top right and the two middle plots represent the *Zarc* element; the two bottom plots show the behaviour from the *Warburg impedance*

## 5.3. Current dependent influences on the model behaviour

The third influence to investigate in detail is the load current, respectively the C-rate. To do so, theoretically there are two possibilities. First, to do EIS measurements within different sine amplitudes and second, pulsed manoeuvres in the time domain with various current rates. Thus, the first method is definitely the more detailed one due to the wide range of frequency influences. In detail, current behaviour can be evaluated on each element of the electric circuit separately. Nevertheless, a large matrix of manoeuvres, respectively a lot of measurement time, is needed. Therefore, due to the limited measurement time, the second method to evaluate the current influence, is used in this thesis. To do so, a pulse manoeuvre on a predefined $SOC = 70.445\,\%$ state and ambient temperature $T_\mathrm{a} = 0\,°\mathrm{C}$ is applied on the test cell as well as the generated cell model in a first step, see Figure 5.7.
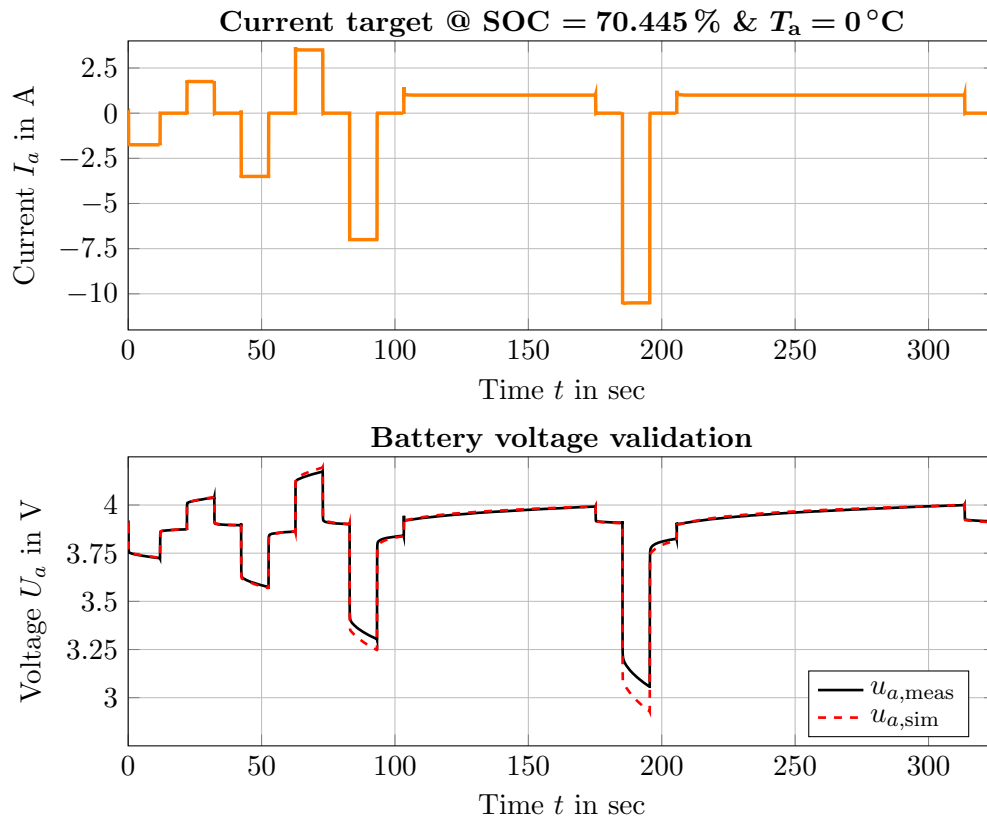


Figure 5.7.: Investigation of various load currents $I_a$ on the cell behaviour, respectively on the battery model, at ambient temperature of $T_\mathrm{a} = 0\,°\mathrm{C}$; the upper plot represents the current pulse target while in the bottom plot the measured voltage $u_{a,\mathrm{meas}}$ and the simulated one from the battery model $u_{a,\mathrm{sim}}$ are presented

In the upper plot of Figure 5.7 the load current target $I_a$ is given. Thus, two positive and four negative pulses are seen. Hence, the reached upper voltage limit within the high positive pulses was the reason why only two positive ones could be applied. Belong to the current target, the measured as well as the simulated cell voltage are presented in the bottom plot. Validating the results from the measured and simulated cell behaviour, it is clearly visible that both match well at lower currents, but worse at higher ones. Thus, remember that the EIS manoeuvres were done with amplitudes of $i_0 = 2\,\text{A}$, which is close to the first two pulses of $i_{0,1/2} = 1.75\,\text{A}$. Therefore, within this area, an error between measured and simulated voltage of about $\Delta u_{1/2} = 3\,\text{mV}$ is given. This indicates a percentage error of $< 1\,\%$.

Nearly the same error behaviour is given at pulse three and four at $i_{0,3/4} = 3.5\,\text{A}$. Nevertheless, an increasing error is given with a rising pulse amplitude. Within the last pulse at $i_{0,6} = 10.5\,\text{A}$, an error of about $\Delta u_6 = 125\,\text{mV}$ is seen. Thus, this shows that the load current definitely has not a negligible influence on cell behaviour. By validating the characteristics, a smaller dynamic voltage drop is desired. From the electro chemical point of view, a different behaviour within the charge transfer between the anode and electrolyte, respectively the cathode and electrolyte is given. Through, this brings changes within the *Zarc* element, in detail in the *Zarc* resistance. Following, by changing the resistance $R_\text{Zarc}$ influences can be modelled. For a detail description, reference to [Buller, 2003] is given.

To do so, the initial setup parameterised from the EIS measurements are used and the $R_\text{Zarc}$ changed, respectively optimised, for each pulse period separately. This results are given within the blue circles in Figure 5.8 on the left side, where each circle represents the optimised resistance for one pulse. Furthermore, for the black solid line the initial resistance out of the EIS is given. Comparing with Figure 5.7, the decreasing behaviour for increasing current is seen in detail. In addition, same behaviour is presented for higher temperature $T_\text{a} = 40\,°\text{C}$ on the right side of Figure 5.8.

To be able to handle also currents between the generated circuits out of each pulse, a model characteristic must be defined. Thus, for the mathematical description of the *Zarc* resistance $R_\text{Z,BV}$, an extended cosinus function is used by

$$R_\text{Z,BV} = B\left(\left(\cos(|c_0 - c_a|)\,C\right) + 1\right) + R_{Z,\min}\,, \tag{5.1}$$

where $c_a$ represents the current C-rate and $c_0$ an offset behaviour on the $x$-axis. Furthermore, the two parameters $B$ and $C$ define the cosine characteristics and are defined by

$$B = \frac{R_\text{Zarc,max} - R_\text{Z,min}}{2} \quad \text{and} \tag{5.2}$$

$$C = \frac{\pi}{\Delta c/2}\,. \tag{5.3}$$
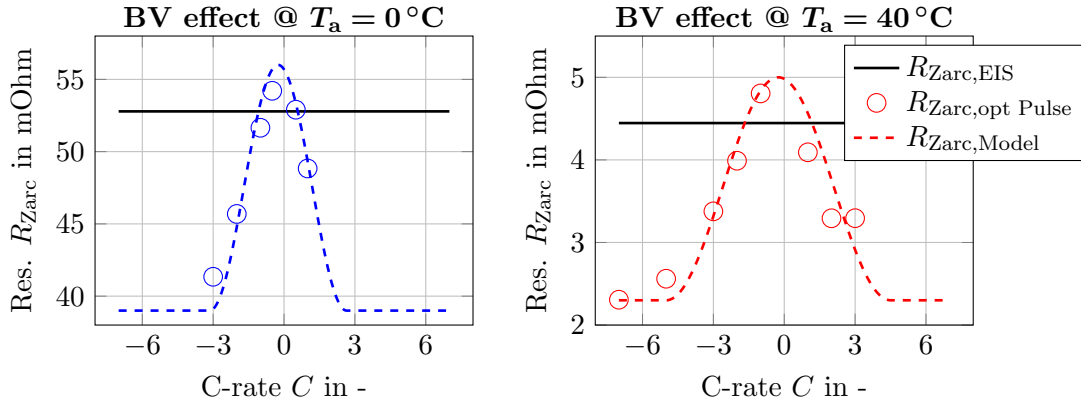
Figure 5.8.: Investigation of different load currents on the *Zarc* resistance; left, for an ambient temperature of $T_a = 0\,°C$ and right for $T_a = 40\,°C$. The black solid line represents the initial value out of the EIS manoeuvre while the circles representing the defined values for each pulse. The dashed line describe the model behaviour respectively

Thus, the parameter $R_{Zarc,max}$ and $R_{Zarc,min}$ represent the maximum and minimum value of the *Zarc* resistance and $\Delta c$ the width of the cosine period. In summary, no explicit optimisation process is needed for this implementation. The semi-physical parameters can be taken out of the results from Figure 5.8 directly, see Table 5.1 respectively.

Finally, the semi-physical model approach is implemented in the battery model and the manoeuvres applied. Thus, results for a $T_a = 0\,°C$ are presented in Figure 5.9 and for $T_a = 40\,°C$ in Figure 5.10. On the upper plot of both figures, the load current target is presented. According thereto, the results of the first and extended model approach are given in the three plots bellow. Hence, the middle plot shows the whole manoeuvre and the two plots bellow detailed zoom areas. Finally, a significant improvement at both temperatures is given, especially at higher load currents.

In summary, it was shown that the load current has an influence on voltage behaviour and should be implemented in some way for an accurate model description. Thus, in this subsection a semi-physical model approach was presented with significant improvements the overall model behaviour.

Table 5.1.: Model parameter to define the BV effect for both ambient temperatures

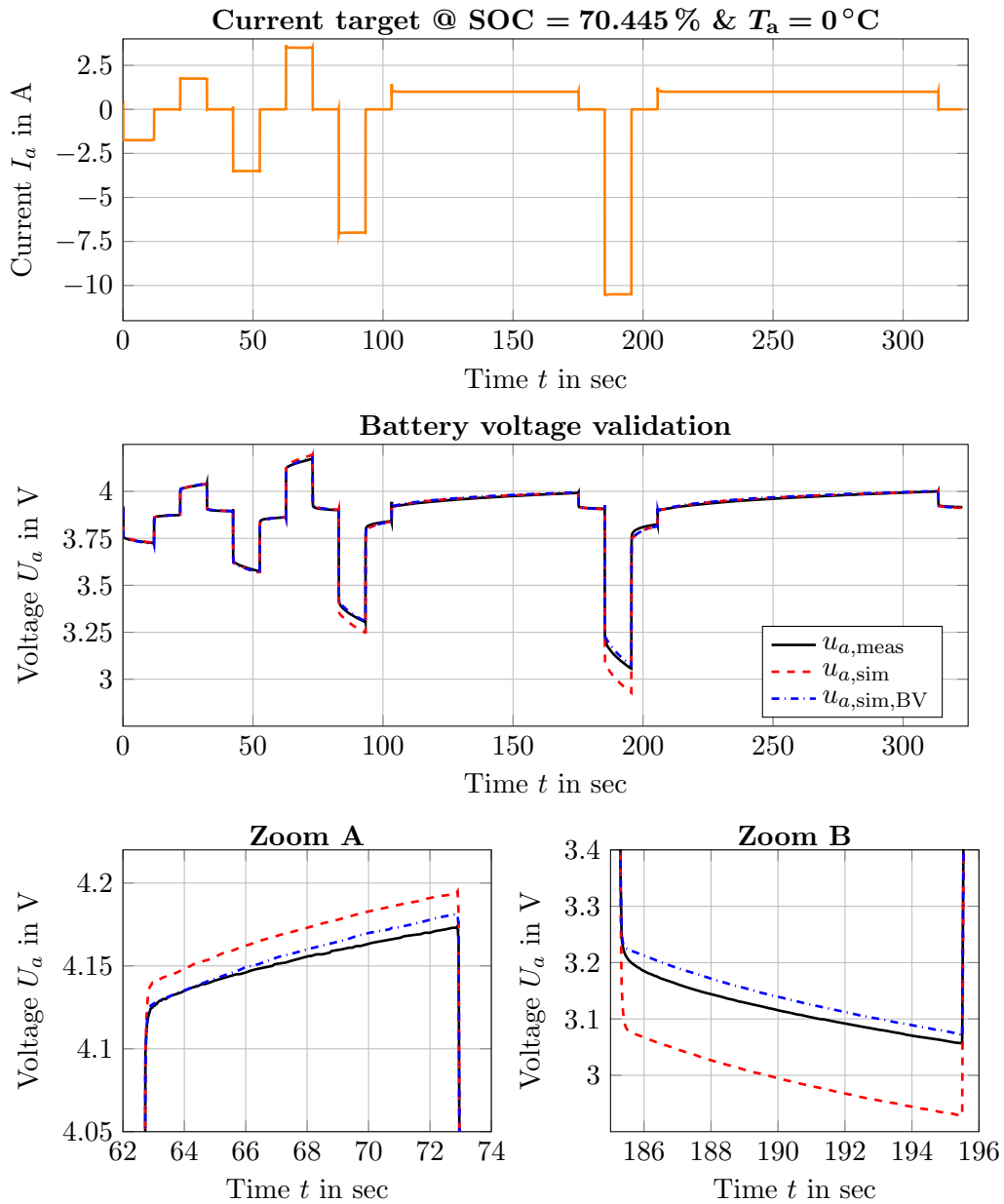| Parameter | $T_a = 0\,°C$ | $T_a = 40\,°C$ | Unit |
|---|---|---|---|
| $R_{Zarc,min}$ | 39 | 2.3 | in m$\Omega$ |
| $R_{Zarc,max}$ | 56 | 5.0 | in m$\Omega$ |
| $\Delta c$ | 5.8 | 9.5 | in - |
| $c_0$ | -0.25 | -0.25 | in - |

Figure 5.9.: Validation of the overall cell model including the BV effect at an ambient temperature of $T_a = 0\,^\circ\mathrm{C}$. The upper plot represents the current target for a defined SOC level, while the three plots bellow show the measured voltage $u_{a,\mathrm{meas}}$, black solid, and the simulated voltages without $u_{a,\mathrm{sim}}$, red dashed, and including the BV model $u_{a,\mathrm{sim,BV}}$, dash dotted blue
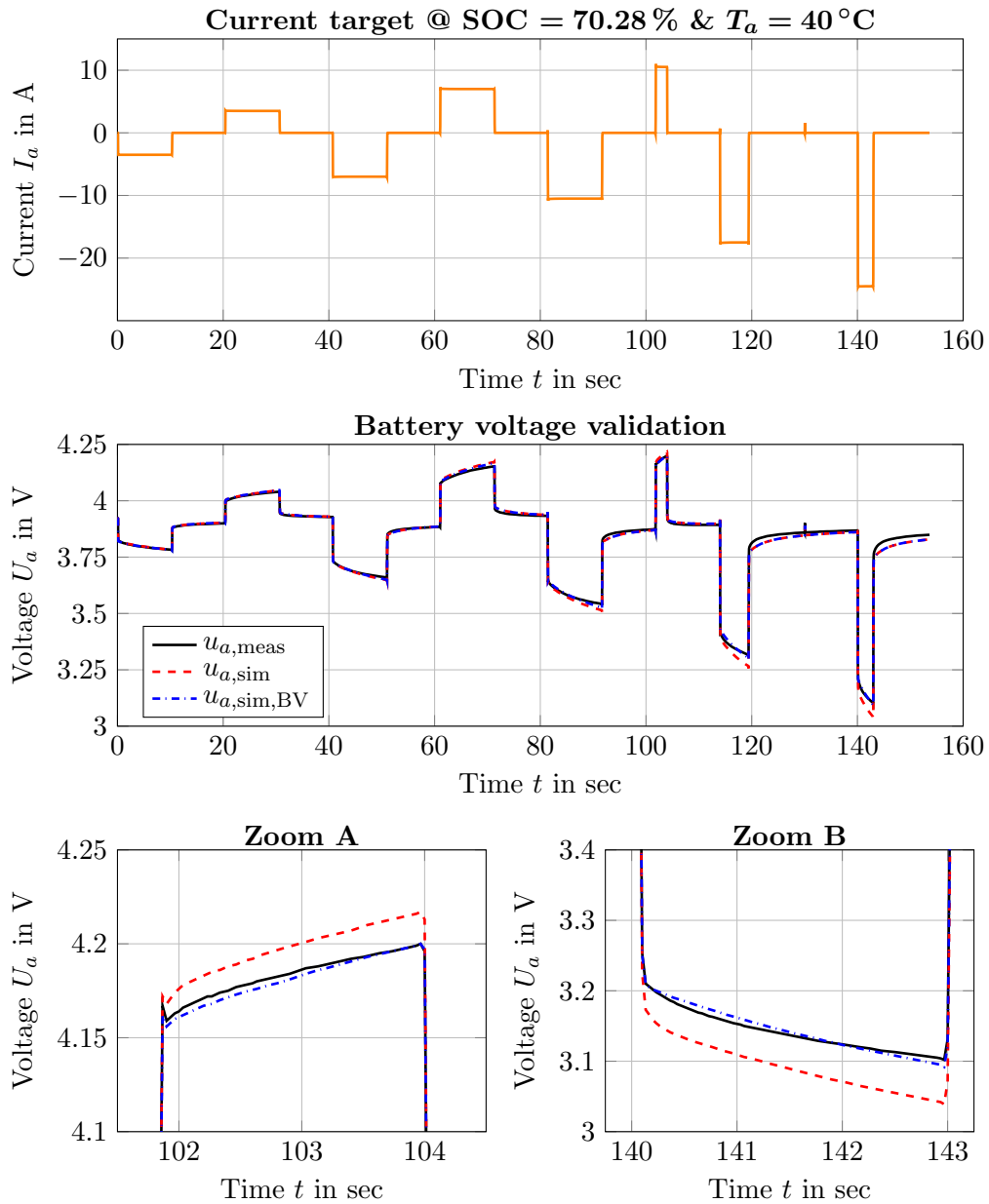
Figure 5.10.: Validation of the overall cell model including the BV effect at an ambient temperature of $T_a = 40\,°\text{C}$. The upper plot represents the current target for a defined SOC level, while the three plots bellow show the measured voltage $u_{a,\text{meas}}$, black solid, and the simulated voltages without $u_{a,\text{sim}}$, red dashed, and including the BV model $u_{a,\text{sim,BV}}$, dash dotted blue

Finally, the developed model was evaluated on different influencing factors, like SOC levels, ambient temperatures and load currents. It was demonstrated that the model, defined with one resistance, one *Zarc* element and one *Warburg impedance* is able to handle SOC and temperature changes by varying a set of parameters respectively. Furthermore, a semi-physical approach to implement the BV effect was given in addition. Within this approach, a wide range of load current can be modelled in a satisfactory way. In summary, the used model approach shows well modelling properties by only using three elements at all.

For the purpose of completeness, a parameterisation process within the time domain is given in the next section to complete the overall model validation. Goal of this investigations is to compare parameters out of the EIS manoeuvre and parameterisation within the time domain.

## 5.4. Equivalent electric circuit parameterisation within the time domain

Finally, a parameterisation process only in the time domain is done in this chapter for the purpose of completeness. Thus, this process as well as the following parameter evaluation, is very useful to compare results from an EIS and a parameterisation within the time domain. Because in few cases no equipment for EIS measurements is available nor time for a wide EIS measurement procedure is applicable. So, this chapter gives an overview how the parameterisation process in the time domain will perform.

To do so, the pulse manoeuvres from the previous section are used to fully parametrise the defined R-Zarc-$Z_W$ model from Figure 4.13. Thus, a non-linear optimisation algorithm defines the parameter from Table 4.2 by using the target current as an input and minimising the resulting error between measured and simulated cell voltage. Finally, the results of these parameterisation processes for both Temperatures $T_a = \{0, 40\}\,°\text{C}$ are presented in Figure 5.11, while in the upper plot conditions of SOC = 70.445 % & $T_a = 0\,°\text{C}$ and in the bottom plot SOC = 70.28 % & $T_a = 40\,°\text{C}$ are given. Thus, the black solid line represents the measured behaviour for both temperatures, while the blue dashed one is defined as simulated behaviour at lower temperature and the red dashed at higher level.

Thus, it is clearly visible that for both temperatures a satisfying match between measured and simulated behaviour is given. Hence, at lower C-rates the simulation under-estimates a little bit while for the larger ones over-estimation is seen. Thus averaging the error without taking the BV effect into account is the result therefore. Extending the model with BV effect brings small improvements but at this point, it is absolutely not necessary because of the already satisfying match. Within this example it can be presented that the model parameterisation is also possible by using measurements within the time domain.
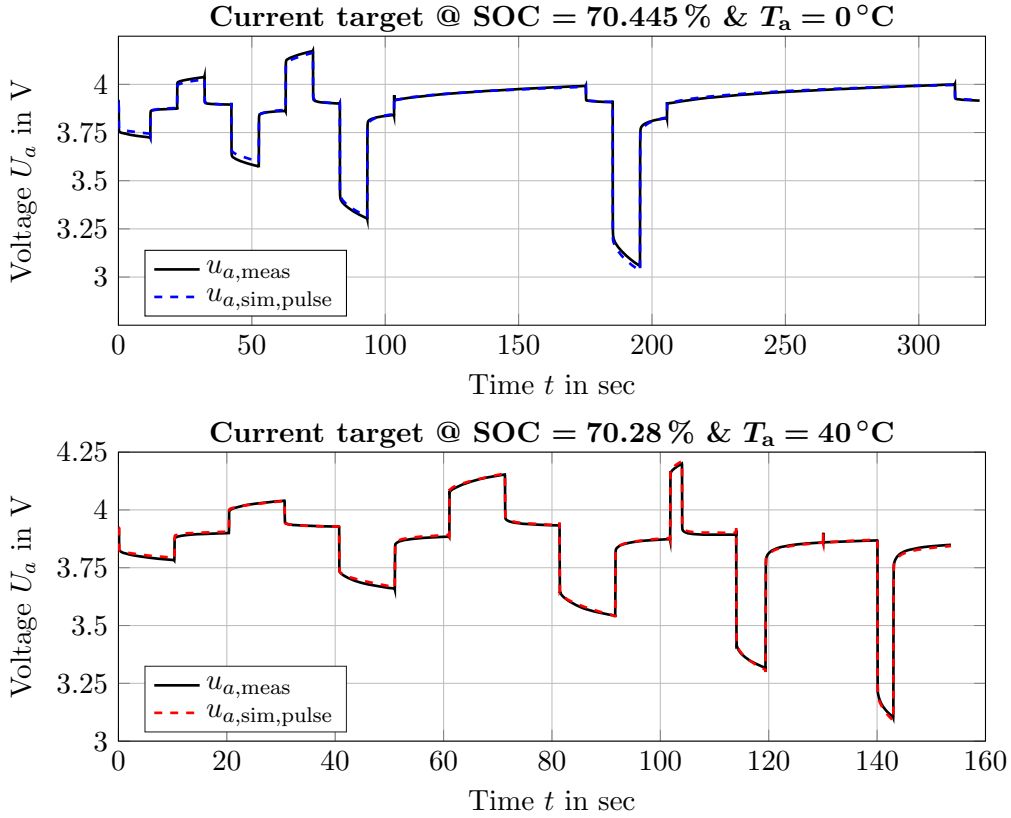
Figure 5.11.: Validation of the parameterised EC within the pulse manoeuvre in time domain for both ambient temperatures $T_\mathrm{a} = \{0, 40\}\,°\mathrm{C}$; conditions of SOC $= 70.445\,\%$ & $T_\mathrm{a} = 0\,°\mathrm{C}$ in the upper plot and SOC $= 70.28\,\%$ & $T_\mathrm{a} = 40\,°\mathrm{C}$ in the bottom plot are given. The measured behaviour $u_{a,\mathrm{meas}}$ is given with the black solid lines, while the simulated ones are given with the dashed blue for $T_a = 0\,°\mathrm{C}$ and dashed red for $T_a = 40\,°\mathrm{C}$

The detailed values, gained from the parameterisation process, are summarised in Table 5.2 and compared with the values out of the EIS measurements. For both temperatures, especially the two resistances $R_0$ and $R_\mathrm{Zarc}$ match well, while a deviation at the four other parameters are seen. Thus, this effect can be explained out of the pulse manoeuvre in combination with the working frequencies of the defined element. Due to the effect that only pulses are used within the time domain manoeuvre this only includes high frequencies. Therefore, the two mentioned parameters can be parameterised easier, where on the contrary low frequencies are not given in these manoeuvres. Therefore, to validate the parameterisation process within the time domain, a manoeuvre with a wider frequency range should be useful for further investigations. Nevertheless, it seems that a adequately parameterisation process is also possible within the time domain.

Table 5.2.: Values comparison out of the parameterisation process based on the EIS method as well as parametrising at time domain for two different ambient temperatures $T_a = \{0, 40\}\,^\circ\mathrm{C}$

| Parameter | Value EIS | Value Pulse | Unit |
|:---:|:---:|:---:|:---:|
| **SOC = 70.445 % & $T_\mathrm{a} = 0\,^\circ\mathrm{C}$** | | | |
| $R_0$ | 26.43 | 24.74 | in mΩ |
| $R_\mathrm{Zarc}$ | 52.79 | 42.62 | in mΩ |
| $\Theta$ | 639.07 | 1356 | in mF |
| $\psi$ | 0.66 | 0.54 | in - |
| $R_\mathrm{W}$ | 69.59 | 67.5 | in mΩ |
| $C_\mathrm{W}$ | 1358 | 1497 | in F |
| **SOC = 70.28 % & $T_\mathrm{a} = 40\,^\circ\mathrm{C}$** | | | |
| $R_0$ | 23.84 | 24.17 | in mΩ |
| $R_\mathrm{Zarc}$ | 4.29 | 5.12 | in mΩ |
| $\Theta$ | 4200 | 8064 | in mF |
| $\psi$ | 0.76 | 1.00 | in - |
| $R_\mathrm{W}$ | 59.82 | 172.2 | in mΩ |
| $C_\mathrm{W}$ | 2373 | 9134 | in F |

In addition, an alternative presentation of the two different parameterisation processes is given in the Nyquist plot in Figure 5.12. Within this plot, the parameters from Table 5.2 are used and behaviour within the frequency domain compared at two different SOC and temperature levels. Out of previous investigations it is visible that the behaviour generated from the EIS procedure $\underline{\boldsymbol{Z}}_{\mathrm{sim,EIS}}(f_\mathrm{sim})$ fits the measured behaviour $\underline{\boldsymbol{Z}}_{\mathrm{meas}}$ quite well. In addition, the characteristic generated from the pulse parameter $\underline{\boldsymbol{Z}}_{\mathrm{sim,pulse}}(f_\mathrm{sim})$ shows a good behaviour at higher frequency levels but get worse for lower frequencies. This confirms the already discussed properties, based on the pulse manoeuvres. Once again, for a more accurate parameterisation process at lower frequencies, a time domain manoeuvre with a wider frequency range should be used.

In summary, the parameterisation process of the elaborated EC was validated in this section. It was shown that parameterising within the time domain brings a good alternative when no EIS measurement equipment is accessible or measurement time limited. Nevertheless, a well defined manoeuvre is needed to handle the parameterisation process for a wide frequency range. Thus, for a detailed comparison different manoeuvres have to be evaluated and compared in a further research step. But overall, the elaborated model shows accurate behaviour in both, frequency and time domain, as well for both parameterisation methods.
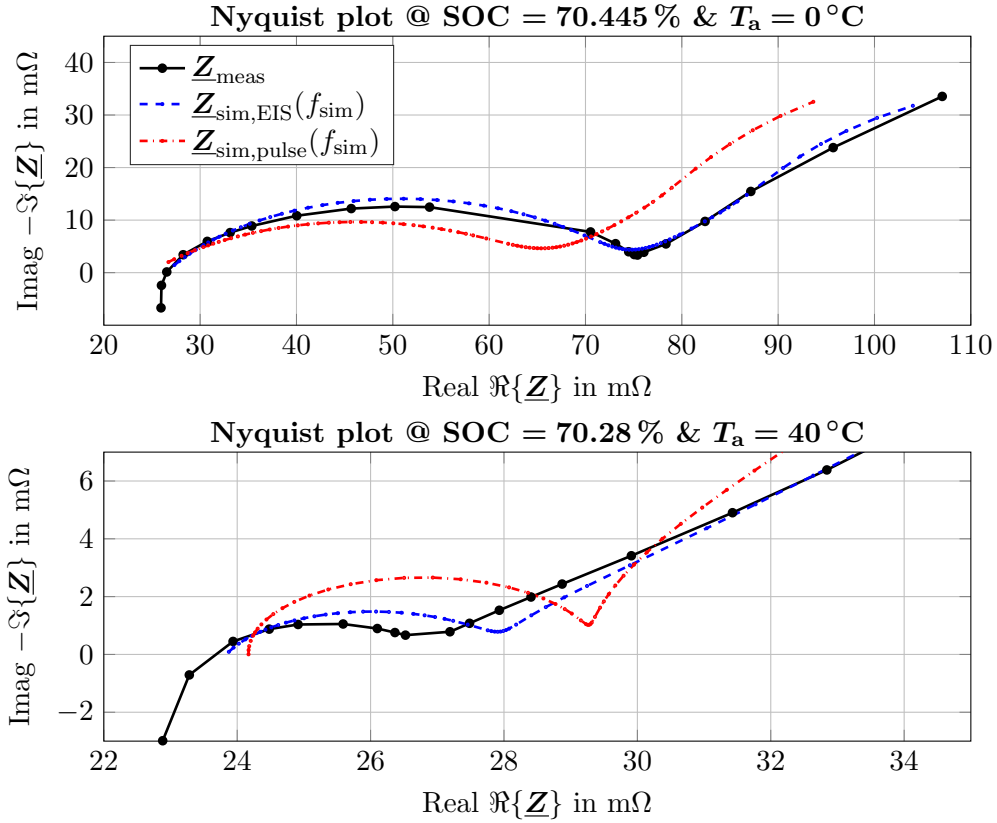
Figure 5.12.: Nyquist plot validation of the EC parametrised via pulse manoeuvre within two different SOC and ambient temperatures. The black solid line $\underline{Z}_{\text{meas}}$ represents the measured behaviour, while the coloured ones represent the simulated characteristics, parameterised via EIS $\underline{Z}_{\text{sim,EIS}}(f_{\text{sim}})$ and via pulse manoeuvre $\underline{Z}_{\text{sim,pulse}}(f_{\text{sim}})$

## 5.5. Comparative conclusion of the model validation process

Finally, after presenting the modelling process in the previous chapters, model validation, based on various external influences, was part of this chapter. Thus, various EIS measurements with different SOC levels were compared and evaluated within the Nyquist plot first. It was presented that the elaborated EC is able to handle various SOC levels quite well. By means of the parameter evaluation it was seen that especially the resistances $R_0$ and the depression factor $\psi_{\text{Zarc}}$ are nearly independent on the SOC, while main influence is given by the two capacities $\Theta_{\text{Zarc}}$ and $C_{\text{W}}$. In addition, the further two resistance $R_{\text{Zarc}}$ and $R_{\text{W}}$ can also kept constant, if no SOC state close to the boundaries must be modelled.

In a second step, same investigations were done with the lower ambient temperature of $T_a = 0\,°\mathrm{C}$ and results compared. Thus, the elaborated EC is also able to handle the cell behaviour at lower temperature quite well. Furthermore it was shown that all model parameters are sensitive to the temperature changes. This means, if the model should be able to handle a wide range of temperatures, the temperature dependency should be implemented in all model parameters.

In a third step, influences on load current, respectively C-rate, was investigated. Based on a pulse manoeuvre within the time domain, it was presented that these influences can not be neglected. Therefore, a semi-physical model approach, based on a current dependent *Zarc* resistance, was developed, implemented and evaluated. It has been demonstrated that this implementation is able to handle the so called BV effect of a battery cell at both temperature levels. This means in detail, that the elaborated EC battery cell model is able to handle all three influences by means of an extended set of parameters.

For the purpose of completeness, a parameterisation process by only using the pulse manoeuvre within the time domain was evaluated in the last section. It was shown that parameterising within the time domain brings a good alternative when no EIS measurement equipment is accessible or measurement time is limited. Nevertheless, a well defined manoeuvre is needed to handle the parameterisation process for a wide frequency range. Thus, for a detailed comparison different manoeuvres have to be evaluated and compared in a further research step.

In summary, the elaborated EC shows accurate modelling behaviour and is able to handle external influence if parameters are implemented accordingly. Furthermore, satisfactory results within the evaluation process in both frequency and time domain as well for parameterisation within the EIS method as well in the time domain are given. Thus, it could be shown that a use for automotive application is possible.

# 6

# Summary and Conclusion

Energy management systems are indispensable to increase the range of *electric vehicles* (EVs) and *hybrid electric vehicles* (HEVs) by using available energy in most sufficient way. To develop, evaluate and validate the strategies behind, modelling and simulation have become a state of the art tool in automotive engineering to reduce development time, limit safety risks and save costs. Thus, the growing demands for lower computation effort, higher accuracy and easier parameterability increase the expectations surrounding environment models, vehicle models as well as drive train models. Accordingly, the demand for higher model accuracy in energy storage systems, which is given by a battery pack in most applications, is a further outcome.

Therefore, this thesis deals with modelling and simulation of the key component of a battery pack, respectively the battery cell. Special focus goes to *equivalent electric circuit* (EC) approaches, which are still widely applied in automotive industry. To provide a knowledge basis, the analysis of these aspects was carried out in different chapters, which are summarised below, concluded with a final statement and finished with an outlook at the end of the chapter.

**Chapter 1: Introduction** In the first chapter the significance of modelling and simulation for EVs and HEVs strategies was presented. Moreover, the statement was made that a vehicle model alone is hardly capable to describe real world conditions. This means that in addition to a realistic vehicle model, a description of the environment, a driver, a drive train model and their interactions are required to handle all conditions precisely. Following, because a hybrid or electric drive train always includes a battery pack in most applications, the cell as core component has to be modelled and understood first. Consequently, cell modelling as foundation for further fundamental investigations on battery storage systems was defined as goal of this project.

**Chapter 2: Modelling and simulation applications of battery cells** Chapter 2 started with the requirements and functionalities of battery cells as fundamental knowledge for the modelling process. Additionally, lithium-ion technologies have proven to be a good choice nowadays, based on the power and energy density needed for automotive applications. Following to functionalities of lithium-ion cells, fundamental chemical effects were gained as introduction to the second part. Thus, three common model applications, based on the literature study, were presented. Thereby, detailed focus was spent on electrochemical models, equivalent electric circuit modelling and neuronal net-

works. Furthermore, advantages and disadvantages of these models within calculation time, accuracy and parameterability were discussed and evaluated. Finally, modelling a battery cell with an equivalent electric circuit was chosen as best trade-off for the given requirements.

**Chapter 3: Open circuit voltage as basis for cell modelling** After defining the preferable model structure in Chapter 2, focus on the first part of the modelling strategy was given in the third chapter. This started with basic considerations on battery cell voltage potentials, for a fundamental cell understanding. Following, the idea to split the modelling process in a steady-state and a transient part was explained and confirmed with the literature. Afterwards, a short overview about the measurement equipment as well as the used test cell was given. The second part of the chapter focused on generating the steady-state cell behaviour described by the *open circuit voltage* (OCV) versus *state of charge* (SOC) characteristic. Because the accuracy of the steady-state characteristic is of major importance for the overall model accuracy, both well-known literature based methods, pulse and constant load currents, were investigated in detail. It was shown that both methods bring advantages and disadvantages but within a correct usage, both are well suitable for practical operation. Furthermore, higher accuracy demand can be generated with increasing measurement time. In summary, the defined OCV versus SOC characteristic dealt as the fundament for the next chapters.

**Chapter 4: Modelling of the transient battery cell behaviour** To model an accurate battery cell behaviour, two main parts are needed. First, a well defined OCV versus SOC characteristic, which was done in Chapter 3. Second, an equivalent electric circuit which is able to model the transient battery cell behaviour. Therefore, this was the goal of this chapter. Starting, investigations on internal cell dynamics have shown a time range from a few micro seconds up to ten thousands of hours. Thus, decision was made to focus on electro chemical reactions as well as on diffusion processes based on applications which occur during driving. Further fundamental investigations have shown that beside working within the time domain, a further method, called *electrical impedance spectroscopy* (EIS), has become quite common nowadays. Because within the EIS approach a wide frequency range can be handled therefore, this method was used within the thesis.

Based on these fundamental investigations the second part focused on the modelling design of the EC model approach. Thus the goal was defined to find an accurate model approach but with less complexity as well as a low number of parameters. Based on separate investigations at different frequency areas, this goal was reached by using three elements, a resistance, a *Warburg impedance* and a *Zarc* element. Finally, together with the steady-state, the model is defined and can be validated in the next chapter.

**Chapter 5: Electric circuit model validation** After defining the EC approach, Chapter 5 focused on the evaluation and parameterisation process. Thus, this was done by validating different external influences like SOC level, ambient temperature and load current, respectively C-rate. In detail, a parameter dependency on each influence were presented and discussed. Based on these behaviours, it was shown that not all

parameters are dependent on all influences and can be kept constant to reduce complexity. In addition, a semi-physical *Buttler Volmer* (BV) model approach was presented and evaluated to implement the current dependency from the technical point of view. In summary, it was shown that the elaborated EC model approach is able to handle all these influences by using dependent model parameters.

For the purpose of completeness, a parameterisation process by only using the pulse manoeuvre within the time domain was evaluated in the last section. It was shown that parameterising within the time domain brings a sophisticated alternative when no EIS measurement equipment is accessible or measurement time is limited. This means, the elaborated EC has presented satisfactory results within both frequency and time domain as well for both parameterisation methods and is therefore suitable for automotive applications.

**Final statement:** The presented thesis provides a well-grounded analysis of battery cell model approaches, which serves as fundamental for energy management system investigations for EV and HEV. Thus, three different types of model approaches were evaluated whereby cell modelling on EC were chosen as trade-off between accuracy, calculation time and parameterability. It is demonstrated that separating the modelling process in two main parts, first steady-state described as OCV versus SOC characteristic and second transient electric circuit, proved to be a good choice. Furthermore, it was shown that the designed model approach is able to handle external influences by using an adapted set of parameters. In addition, parameterisation is able in frequency as well as time domain, but advantages and disadvantages must be taken into account accordingly. In summary, the presented model approach can be used for further practical and theoretical investigations.

**Outlook:** As further research step, an evaluation within a wider ambient temperature range as well as EIS measurements with different manoeuvre amplitudes can be named at this point. Nevertheless, this extended measurements bring long measurement times and costs, but afterwards an application independent on the operation point can be proved. Practically, parameterisation and evaluation with different manoeuvres within the time domain can be done as well. Examples are the well known drive cycles like the New European Drive Cycle (NEDC) or the Urban Driving Cycle (UDC), but also data from real measurement data.

Furthermore, the cell model can be implemented in a first overall battery pack model approach to investigate the behaviour when cells in series or parallel are used. Thus, this are just a few further application cases and confirms the statement that the cell model approach can be used for further practical and theoretical investigations.
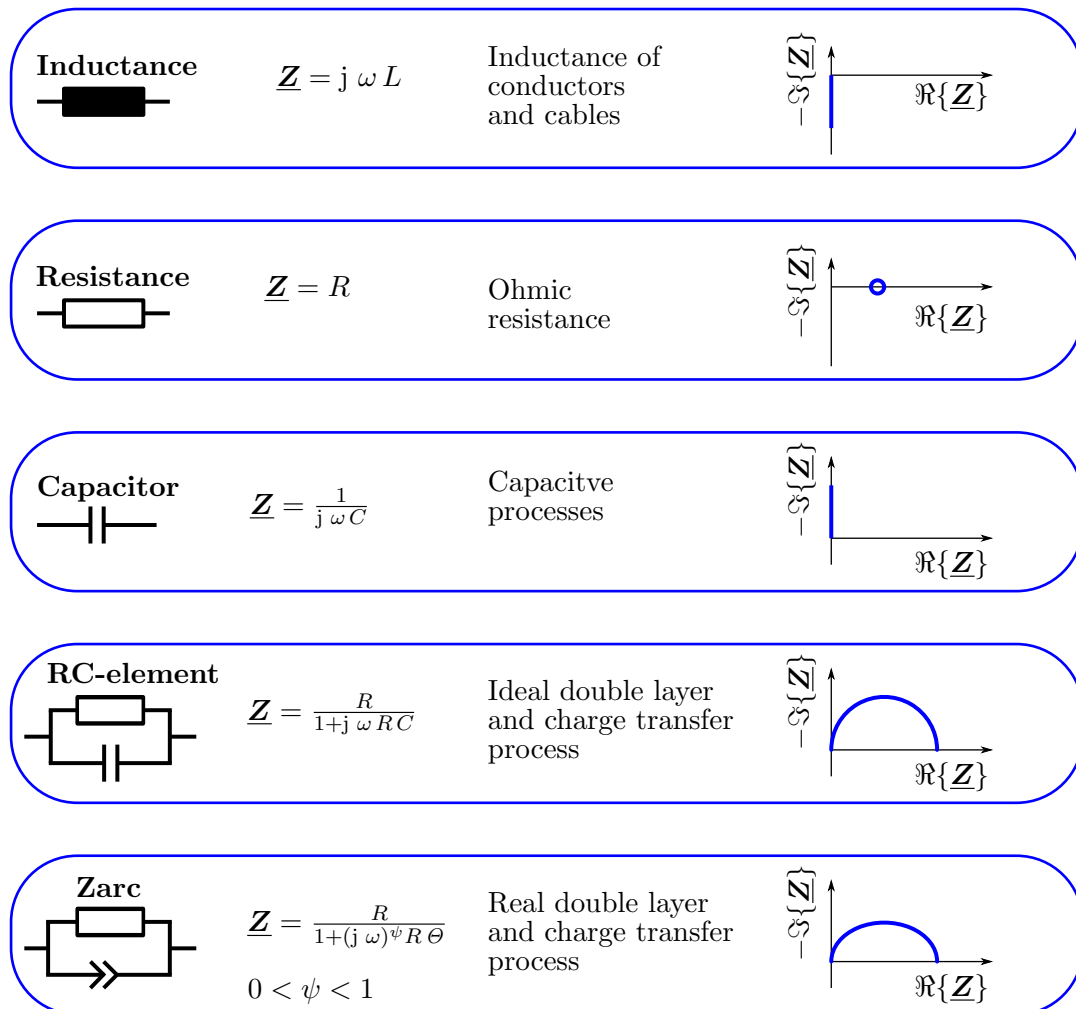
# A

# Electric circuit - fundamental elements

**Inductance**

$$\underline{Z} = \mathrm{j}\,\omega\,L$$

Inductance of
conductors
and cables

**Resistance**

$$\underline{Z} = R$$

Ohmic
resistance

**Capacitor**

$$\underline{Z} = \frac{1}{\mathrm{j}\,\omega\,C}$$

Capacitve
processes

**RC-element**

$$\underline{Z} = \frac{R}{1+\mathrm{j}\,\omega\,R\,C}$$

Ideal double layer
and charge transfer
process

**Zarc**

$$\underline{Z} = \frac{R}{1+(\mathrm{j}\,\omega)^{\psi}R\,\Theta}$$

$$0 < \psi < 1$$

Real double layer
and charge transfer
process

Figure A.1.: Equivalent electric elements based on battery cell behaviours, in-
cluding there *Nyquist plots*, adapted from [Andre et al., 2011b] and
[Weber, 2018]

.

# List of Figures

# List of Tables

# Bibliography

[Amiribavandpour et al., 2013] Amiribavandpour, P., Shen, W., & Kapoor, A. (2013). Development of thermal-electrochemical model for lithium ion 18650 battery packs in electric vehicles. In *2013 IEEE Vehicle Power and Propulsion Conference (VPPC)* (pp. 1–5). DOI:10.1109/VPPC.2013.6671675.

[Andre et al., 2011a] Andre, D., Meiler, M., Steiner, K., Wimmer, C., Soczka-Guth, T., & Sauer, D. (2011a). Characterization of high-power lithium-ion batteries by electrochemical impedance spectroscopy. I. Experimental investigation. *Journal of Power Sources*, 196, 5334–5341. DOI: 10.1016/j.jpowsour.2010.12.102.

[Andre et al., 2011b] Andre, D., Meiler, M., Steiner, K., Wimmer, C., Soczka-Guth, T., & Sauer, D. (2011b). Characterization of high-power lithium-ion batteries by electrochemical impedance spectroscopy. II: Modelling. *Journal of Power Sources*, 196, 5349–5356. 10.1016/j.jpowsour.2010.07.071.

[Ashwin et al., 2017] Ashwin, T., McGordon, A., & Jennings, P. (2017). Electrochemical modelling of li-ion battery pack with constant voltage cycling. *Journal of Power Sources*, 341, 327 – 339.

[Barai et al., 2016] Barai, A., Widanage, W. D., McGordon, A., & Jennings, P. (2016). The influence of temperature and charge-discharge rate on open circuit voltage hysteresis of an lfp li-ion battery. In *2016 IEEE Transportation Electrification Conference and Expo (ITEC)* (pp. 1–4). DOI: 10.1109/ITEC.2016.7520299.

[Barsoukov & Macdonald, 2005] Barsoukov, E. & Macdonald, J. R. (2005). *Impedance Spectroscopy: Theory, Experiment, and Applications*. John Wiley & Sons, Inc., second edition. ISBN: 978-0-471-64749-2.

[Battery University, 2019] Battery University (2019). BU-205: Types of Lithium-ion. `https:https://batteryuniversity.com/learn/article/types_of_lithium_ion`. Accessed on 22 July 2019.

[Batteryforum, 2019] Batteryforum, D. (2019). Lithium-Ionen-Batterien. `https://https://www.batterieforum-deutschland.de/infoportal/batterie-kompendium/sekundaere-batterie/metall-ionen-batterien/lithium-ionen-batterien/`. Accessed on 03 July 2019.

[Buller, 2003] Buller, S. (2003). *Impedance-Based Simulation Models for Energy Storage Devices in Advanced Automotive Power Systems*. PhD thesis, Institut für Leistungselektronik und Elektrische Antriebe, RWTH Aachen University, Aachen, Germany. ISBN: 978-3-8322-1225-4.

[Chemali et al., 2018] Chemali, E., Kollmeyer, P. J., Preindl, M., Ahmed, R., & Emadi, A. (2018). Long short-term memory networks for accurate state-of-charge estimation

of li-ion batteries. *IEEE Transactions on Industrial Electronics*, 65(8), 6730–6739. DOI: 10.1109/TIE.2017.2787586.

[Dubarry et al., 2019] Dubarry, M., Baure, G., Pastor-Fernandez, C., Yu, T. F., Widanage, W. D., & Marco, J. (2019). Battery energy storage system modeling: A combined comprehensive approach. *Journal of Energy Storage*, 21, 172–185. DOI: 10.1016/j.est.2018.11.012.

[European Commission, 2018a] European Commission (2018a). 2050 long-term strategy. `https://ec.europa.eu/clima/policies/strategies/2050_en`. Accessed on 03 July 2019.

[European Commission, 2018b] European Commission (2018b). A Clean Planet for all A European strategic long-term vision for a prosperous, modern, competitive and climate neutral economy. *Communication from the European Commission*, 773, 25. Published: 28. November 2018.

[European Commission, 2018c] European Commission (2018c). Our Vision for A Clean Planet for All: Industrial Transition. `https://https://lionknowledge.com/2-funktionsweise-von-lithium-ionen-batterien/2-1-chemische-reaktionen/`. Accessed on 03 July 2019.

[Farmann & Sauer, 2017] Farmann, A. & Sauer, D. U. (2017). A study on the dependency of the open-circuit voltage on temperature and actual aging state of lithium-ion batteries. *Journal of Power Sources*, 347, 1–13. DOI: 10.1016/j.jpowsour.2017.01.098.

[Farmann & Sauer, 2018] Farmann, A. & Sauer, D. U. (2018). Comparative study of reduced order equivalent circuit models for on-board state-of-available-power prediction of lithium-ion batteries in electric vehicles. *Applied Energy*, 225, 1102 – 1122. DOI: doi.org/10.1016/j.apenergy.2018.05.066.

[Frölich, 2006] Frölich, O. (2006). Einführung in Neuronale Netze. Lecture notes.

[Han et al., 2015a] Han, X., Ouyang, M., Lu, L., & Li, J. (2015a). Simplification of physics-based electrochemical model for lithium ion battery on electric vehicle. Part I: Diffusion simplification and single particle model. *Journal of Power Sources*, 278, 802 – 813. DOI: 10.1016/j.jpowsour.2014.12.101.

[Han et al., 2015b] Han, X., Ouyang, M., Lu, L., & Li, J. (2015b). Simplification of physics-based electrochemical model for lithium ion battery on electric vehicle. Part II: Pseudo-two-dimensional model simplification and state of charge estimation. *Journal of Power Sources*, 278, 814 – 825. DOI: doi.org/10.1016/j.jpowsour.2014.08.089.

[Handschuh, 2007] Handschuh, T. (2007). *Untersuchung des Betriebs- und Alterungsverhaltens von Blei-Säure-Akkumulatoren bei für Hybridantriebssysteme typischen Belastungen*. PhD thesis, Fakultät für Ingenieurwissenschaften und Informatik, Ulm, Germany. DOI: 10.18725/OPARU-379.

[He et al., 2014] He, W., Williard, N., Chen, C., & Pecht, M. (2014). State of charge estimation for li-ion batteries using neural network modeling and unscented kalman

filter-based error cancellation. *International Journal of Electrical Power & Energy Systems*, 62, 783 – 791.

[Huang & Chow, 2016] Huang, C. & Chow, M. (2016). Accurate thevenin's circuit-based battery model parameter identification. In *2016 IEEE 25th International Symposium on Industrial Electronics (ISIE)* (pp. 274–279). DOI: 10.1109/ISIE.2016.7744902.

[Huria et al., 2012] Huria, T., Ceraolo, M., Gazzarri, J., & Jackey, R. (2012). High fidelity electrical model with thermal dependence for characterization and simulation of high power lithium battery cells. In *2012 IEEE International Electric Vehicle Conference* (pp. 1–8). DOI: 10.1109/IEVC.2012.6183271.

[Hussein, 2019] Hussein, A. A. (2019). Adaptive Artificial Neural Network-Based Models for Instantaneous Power Estimation Enhancement in Electric Vehiclesâ€™ Li-Ion Batteries. *IEEE Transactions on Industry Applications*, 55(1), 840–849. DOI: 10.1109/TIA.2018.2866102.

[Jeon & Baek, 2011] Jeon, D. H. & Baek, S. M. (2011). Thermal modeling of cylindrical lithium ion battery during discharge cycle. *Energy Conversion and Management*, 52(8), 2973 – 2981. DOI: 10.1016/j.enconman.2011.04.0130.

[Jiang et al., 2017] Jiang, J., Liang, Y., Ju, Q., Zhang, L., Zhang, W., & Zhang, C. (2017). An equivalent circuit model for lithium-sulfur batteries. *Energy Procedia, 8th International Conference on Applied Energy, ICAE2016, 8-11 October 2016, Beijing, China*, 105, 3533 – 3538. DOI: doi.org/10.1016/j.egypro.2017.03.810.

[Karden et al., 2000] Karden, E., Buller, S., & De Doncker, R. (2000). A method for measurement and interpretation of impedance spectra for industrial batteries. *Journal of Power Sources*, 85(1), 72–78. DOI: doi.org/10.1016/S0378-7753(99)00385-7.

[Khan & Kaer, 2016] Khan, M. R. & Kaer, S. K. (2016). Three dimensional thermal modeling of li-ion battery pack based on multiphysics and calorimetric measurement. *2016 IEEE Vehicle Power and Propulsion Conference (VPPC)*, (pp. 1–6). DOI: 10.1109/VPPC.2016.7791803.

[Kölbel, 2019] Kölbel, D. A. (2019). Lithium-Ionen-Batteriesysteme. `https://lionknowledge.com/`. Accessed on 13 August 2019.

[Kollmeyer et al., 2017] Kollmeyer, P., Hackl, A., & Emadi, A. (2017). Li-ion battery model performance for automotive drive cycles with current pulse and eis parameterization. In *2017 IEEE Transportation Electrification Conference and Expo (ITEC)* (pp. 486–492). DOI: 10.1109/ITEC.2017.7993319.

[Kraus, 2016] Kraus, H. (2016). *Development of an Operation Strategy for Plug-in Hybrid Electric Vehicles - Long-term Prediction and Adaptation based on Past Vehicle and Driver Data*. PhD thesis, Graz University of Technology, Graz, Austria.

[Lösche-ter Horst, 2015] Lösche-ter Horst, T. (2015). Batterien als Bestandteil zukünftiger Antriebstechnik. *4. Kompetenztreffen Elektromobilität*.

[Mauracher & Karden, 1997] Mauracher, P. & Karden, E. (1997). Dynamic modelling of lead/acid batteries using impedance spectroscopy for parameter identification. *Journal of Power Sources*, 67(1), 69–84. Proceedings of the Fifth European Lead Battery Conference.

[McCulloch & Pitts, 1943] McCulloch, W. S. & Pitts, W. (1943). A logical calculus of the ideas immanent in nervous activity. *The bulletin of mathematical biophysics*, 5(4), 115–133. DOI: 10.1007/BF02478259.

[Mousavi G. & Nikdel, 2014] Mousavi G., S. & Nikdel, M. (2014). Various battery models for various simulation studies and applications. *Renewable and Sustainable Energy Reviews*, 32, 477 – 485. DOI: 10.1016/j.rser.2014.01.048.

[Müller-Wondorf, 2017] Müller-Wondorf, R. (2017). Elektrooffensive mit Wenn und Aber. *VDI Nachrichten - Technik, Wirtschaft, Gesellschaft*, Volume 37, Page 14. Published: 15. September 2017.

[Petzl & Danzer, 2013] Petzl, M. & Danzer, M. A. (2013). Advancements in ocv measurement and analysis for lithium-ion batteries. *IEEE Transactions on Energy Conversion*, 28(3), 675–681. DOI: 10.1109/TEC.2013.2259490.

[Rahimzei et al., 2015] Rahimzei, E., Sann, K., & Vogel, M. (2015). Kompendium:Li-Ionen-Batterien - Grundlagen, Bewertungskriterien, Gesetze und Normen. *BMWi Förderprogramm IKT für Elektromobilität*, II, 66.

[Randles, 1947] Randles, J. E. B. (1947). Kinetics of rapid electrode reactions. *Discuss. Faraday Soc.*, 1, 11–19. DOI: 10.1039/DF9470100011.

[Rumelhart & McClelland, 1987] Rumelhart, D. E. & McClelland, J. L. (1987). *Learning Internal Representations by Error Propagation*, (pp. 282 – 317). MITP. ISBN: 9780262291408.

[Samsung INR18650-35E, 2019] Samsung INR18650-35E (2019). Samsung INR18650-35E 3500mAh (Pink). `https://lygte-info.dk/review/batteries2012/Samsung%20INR18650-35E%203500mAh%20%28Pink%29%20UK.html`. Accessed on 28 August 2019.

[Schweighofer et al., 2013] Schweighofer, B., Recheis, M., Gallien, T., & Wegleiter, H. (2013). Fast and accurate battery model including temperature dependency. In *IECON 2013 - 39th Annual Conference of the IEEE Industrial Electronics Society* (pp. 6740–6745). DOI: 10.1109/IECON.2013.6700248.

[Schweighofer et al., 2012] Schweighofer, B., Wegleiter, H., Recheis, M., & Fulmek, P. (2012). Fast and accurate battery model applicable for ev and hev simulation. In *2012 IEEE International Instrumentation and Measurement Technology Conference Proceedings* (pp. 565–570). DOI: 10.1109/I2MTC.2012.6229525.

[Smith et al., 2010] Smith, K. A., Rahn, C. D., & Wang, C. Y. (2010). Model-Based Electrochemical Estimation and Constraint Management for Pulse Operation of Lithium

Ion Batteries. *IEEE Transactions on Control Systems Technology*, 18(3), 654–663. DOI: 10.1109/TCST.2009.2027023.

[Somakettarin & Funaki, 2017] Somakettarin, N. & Funaki, T. (2017). Study on factors for accurate open circuit voltage characterizations in mn-type li-ion batteries. *Batteries*, 3, 8. DOI: 10.3390/batteries3010008.

[Statista GmbH, 2019a] Statista GmbH (2019a). Anzahl der Elektroautos in Deutschland von 2006 bis 2019. `https://de.statista.com/statistik/daten/studie/265995/umfrage/anzahl-der-elektroautos-in-deutschland/`. Accessed on 03 July 2019.

[Statista GmbH, 2019b] Statista GmbH (2019b). Anzahl der Neuzulassungen von Elektroautos in Deutschland von 2003 bis 2019. `https://de.statista.com/statistik/daten/studie/244000/umfrage/neuzulassungen-von-elektroautos-in-deutschland/`. Accessed on 03 July 2019.

[Statista GmbH, 2019c] Statista GmbH (2019c). Weltweite Preisentwicklung für Lithium-Ionen-Batterien von 2013 bis 2020 (in Euro/kWh). `https://de.statista.com/statistik/daten/studie/534429/umfrage/weltweite-preise-fuer-lithium-ionen-akkus/`. Accessed on 04 July 2019.

[Sung et al., 2016] Sung, W., Hwang, D. S., Jeong, B.-J., Lee, J., & Kwon, T. (2016). Electrochemical battery model and its parameter estimator for use in a battery management system of plug-in hybrid electric vehicles. *International Journal of Automotive Technology*, 17(3), 493 – 508. DOI: 10.1007/s12239-016-0051-8.

[Sung & Shin, 2015] Sung, W. & Shin, C. B. (2015). Electrochemical model of a lithium-ion battery implemented into an automotive battery management system. *Computers & Chemical Engineering*, 76, 87 – 97. DOI: 10.1016/j.compchemeng.2015.02.007.

[Tao et al., 2017] Tao, L., Ma, J., Cheng, Y., Noktehdan, A., Chong, J., & Lu, C. (2017). A review of stochastic battery models and health management. *Renewable and Sustainable Energy Reviews*, 80, 716 – 732. DOI: 10.1016/j.rser.2017.05.127.

[Vetter, 2018] Vetter, M. (2018). Batteriespeicher in der stationären Anwendung. Lecture notes.

[Weber, 2018] Weber, A. (2018). Batteriemodellierung mit MATLAB. Lecture notes, winter term 2018. Institut für Angewandte Materialien, Karlsruher Institut für Technologie.

[Wegleiter & Schweighofer, 2017] Wegleiter, H. & Schweighofer, B. (2017). Entwurf und Modellierung mobiler Energiespeichersysteme. Lecture notes, summer term 2017. Institute of Electrical Measurement and Measurement Signal Processing, Graz University of Technology.

[Westerhoff et al., 2016] Westerhoff, U., Kurbach, K., Lienesch, F., & Kurrat, M. (2016).

Analysis of lithium-ion battery models based on electrochemical impedance spectroscopy. *Energy Technology*, 4(12), 1620–1630. DOI: 10.1002/ente.201600154.

[Yang et al., 2017] Yang, D., Wang, Y., Pan, R., Chen, R., & Chen, Z. (2017). A neural network based state-of-health estimation of lithium-ion battery in electric vehicles. *Energy Procedia, 8th International Conference on Applied Energy, ICAE2016, 8-11 October 2016, Beijing, China*, 105, 2059 – 2064. DOI: 10.1016/j.egypro.2017.03.583.